Jagiellonian University in Kraków
Faculty of Physics, Astronomy and Applied Computer Science
Marian Smoluchowski Institute of Physics

PHD IN THE FIELD OF SCIENCE OF PHYSICS

EXPERIMENTAL STUDIES ON THE MULTINUCLEON TRANSFER REACTIONS AS A PATH TO SUPERHEAVY NUCLEI CREATION

Doctoral Dissertation of:

Kamila Zelga

Supervisor:
prof. dr hab. Roman Płaneta
Department of Hot Matter Physics, FAIS UJ

Kraków, September 14, 2020

Wydział Fizyki, Astronomii i Informatyki Stosowanej
Uniwersytet Jagielloński

Oświadczenie

Ja niżej podpisana Kamila Zelga (numer albumu: 1109244), doktorantka Wydziału Fizyki, Astronomii i Informatyki Stosowanej Uniwersytetu Jagiellońskiego oświadczam, że przedłożona przeze mnie rozprawa doktorska pt. *Experimental studies on the multinucleon transfer reactions as a path to superheavy nuclei creation* jest oryginalna i przedstawia wyniki badań wykonanych przeze mnie osobiście, pod kierunkiem prof. dr hab. Romana Płanety. Pracę napisałam samodzielnie. Oświadczam, że moja rozprawa doktorska została opracowana zgodnie z Ustawą o prawie autorskim i prawach pokrewnych z dnia 4 lutego 1994 r. (Dziennik Ustaw 1994 nr 24 poz. 83 wraz z późniejszymi zmianami). Jestem świadoma, że niezgodność niniejszego oświadczenia z prawdą ujawniona w dowolnym czasie, niezależnie od skutków prawnych wynikających z ww. ustawy, może spowodować unieważnienie stopnia nabytego na podstawie tej rozprawy.

Kraków, September 14, 2020 .....
podpis doktoranta

Abstract

The purpose of this doctoral dissertation is to introduce a multinucleon transfer method (MNT) as an alternative to the classic technique of superheavy elements (SHE) production - complete fusion. It is expected that the cross section for the creation of the next SHE using the standard procedure is on the order of tens of femto barns. Which, together with technical difficulties associated with the preparation of the appropriate target and beam energy, crates a serious limitation. The proposed MNT method was tested for the reaction ^{197}Au + ^{232}Th, 7.5 AMeV in terms of searching for both short-lived and long-lived superheavy elements. The obtained results turned out to be optimistic for both SHEs life categories. This work will present detection systems dedicated to these experiments and prepared by a collaboration of Jagiellonian University and Texas A&M University groups. The process of analysis will also be presented, focusing on the search for the radioactive decay of MNT reaction products registered in the scintillation material of the detector. The work has a pilot character, therefore it contains a historical outline of the process of discovering the next superheavy elements together with an explanation of the methods used for their production and identification. It also explains exactly why the search for an alternative method of producing new SHEs is considered as necessary.

Streszczenie

Celem niniejszej rozprawy doktorskiej jest przedstawienie metody transferu wielonukleonowego (MNT) jako alternatywy dla klasycznej metody produkcji nowych pierwiastków superciężkich (SHE) - kompletnej fuzji. Szacuje się że przekrój czynny na utworzenie kolejnego SHE przy pomocy standardowej procedury osiąga wartości rzędu dziesiątek femto barnów. Co wraz z technicznymi utrudnieniami związanymi z przygotowaniem odpowiedniej tarczy oraz energii wiązki stanowi obecnie poważne ograniczenie. Zaproponowana metoda MNT była badana dla reakcji ^{197}Au + ^{232}Th, 7.5 AMeV pod kątem poszukiwania zarówno krótkożyciowych jak i długożyciowych pierwiastków superciężkich. Otrzymane wyniki okazały się optymistyczne dla obu kategorii czasów życia SHE. W pracy przedstawione zostaną dedykowane tym eksperymentom układy detekcyjne przygotowane przez naukowców z kolaboracji Uniwersytetu Jagiellońskiego z Uniwersytetem Teksas A&M. Zostanie również przedstawiony proces przeprowadzanej analizy, skupiającej się na poszukiwaniu rozpadów radioaktywnych produktów reakcji MNT zarejestrowanych w materiale scyntylacyjnym detektora. Praca ma charakter pilotażowy, dlatego też zawiera rys historyczny procesu odkrywania kolejnych pierwiastków superciężkich wraz z wyjaśnieniem stosowanych wówczas metod na ich produkcję oraz identyfikację. W pracy wyjaśniono również dokładnie powód dla którego poszukiwanie alternatywnej metody na wytworzenie nowych SHE jest uznawane za konieczne.

Contents

Introduction

Our quest for discovery fuels our creativity in all fields, not just science. If we reached the end of the line, the human spirit would shrivel and die. But I don't think we will ever stand still: we shall increase in complexity, if not in depth, and shall always be the center of an expanding horizon of possibilities.

THE UNIVERSE IN A NUTSHELL
- Stephen Hawking, 2001.

The search for new chemical elements has a very long history. Its beginnings are reaching times when the periodic table does not exist yet and people were already discovering metals with their different properties. Then the main goal was, for example, refining decorative elements or strengthening weapons. In addition to various thermal processing techniques such as heating and quenching, materials were sought that could be mixed with known metal alloys. Since then, humanity has greatly evolved and the progress of technology and science has made it possible to name, categorize and characterize each of the discovered element. What is more, the current level of science allows us to predict certain properties of elements that have not yet been created.

Searching for new heavier elements is still one of the leading issues in chemistry and nuclear physics. Current knowledge and technology status allowed production of the element over four times heavier than iron known since the dawn of civilization, or almost 20 times heavier than even longer known coal. The hunger for discoveries is constantly growing as new elements are created. This is caused not only due to the vision of the possible usability of the new isotopes but primarily because of the desire to push the boundaries of the impossible.

From over 60 years, scientists are focusing on searching superheavy elements (SHE), i.e. these with proton number (Z, also known as atomic number) is greater than 103. However, this is not the only challenge of this search, because scientists are striving to discover a stable element, or at least

long-lived that would allow further development of science. At the moment all elements heavier than lead with Z = 82 ($_{82}$Pb) are more or less unstable. Admittedly, bismuth ($_{83}$Bi), thorium ($_{90}$Th) or uranium ($_{92}$U) have isotopes that have a half-life of billions of years - which is why it can be found on Earth - but none of them are stable.

All SHE isotopes already discovered are created in a standard procedure with use of the complete fusion reaction. This process consist joining two lighter nuclei into one heavier nucleus, and it will be explained in detail later in this work. SHEs created in such a way are not only unstable but also are characterized by short lifetimes on the level of few minutes or less. However, at the same time, nuclear models predicts existence of long-lived (even billions of years) superheavy elements. This is most clearly seen in the area of the island of stability which existence was suggested in 1957 by Gertrude Scharff-Goldhaber as a new region of relative stability for the double magic nucleus $^{310}_{126}X$ [1].

Later on, in the 1960s, Glenn Seaborg popularizes this idea. The hypothesis he proclaims was also using magic numbers and it was based on the nuclear shell model in a manner similar to electron shells in an atom. The similarity to electron physics does not end just on the nucleus structure but also explains what is called a magic number in nuclear physics. When the outermost atomic orbital is completely filled with electrons the noble gases gain their chemical stability. Such electrons number is called the magic number. Likewise in the case of nucleus stability, it is assumed that if the energy levels of a given nucleus shell are completely filled by protons and neutrons, the nucleon binding energy will reach the maximum value. Such a maximum will lead to a strongly bound configuration with a longer lifetime than those configurations that do not completely fill their shells and the nucleus will be stable. Those numbers of protons (Z) and neutrons (N) for which the shells are filled are also called magic numbers. Theoretical research based on the nuclear shell model allowed Seaborg to postulate that such a situation will take place for elements with Z=114, N=184, 196 and Z=164, N=318. A significant role in developing the theory applied to these predictions had Polish scientists, Władysław Świątecki and Adam Sobiczewski. What is more, W. Świątecki together with W. D. Myers in 1966 also based on the shell model indicated that the magic numbers will be Z=126 and N=184 [2]. In the same year A. Sobiczewski, F.A. Gareev and B.N. Kalinkin, again working on the same model, suggested a bit different magic numbers: Z=114 and N=184 [3].

Discovery of the flerovium (Fl) element triggered an excitation in a researcher's society, because of its atomic number Z=114. Unfortunately, isotopes that were produced, are neutron deficient and they do not reach the island of stability. Nevertheless, it is one of SHEs that is closest to it. So far,

it has not yet been possible to obtain a superheavy nucleus that will reach one of the two postulated stability islands.

Flerovium, although, was not the heaviest already discovered element. This honor belongs to oganesson with Z =118 ($_{118}Og$). It was synthesized as a result of the bombardment of californium nuclei with calcium ions. Unfortunately, further research on new SHEs creation seems to be limited due to the ever smaller active cross-sections for the heavier elements production by complete fusion reactions used so far.

To exceed the limitations associated with the technical and physical limitations on the production of new SHEs the collaboration of the Jagiellonian University with Texas A & M University, University of Silesia and several other universities was established. Its main goal was to find an alternative method of new superheavy elements creation. Multinucleon transfer (MNT), because that is the name of this method, was tested under two realizations. First type of experiments were focused on searching very short-lived SHEs, with lifetime on the level of few ns, while second type was devoted to searching long-lived SHEs. Those both types of tests required different detection setups and were using different analysis methods. Both of them were also conducted in two different places. First group of experiments was made at the Cyclotron Institute of Texas A & M University while second is fully conducted at Jagiellonian University in Kraków. Listed above researches on the MNT are the main content of this work.

This dissertation is divided into four parts. First part contains Chapter 1 end 2 and it is focusing on a historical overview of all heavier than $_{92}$U elements creation. There can be found not only methods of their creation and identification but also description of example detection setup used for their discovery. There are also presented difficulties related to the limitation of a standard approach for searching for new heavier elements.

An attempt to overcome the above mentioned difficulties is associated with the need for an alternative SHE creation approach. Multinucleon transfer and experiments testing its possibilities will be presented in the second part of this work, in Chapter 3. This part is devoted to the experiments focused on searching very short-lived SHEs. Its goal is to present a short historical outline of multinucleon transfer experiments conducted by UJ and TAMU groups. In this part two final detection setups will be introduced together with the most promising results which allowed further experimental setup development.

The third part of this dissertation, contained in Chapters 4, 5 and 6, is devoted to testing MNT method as a way of long-lived SHE creation. Because this is a relatively young experiment, and the formation of a dedicated detection system was also my task, this part will include its detailed descrip-

tion along with the stages of its preparation. The experiment is in the initial phase of research and continuous evolution, so only some of the obtained results will be presented in the work.

The last part contains appendixes A and B with some additional informations and shortcuts explanations.

1 | Historical outline

In this chapter the history of discovering heavy elements: actinides and transactinides will be presented. Method of production selected isotopes will be discussed, together with their discoverers and accompanying circumstances.

1.1 History of transuranic elements

History of searching for superheavy elements has beginnings in the discovery of the heaviest element occurring in Nature. That unique element is uranium with atomic number 92 ($_{92}$U). Uranium was discovered in 1789 by Martin Klaproth at an experimental laboratory in Berlin and in its pure form was first separated by Eugène-Melchior Péligot in 1841 at the Central School of Arts and Manufactures in Paris. At that time the heavier elements could not be created because of lack of the experimental methods of their production, and what is more, scientists did not consider anything heavier than uranium. Finally, the thirties of the twentieth century nuclear theory has appeared what led to the formation of the first transuranium element. The transuranium group increases with time. Currently, it can be divided into two smaller subgroups: actinides (with an atomic number from the interval 93 - 103) and transactinides (with an atomic number greater than 103). Let us look at the history of their discovering.

1.1.1 Actinides

Discovery of the neutron by James Chadwick in 1932 initiated the process of producing transuranic elements. Two years later Enrico Fermi proposed a breakthrough hypothesis of the possible method for new heavier elements production [4]. He notes that the β^- decay which accompanied the bombarding of uranium by neutrons can be proof of the new heavy element creation. The method he proposes was the neutron capture. This type of nuclear reactions is a result of joining the neutron to the nucleus ($^A_Z X$) with Z atomic

number and A mass number (A = number of neutrons(N) + number of protons(Z)). So created new nucleus (${}^{A+1}_{Z}X^{*}$) is excited to average value about 8 MeV. Than the excitation energy is emitted in the form of γ quantum, with emission time on a level 10^{-8}s. Such a reaction is presented on a scheme 1.1. Nucleus formed in such way (${}^{A+1}_{Z}X$) is usually β^{-} radioactive, and by emission of the electron (e^{-}) in accompaniment of the antineutrino ($\tilde{\nu}$) increases its atomic number by one and thus creates a new element (${}^{A+1}_{Z+1}X$), scheme 1.2.

$$ {}^{A}_{Z}X + {}^{1}_{0}n \longrightarrow {}^{A+1}_{Z}X^{*} \longrightarrow {}^{A+1}_{Z}X + \gamma \tag{1.1} $$

$$ {}^{A+1}_{Z}X \longrightarrow {}^{A+1}_{Z+1}X + e^{-} + \tilde{\nu} \tag{1.2} $$

Neutron capture method described above has opened the path for the production of new heavier elements and consequently allowed Edwin McMillan and Philip Abelson received a first transuranic element - neptunium ($_{93}$Np). Its origin reaction is presented in table 1.1.

Neptunium was produced by bombarding uranium target with neutrons beam. With time other types of beams began to be used, such as helium ($_{2}$He) or heavier. Table 1.1 presents all reactions used for actinides creation. Almost all actinides were discovered at the Lawrence Berkeley National Laboratory at the University of California (LBNL). The exception were einsteinium ($_{99}$Es), fermium ($_{100}$Fm) and nobelium ($_{102}$Nb) elements. Nobelium was created at Joint Institute for Nuclear Research at Dubna (JINR) while einsteinium and fermium were not discovered in a laboratory environment at all. Both of them were firstly found in the fallout from the nuclear test, called Ivy Mike, by Albert Ghiorso with his fellow-workers from the University of California, Argonne National Laboratory and Los Alamos National Laboratory.

Ivy Mike was the first hydrogen bomb detonated on the Marshall Islands at the Manhattan Project initiated by Franklin Roosevelt during II World War. This nuclear bomb detonated in 1952 had explosion power higher than 10 megatons of TNT. Despite the enormous power of nuclear bomb destruction military efforts had often provided fields for further research and development of science. This time was similar. Einsteinium was produced by neutron capture of 15 neutrons when fermium absorbed 17 of them. Identification of both elements was possible thanks to a specific energy of the α particles which were emitted by decaying $_{99}$Es and $_{100}$Fm. For $_{99}$Es α energy was 6.6 MeV and for $_{100}$Fm it was 7.02 MeV. This results were hidden from society, the reason was of course their connection with military and nuclear bomb, and rivalry with Soviet Union in field of nuclear physics and technologies. Meanwhile team from Berkeley and Argonne laboratories were working

parallel on producing this elements in laboratory conditions. To produce them they were irradiating californium (e.g. reaction 1.3) or plutonium.

$$^{252}_{98}Cf \xrightarrow{(n,\gamma)} {}^{253}_{98}Cf \xrightarrow[17{,}81\ d]{\beta^-} {}^{253}_{99}Es \xrightarrow{(n,\gamma)} {}^{254}_{99}Es \xrightarrow{\beta^-} {}^{254}_{100}Fm \tag{1.3}$$

Laboratory obtained results were presented in articles in 1954 with a note that it was not the first time of $_{99}Es$ and $_{100}Fm$ production [5, 6, 7, 8, 9, 10]. Results of experiments made on Ivy Mike were declassified and shown to the public in 1955.

Element	**Origin reactions**	**Y. Lab. Ref.**
Neptunium	$^{238}_{92}U + {}^{1}_{0}n \longrightarrow {}^{239}_{92}U^* \xrightarrow[23\ min]{\beta^-} {}^{239}_{93}Np$	1940, LBNL, [11]
Plutonium	$^{239}_{93}Np \xrightarrow[2{,}35\ d]{\beta^-} {}^{239}_{94}Pu$	1940, LBNL, [12]
Americium	$^{239}_{94}Pu \xrightarrow{(n,\gamma)} {}^{240}_{94}Pu \xrightarrow{(n,\gamma)}$ $^{241}_{94}Pu \xrightarrow[14.35\ yr]{\beta^-} {}^{241}_{95}Am$	1944, LBNL, [13]
Curium	$^{239}_{94}Pu + {}^{4}_{2}He \longrightarrow {}^{242}_{96}Cm + {}^{1}_{0}n$	1944, LBNL, [14]
Berkelium	$^{241}_{95}Am + {}^{4}_{2}He \longrightarrow {}^{243}_{97}Bk + 2{}^{1}_{0}n$	1949/1950, LBNL, [15, 16]
Californium	$^{242}_{96}Cm + {}^{4}_{2}He \longrightarrow {}^{245}_{98}Cf + {}^{1}_{0}n$	1949/1950, LBNL, [17, 18]
Einssteinium	found in nuclear fallout	see text
Fermium	found in nuclear fallout	see text
Mendelevium	$^{253}_{99}Es + {}^{4}_{2}He \longrightarrow {}^{256}_{101}Md + {}^{1}_{0}n$	1955, LBNL,[19]
Nobelium	$^{238}_{92}U + {}^{22}_{10}Ne \longrightarrow {}^{260}_{102}No^* \longrightarrow {}^{254}_{102}No + 6{}^{1}_{0}n$	1966, JINR, [20]
Lawrencium	$^{252}_{98}Cf + {}^{11}_{5}B \longrightarrow {}^{263}_{103}Lr^* \longrightarrow {}^{258}_{103}Lr + 5{}^{1}_{0}n$	1961, LBNL,[21]

Table 1.1: List of origin reactions for actinides with year (Y) and place (Lab) of its discovery, and references (Ref) to publication considered each element.

Additionally in table A.1 in appendix A are presented decay modes and half-lifes of all discovered until this time actinide isotopes.

1.1.2 Transactinides - SHE

Currently, the existing elements do not end on actinides. Heavier than them, i.e. with an atomic number higher than 103, according to Seaborg's suggestion, are qualified to the group of transactinides. Transactinides, also known as superheavy elements (SHE), like all transuranic elements were created in artificial conditions.

All elements from this group were synthesized by use of the fusion reaction, also known as a complete fusion, which is the process of combining two lighter nuclei into a heavier one. It is usually accompanied by releasing some energy and the emission of several neutrons. Scheme of this reaction is presented in Figure 1.1. This process is well known from the twenties (in 1920 Arthur Eddington as a first correctly suggested and described that source of the solar energy was a fusion mechanism of hydrogen into helium [22, 23]), but first time in the laboratory environment it appears in 1932 during discovery of helium-3 and tritium by physics Mark Oliphant [24, 25, 26, 27].

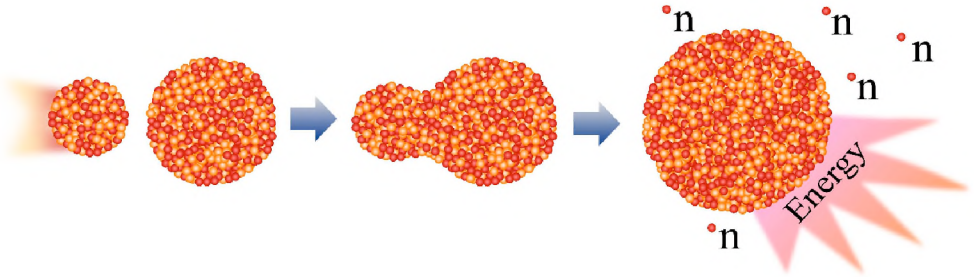

Figure 1.1: Scheme of the fusion reaction on an example of hot fusion process.

A number of conditions must be met for a fusion to occur. Coulomb repulsion of the nuclei involved in the reaction is so large that adequate collision energy is needed to overcome the Coulomb barrier, but at the same time, the collision energy can not be too large to avoid splitting just created nucleus. This process requires also a central collision between both nuclei (projectile and target nuclei). As nuclear fusion is an exothermic reaction the excited compound nucleus (CN) is created. Excited nucleus is cooling down to the ground state by emitting mainly neutrons (protons) and gammas. The competitive process which destroyed the compound nucleus is immediate fission. Many of those factors affect strongly on the probability of creating a new element.

Due to excitation energy of the compound nucleus fusion can be divided into two varieties, hot and cold one:

Hot fusion - is a process in which the energy of the excited compound nucleus is about 30 to 50 MeV. In such a case nucleus evaporates several, 3 to 5, neutrons or undergoes with immediate fission. At such high excitation energy fission have high probability.

Cold fusion - is a process in which the energy of the excited compound nucleus is about 10 to 15 MeV. The amount of emitted neutrons is low, 1-2 neutrons. An important advantage of cold fusion is the relatively low

probability of immediate fission of the produced nucleus.

According to the above explained mechanism of complete fusion reaction scientists from several institutes located in different parts of the world began their experiments. The main research laboratories responsible for currently known SHE discoveries are Joint Institute for Nuclear Research (JINR) in Dubna, Helmholtz Centre for Heavy Ion Research (GSI) in Darmstadt, Lawrence Berkeley National Laboratory (LBNL) in California, Lawrence Livermore National Laboratory (LLNL)in California and Institute of Physical and Chemical Research - Rikagaku Kenkyujo Nishina Center for Accelerator-Based Science (RIKEN) in Wako Saitama. List of obtained until those days SHEs is presented in the table 1.2 together with origin reaction, year and place of their creation.

Against the backdrop of all the reactions listed in the table, history of nihonium ($_{113}$Nh) deserves to be emphasized. This element as the only one from the transactinides group was produced in both fusion varieties (hot and cold fusion). Six preceding it elements were made by using cold fusion reaction, which was pioneered by Yuri Oganessian in 1974, unfortunately, it was found that efficiency of cold fusion is decreasing with a growing atomic number. Nuclei which were produced in such a way were neuron-deficient and had a very short lifetime. What is more group from GSI was trying to create element Z=113 using this technique without success. Those facts led Oganessian in direction of hot fusion method, which was normally used before seaborgium $_{106}$Sg discovery. In 1998 JINR group together with LLNL were bombarding plutonium target with calcium ions. In this way, they discovered element flerovium ($_{114}$Fl) and as a decay product, they obtained for the first time nihonium ($_{113}$Nh). A few years later the same group by using hot fusion method on americium target were found moscovium ($_{115}$Mc), also with nihonium element as a decay product from element Z=115.

In 2003 the Japanese group from RIKEN, lead by Kōsuke Morita using the already abandoned method of cold fusion, finally obtained nihonium directly from the reaction of bombarding bismuth by zinc isotopes. Because of this direct creation the RIKEN group has been honored with the title of nihonium discoverers.

Element	Origin reactions	Y. Lab. Ref.
Rutherfordium	$^{242}_{94}Pu + ^{22}_{10}Ne \longrightarrow ^{259}_{104}Rf + 5^{1}_{0}n$	1964, JINR, [28, 29]
	$^{249}_{98}Cf + ^{12}_{6}C \longrightarrow ^{257}_{104}Rf + 4^{1}_{0}n$	1969, LBNL, [30]
Dubnium	$^{243}_{95}Am + ^{22}_{10}Ne \longrightarrow ^{261}_{105}Db + 4^{1}_{0}n$	1968, JINR,[31]
	$^{243}_{95}Am + ^{22}_{10}Ne \longrightarrow ^{260}_{105}Db + 5^{1}_{0}n$	
	$^{249}_{98}Cf + ^{15}_{7}N \longrightarrow ^{260}_{105}Db + 4^{1}_{0}n$	1970, LBNL, [32]
Seaborgium	$^{208}_{82}Pb + ^{54}_{24}Cr \longrightarrow ^{260}_{106}Sg + 2^{1}_{0}n$	1974, JINR,[33]
	$^{207}_{82}Pb + ^{54}_{24}Cr \longrightarrow ^{260}_{106}Sg + ^{1}_{0}n$	
	$^{249}_{98}Cf + ^{18}_{8}O \longrightarrow ^{259}_{106}Sg + 4^{1}_{0}n$	1974, LBNL, [34]
Bhorium	$^{209}_{83}Bi + ^{54}_{24}Cr \longrightarrow ^{262}_{107}Bh + ^{1}_{0}n$	1976, JINR,[35]
		and 1981, GSI, [36]
Hassium	$^{209}_{83}Bi + ^{55}_{25}Mn \longrightarrow ^{263}_{108}Hs + ^{1}_{0}n$	1983, JINR,[37, 38]
	$^{226}_{88}Ra + ^{48}_{20}Ca \longrightarrow ^{270}_{108}Hs + 4^{1}_{0}n$	
	$^{208}_{82}Pb + ^{58}_{26}Fe \longrightarrow ^{264}_{108}Hs + 2^{1}_{0}n$	1984, GSI,[39]
Meitnerium	$^{209}_{83}Bi + ^{58}_{26}Fe \longrightarrow ^{266}_{109}Mt + ^{1}_{0}n$	1982, GSI, [40]
Darmstadium	$^{208}_{82}Pb + ^{62}_{28}Ni \longrightarrow ^{269}_{110}Ds + ^{1}_{0}n$	1994, GSI,[41]
	$^{208}_{82}Pb + ^{64}_{28}Ni \longrightarrow ^{271}_{110}Ds + ^{1}_{0}n$	
Roentgenium	$^{209}_{83}Bi + ^{64}_{28}Ni \longrightarrow ^{272}_{111}Rg + ^{1}_{0}n$	1994, GSI,[42]
Copernicium	$^{208}_{82}Pb + ^{70}_{30}Zn \longrightarrow ^{277}_{112}Cn + ^{1}_{0}n$	1996, GSI, [43]
Flerovium	$^{244}_{94}Pu + ^{48}_{20}Ca \longrightarrow ^{290}_{114}Fl + 2^{1}_{0}n + e^{-}$	1998, LLNL + JINR, [44]
Moscovium	$^{243}_{95}Am + ^{48}_{20}Ca \longrightarrow ^{288}_{115}Mc + 3^{1}_{0}n$	2003, JINR, [45]
	$^{243}_{95}Am + ^{48}_{20}Ca \longrightarrow ^{287}_{115}Mc + 4^{1}_{0}n$	
Nihonium	$^{209}_{83}Bi + ^{70}_{30}Zn \longrightarrow ^{279}_{113}Nh + ^{1}_{0}n$	2003, RIKEN, [46]
Livermorium	$^{248}_{96}Cm + ^{48}_{20}Ca \longrightarrow ^{296}_{116}Lv + 3^{1}_{0}n$	2000, JINR, [47]
Tennessine	$^{249}_{97}Bk + ^{48}_{20}Ca \longrightarrow ^{294}_{117}Ts + 3^{1}_{0}n$	2010, JINR,[48]
	$^{249}_{97}Bk + ^{48}_{20}Ca \longrightarrow ^{293}_{117}Ts + 4^{1}_{0}n$	
Oganesson	$^{249}_{98}Cf + ^{48}_{20}Ca \longrightarrow ^{294}_{118}Og + 3^{1}_{0}n$	2006, JINR, [49]

Table 1.2: List of origin reactions for SHEs with year (Y) and place (Lab) of its discovery, and references (Ref) to publication considered each element.

Similar like in the case of actinides also for SHEs table with their decay modes and half-lifes was prepared (table A.2) and can be found in appendix A.

1.2 Difficulties with the synthesis of SHEs heavier than $_{118}$Og

It seems that fusion itself as a method of heavier then Z=118 SHE production is no longer effective. In both cases, cold and hot fusion, the probability of creating new element is decreasing with increasing atomic number of the created element (Fig. 1.2). The cross section (σ) for an element with Z>118 could be on a level of 0.1 pb, or lower.

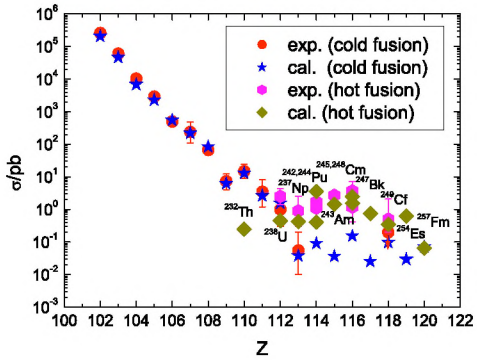

Figure 1.2: Cross section for superheavy elements production in two types of reaction: cold and hot fusion [50].

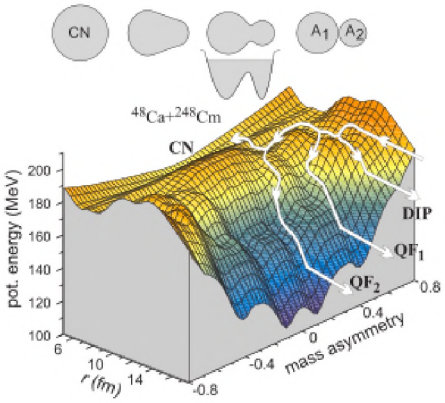

Figure 1.3: Map of adiabatic potential energy for ^{48}Ca on ^{248}Cm collision.White trajectories represents competitive processes preventing compound nucleus formation [51].

It happens not only because of increasing Coulomb repulsion between reaction components but also because of competitive processes occurring during collision of reaction partners. Example of such processes are presented in Figure1.3, where two processes are shown, which prevent compound nucleus creation. The first one is deep inelastic scattering reaction marked as a DIP in a figure, where the large portion of the mass and kinetic energy of reaction partners is exchanged, then re-separation of nuclei occurs. In consequence compound nucleus(CN) can not be created. The other process of the collision is more violent (larger mass and kinetic energy is exchanged) and it is called quasi-fission, marked as QF_1, QF_2 in the figure. In this process reaction partners loose their initial identity but re-separation still occurs and similarly, CN can not be created. Only with very small probability collision dynamics lead to the potential hole - compound nucleus.

However, even if CN is created it does not mean that heavy/superheavy

element will be synthesized. Such CN is an excited object which requires cooling, by light particles evaporation (neutrons, protons or gammas) in order to reach ground state and became SHE (residue evaporation - EvR). The competitive cooling process which destroys CN is splitting on two fragments, known as immediate fission (IF).

The cross section for evaporation residue, is given by formula 1.4, which takes into account consecutive stages of the collision. Here P_{cont} is a probability of a contact configuration (also named capture or Coulomb barrier overcome), P_{CN} is a probability of excited compound nuclei formation, P_{xn} is a probability of x number neutron emission from excited CN, E is collision energy, E^* excitation energy of CN and finally l is angular momentum.

$$\sigma_{EvR}^{xn}(E) = \frac{\pi}{k^2}\sum_{l=0}^{\infty}(2l+1)P_{cont}(E,l)\cdot P_{CN}(E^*,l)\cdot P_{xn}(E^*,l) \tag{1.4}$$

As can be seen from the formula, many factors affect the formation of evaporation residue. This is illustrated in Figure 1.4 on an example of $^{58}Fe +^{208} Pb \longrightarrow^{266}_{108} Hs$ reaction. The upper panel of the figure is well showing competition between main channels like IF, DIP, QF and EvR formation. It is clear that even if capture cross section (marked by black solid line) is quite high the formation of the evaporation residue by emission of only few neutrons (colorful dashed lines) becomes extremely unlikely, even on the level of 0.01 - 10 nb. At the same time bottom panel of the figure shows a competition between neutron evaporation and IF process after compound nucleus formation. For simplicity, it was assumed that $P_{CN} = 1$. More such examples are presented in the paper [52].

However, departing from the physics limitations on the use of a complete fusion method to produce heavier SHEs, one should also mention technical problems that we currently encounter in SHE synthesis. Elements that seem to be within our reach are Z=119, Z=120 and maybe Z=121. Table 1.3 is presenting suggested reactions for their creation [53, 54].

The easiest way for their synthesis seems to be the use of reaction with ^{50}Ti beam. Unfortunately, this type of beam needs development in the direction of higher intensity, because of very small cross sections expected in this case. Besides currently available Cf targets - especially ^{251}Cf, are a mixture of several Cf isotopes. This isotope constitutes 10%-40% of this mixture. Which means, that such compound require special chemical processing and isotopic separation. This is an additional difficulty for targets production.

The probability of the above mentioned SHEs synthesis increases while switching to the ^{254}Es target. Here, however, a technical problem arises with the inability to produce such a heavy target. High Flux Isotope Reactor

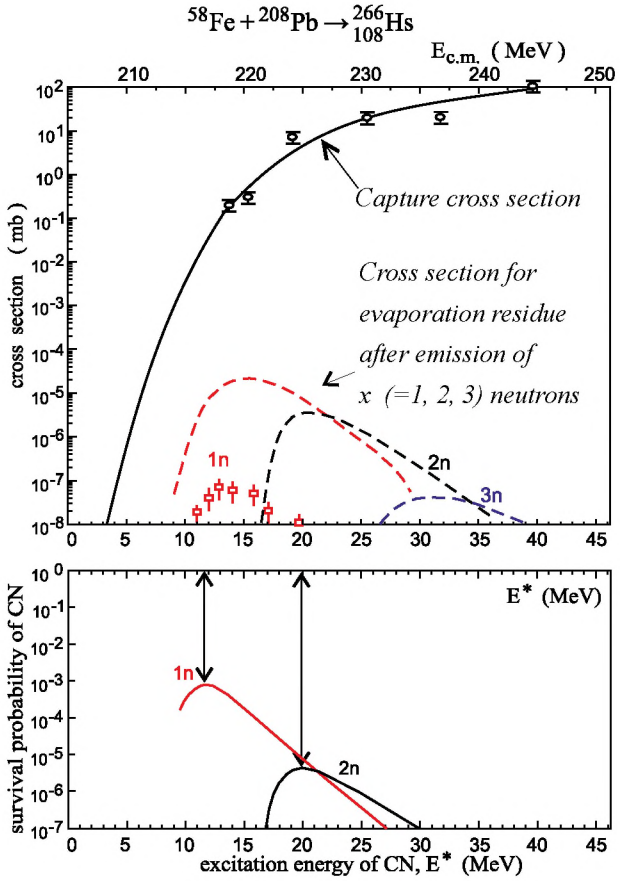

Figure 1.4: Upper panel: cross section for contact configuration (capture) and cross section for EvR as a function of center of mas collision energy. Symbols with error bars represent experimental data. Bottom panel: probability of EvR formation after CN formation as a function of CN excitation energy [52].

Z	Target	Beam
119	^{249}Bk	^{50}**Ti**
	^{254}**Es**	^{48}Ca
120	^{249}Cf	^{50}**Ti**
	^{251}Cf	^{50}**Ti**
121	^{254}**Es**	^{50}**Ti**

Table 1.3: Suggested reaction for obtaining SHE with Z listed in the table - using complete fusion method [54].

(HAFIR) at Oak Ridge National Laboratory (ORNL), a laboratory where all targets for currently conducted SHE experiments are made, can produce only μg quantities of ^{254}Es, while the necessary amount is on the level of mg at least.

Another possibility for synthesis SHEs with a complete fusion method is to use radioactive beams as model calculations shows. However present development of radioactive beams facilities can not deliver appropriate intensity of projectiles ions and it does not seem that in near future large enough intensity can be achieved.

2 Procedures of new element identification

2.1 Identification methods

There are various approaches for identifying elements that depend on the atomic number of the studied element. In this chapter, it will be presented main methods of heavy nuclei identification and as an example the detection setup for the nihonium element will be discussed in more detail.

Over the years, many identification methods have been used, some of them have been modernized, others are used unchanged. For elements with an atomic number less than 104, the radiochemical tests are used, which are checking what type of decay element undergoes. If it was α, β decay or spontaneous fission products emission, then the half life of the studied element is measured. Another possibility in this field of investigation is an observation of the elements decay in the Wilson cloud chamber or (more recently) in the bubble chamber, which are devices used to detect radiation by observing traces of emitted particles. Of course, there exist other then radiochemical methods for elements identification, such as chemical tests or chromatography. Chromatography is very useful especially for identifying components of various mixtures, what is possible by determining the different transport speeds of these components (elements) in the tested medium: gas or liquid. Chemical studies use the comparison of properties between new element and particles already known, like flammability or chemical activity in behavior with other substances. On larger samples of a given element, the state of matter, density, boiling and melting points, solubility in water, thermal and electrical conductivity, color, gloss or toughness may also be tested. All those properties can be helpful for lighter elements identification.

In the case of superheavy elements physics, the most known approaches for SHE identification is the alpha chain method dedicated for SHE decaying via α particles emission, and Viola formula for SHE decaying through spon-

taneous fission (SF). Let us note that the alpha chain method is not only reserved for the identification of superheavy elements, it can be also used for all α-radioactive elements.

2.1.1 Alpha chains method

The alpha chain is a result of the decaying superheavy nucleus. Synthesized SHE in the collision of beam ion and target nucleus is implanted into the detector material (e.g. silicon position detector) where it starts to decay via α/SF particles emission. If SHE (parent nucleus) decays via α particles then the nucleus with Z reduced by two is formed (daughter nucleus). The daughter nucleus can again decay via α/SF particles. Such a decay process can be repeated (daughter, granddaughter, and so on) until the SF terminates decay process or very long lived nucleus is reached. The consecutive α particles emitted during this process are called alpha chain. An example of such chain is presented in Figure 2.1. It is worth mentioning that alpha particles emitted from a particular parent nucleus have strictly defined energies, which is a helpful tool during SHE identification.

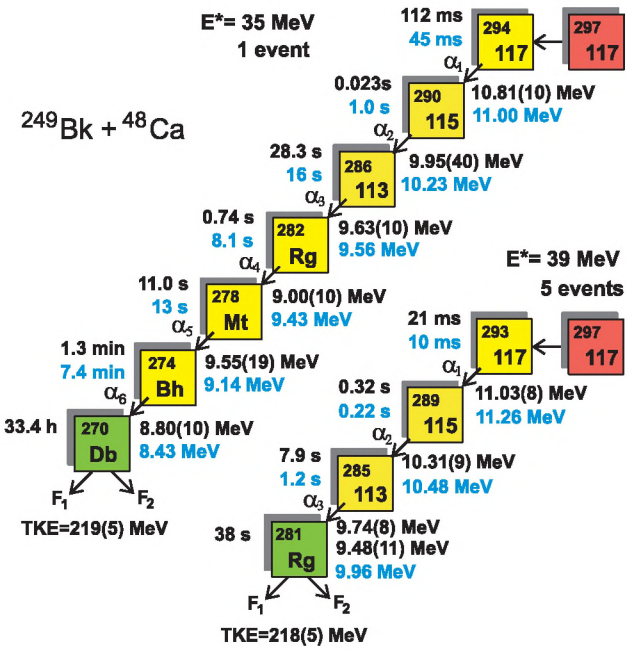

Figure 2.1: Example of two detected alpha chains for element $_{117}$Ts. Measured (blue font) and predicted (black font) half-life times and particle energies are shown on the picture with total kinetic energy (TKE) for spontaneous fission fragments terminating decaying process [48].

The alpha chain has to be properly reconstructed from the measured data. One of the main criteria in such a reconstruction is to check whether the observed signals coming from the superheavy nucleus, from α particles, or from spontaneous fission fragments are registered in the same place of the detector. If this criterion is satisfied, the next step is to get kinetic energy for each emitted α/SF and its emission time which is used to determine the lifetime of the registered isotope. There are several possibilities for alpha chain termination. The first situation is when the chain ends with α which has an energy that corresponds to the α emission energy from the already known isotope then one can trace back along the alpha chain and identify implanted SHE.

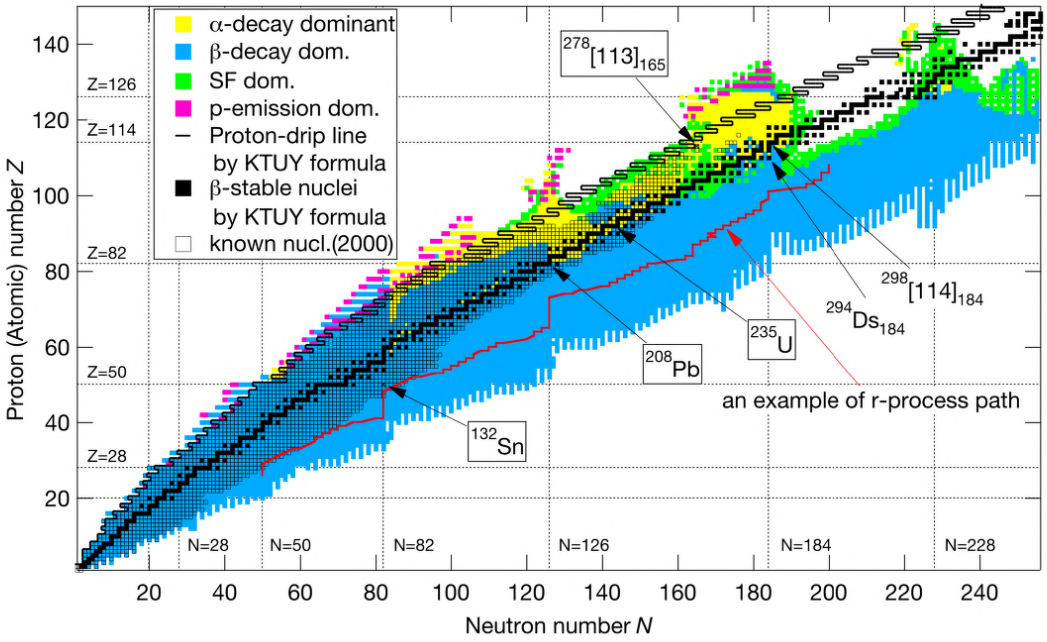

Figure 2.2: Extended nuclide chart according to calculations of Hiroyuki Koura and his group from Japan Atomic Energy Agency and from Advanced Science Research Center [55, 56]. With different colors (described in the picture) the different dominant decays channels were marked. For comparison the already known nucleus were also applied on this chart by empty black squares.

Second situation occurs when the energy of the last α in the chain does not match α energy of any known radioactive isotope. In such case identification is strictly related to information on Z number of target and beam elements and energy of the collision. Assuming complete fusion took place, excitation

energy can be calculated then the number of evaporated neutrons is estimated hence the SHE isotope is predicted. Reconstructed chain is also compared with theoretical calculations of dominant decay channels for new elements. Such a comparison can confirm that the detected element can indeed produce the observed alpha chain. Nuclide chart containing this type of expectation is presented in Figure 2.2.

One should also mention about experimental systematics that facilitate the identification of created SHE. The first one is a correlation between total energy released in the α decay process (Q_α) and the Z and N number of the parent element. Such a correlation may give additional confirmation that α decay chain was properly identified. Namely with increasing of the SHE atomic number Q_α is also increasing as it is presented in Figure 2.3 which shows the dependence of Q_α value on neutron number of parent elements.

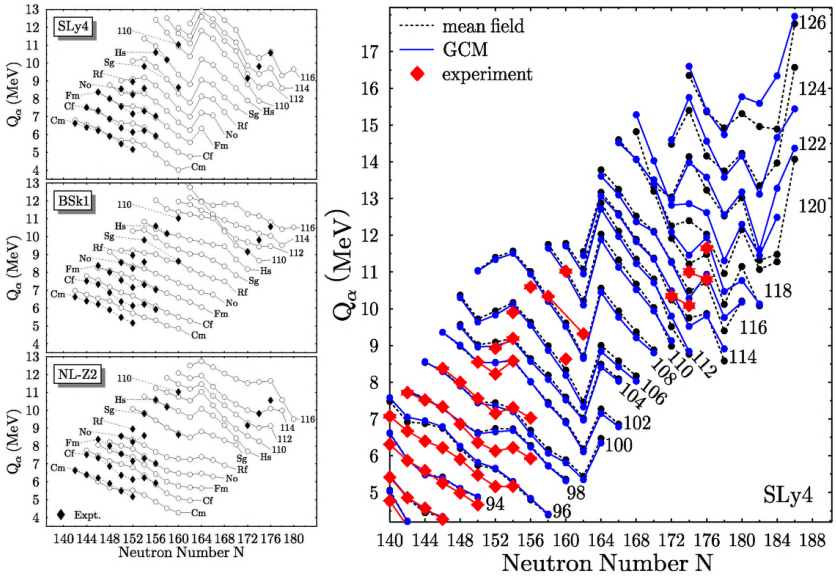

Figure 2.3: Q_α values for α particles emitted from even-even nuclei as a function of neutron number for different Z of heavy and superheavy nuclei. Data and model calculations are presented. Figure on the left panel is taken from [57], while figure on the right is taken from [58].

In the left column for comparison with data (full black diamonds) three model calculations (empty circles) are presented for even-even isotopes of elements from $_{96}$Cm to $_{116}$Lv [57]. The top panel shows results of the Hartree-Fock-Bogoliubov (HFB) method with a Skyrme effective interaction and SLy4 parameter set [59, 60, 61]. The middle panel presents also HFB results with the same interaction, but this time with BSk1 parameter set [62]. Bottom

panel shows the results obtained from predictions of relativistic mean field (RMF) models [63, 64]. The right panel of the figure presents a comparison of self-consistent mean field calculation (black dotted line) with beyond mean field calculation GCM (blue solid line) [58]. Also in this figure by diamonds (red color) are marked experimental data. It is interesting to note that predictions are showing Q_α values for SHEs heavier than 118.

All presented model calculations are reproducing the data quite well and it is difficult to judge which of the models is more realistic. What is more, they should have similar predictive power, so one can expect that for heaviest, undiscovered SHEs, Q_α values can be as high as 17 MeV (results are shown on the right panel).

The second experimental systematics that concerns Q_α values is dependence of $log(T_{1/2})$ on $Q_\alpha^{-1/2}$. Figure 2.4 shows this dependence for several elements from Pt to Og marked by different colors and connected by lines to guide the eye for each element. From the figure it can be seen that isotopes of elements heavier than Pu tend to shorten their half-life with increasing Q_α value. This type of relation is described by the Geiger-Nuttall law given by formula 2.1.

$$logT_{1/2} = aQ_\alpha^{-1/2} + b \tag{2.1}$$

where coefficients a and b are determined by fitting experimental data to each isotopes series (all isotopes of a given element).

This relationship can also significantly facilitate the analysis of data for the identification of superheavy elements especially when the registered alpha chain ends with an unknown element, or only a fragment of the alpha chain has been recorded.

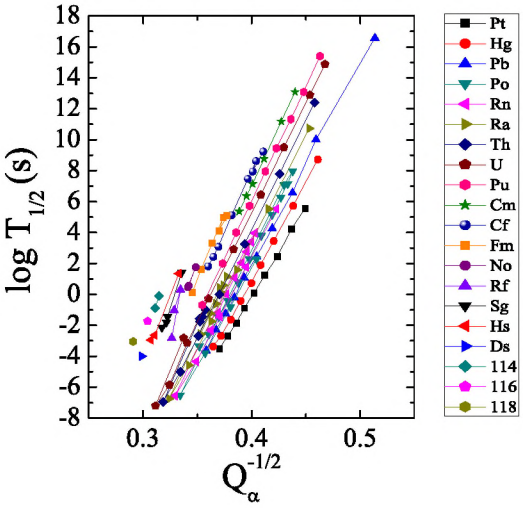

Figure 2.4: Geiger Nuttall relation for nuclei with atomic number from 78 to 118 (and their isotopes). Q_α is presented in MeV [65].

It should be noted that the spontaneous fission process strongly competes with an α decay channel of synthesized SHE. This is why some of SHEs produce α decay chain that terminates with the SF process or even decays directly via SF process with no α emission. In such a case kinetic energy of both fission fragments can be compared with so called Viola systematic to assign Z number of registered SHE and this will be discussed

in the next section.

2.1.2 Viola systematics

There is also a possibility that synthesized SHE undergoes spontaneous fission (SF) which actually strongly competes with the emission of α particles. In such cases Viola systematic becomes the main method of the parent nucleus identification.

Viola systematic is showing the dependence of the total kinetic energy (TKE) released in a fission process on atomic number and element mass. It appears that TKE depends linearly on $Z^2/A^{1/3}$. Presently two version of this linear dependence are used (2.2) and (2.3). The first one was fitted to data obtained until 1966 while the second one is improved version in the year 1984 because new data appeared [66].

$$TKE = 0.1071\frac{Z^2}{A^{1/3}} + 22.2MeV \quad \text{(from 1966)} \tag{2.2}$$

$$TKE = 0.1189\frac{Z^2}{A^{1/3}} + 7.3MeV \quad \text{(from 1984)} \tag{2.3}$$

This systematics is shown in Figure 2.5. The left panel is showing all the data (symbols in the figure) which were used to obtained equations (2.2) and (2.3). In case of equation (2.3) fission of element $^{52}_{26}$Fe was taken into account. The right panel is showing the upper part of Viola systematic which presents the region of heavy and superheavy nuclei with data collected after 1984. Open squares represent mainly heavy nuclei starting from Z = 96 while black symbols are for spontaneous fission isotopes with Z $\geq$ 104. As one can see a large part of the data is reproduced by the Viola systematics (two dashed lines in the figure) while the data in the dashed rectangular which are outside the systematics can be explained according to the model [67, 68] as symmetric spontaneous fission.

From both panels of Figure 2.5 it is well seen that TKE is increasing with increasing atomic number. This observation can be used to estimate Z of a superheavy element which decays by SF process.

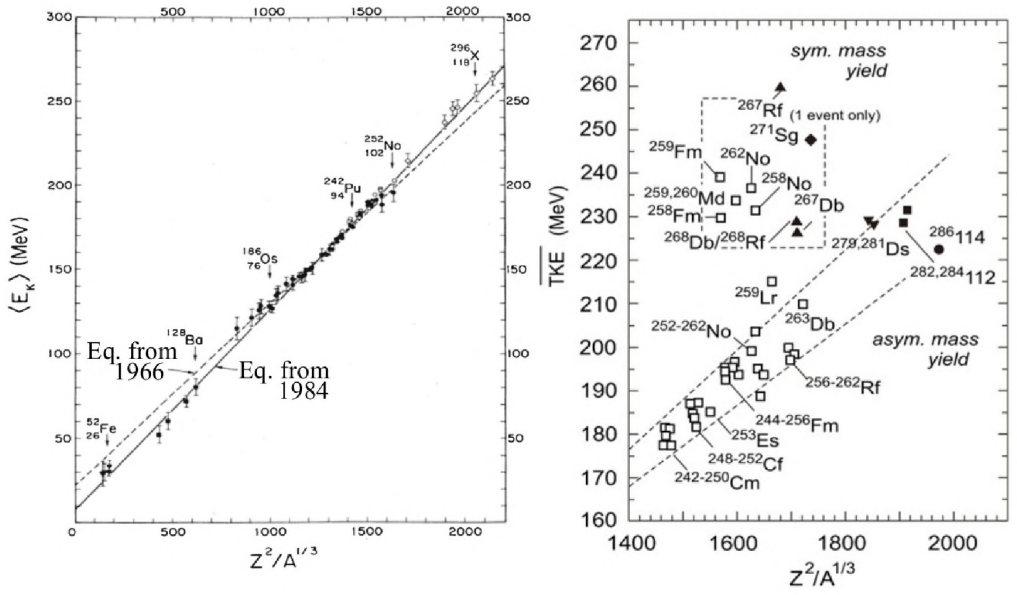

Figure 2.5: TKE dependence on parameter $Z^2/A^{1/3}$ of fissioning nucleus. Left panel is taken from [69] while right one is from [70].

2.2 RIKEN - $_{113}$Nh synthesis

The full process of superheavy element synthesis is shortly presented on the example of $_{113}$Nh. As was mentioned in chapter 1.1.2 nihonium was synthesized in 2003 by the Morita group at RIKEN laboratory, and it is the heaviest element produced by the method known as cold fusion [46]. The studied reaction is presented below.

$$^{209}_{83}Bi + ^{70}_{30}Zn \longrightarrow ^{279}_{113}Nh + ^{1}_{0}n \tag{2.4}$$

As a beam $^{70}_{30}$Zn was used which was provided by RIKEN Linear Accelerator Facility (RILAC). The energy of extracted beam was 352.6 MeV with accuracy ± 0.6 MeV, and with intensity 2.4×10^{12} particles/s^{-1}.

Bismuth target was prepared by vacuum evaporation of metallic $^{209}_{83}$Bi onto carbon foil with 30 μg/cm^2 thickness. A layer of bismuth was much thicker, 450 μg/cm^2, and also coated with another carbon layer, this time with thickness about 10 μg/cm^2. Because of the energy loss process of the beam in the target (about 5.4 MeV) the final energy at the half-depth of the target reached 349.0 MeV. Several small targets were placed on the rotating disk with 2000 rpm, right in front of the GARIS detectors setup - Figure 2.6.

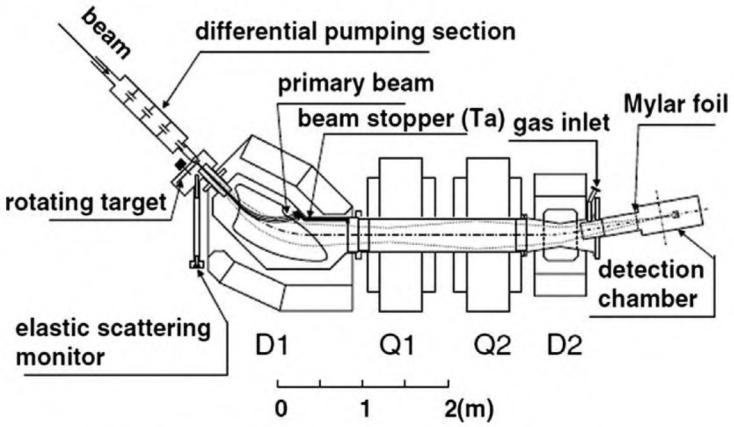

Figure 2.6: GARIS scheme [71]. Gas-filled recoil ion separator contains two dipole magnets (D1, D2) and two quadrupole magnets (Q1, Q2). All of them were mounted there to reduce events from the background and to increase resolving power at the focal plane. The primary beam is stopped in a tantalum plate mounted in D1 section, while section D2 is reducing background from lighter elements. Pressure of a helium inside GARIS during that experiment reached 86 Pa.

Gas-filled recoil ion separator, called GARIS, is a set of dipoles and quadrupoles where the reaction products are separated from the projectile like elements. It allows isolate the evaporation residue (SHE) from non-superheavy elements. After separation, the reaction products are directed to the detector in the focal plane of a GARIS separator. Figure 2.7 is presenting plane view of that detection setup. Then evaporation residues are overcoming two timing detectors (MCP) to finally reach the position sensitive silicon detector (PSD) detector where are implanted. MCP detectors are returning information about time of flight, and together with energy measured in the PSD detector enables to calculate mass number of ER. During the experiment one event was observed with four correlated to ER α particles. The alpha chain was terminated by registered SF. That element was identified as an evaporation residue of the nihonium implanted in the PSD detector and ended by the spontaneous fission reaction. First and last α were found only in PSD detector, while second and third α were detected in both, SSD and PSD detectors. Energies of these particles and time difference between registration of successive αs are presented in Figure 2.8.

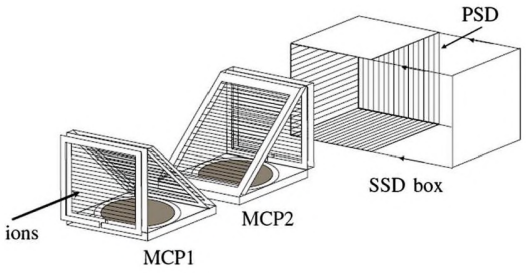

Figure 2.7: Scheme of the detection setup at the focal plane of GARIS [72]. It contains SSD box which is a set of silicon semiconductors, and two timing detectors built with micro-channel plates (MCP). MCP is used for electron detection emitted from mylar foil (see Figure 2.6) as a result of ions passing through that foil. SSD box contains two types of silicon detectors: PSD (strips detector) which is returning information about α and ER position, and the detector which purpose is to detect α/SF particles from decaying evaporation residues implanted in PSD [46].

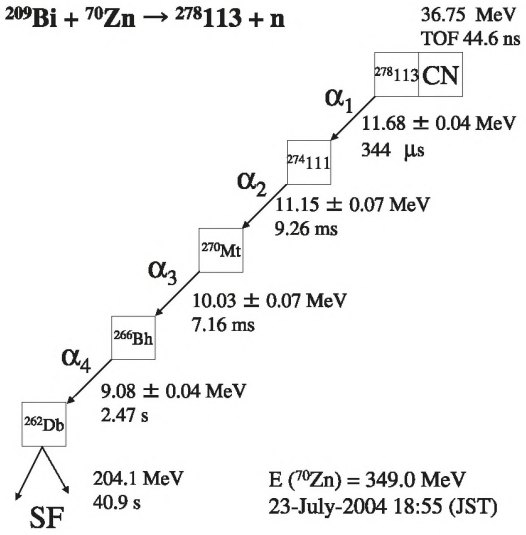

Figure 2.8: Alpha chain for $_{113}$Nh created with cold fusion method [46].

3 Searching for short-lived SHEs with use of multinucleon transfer method

For a few decades physics had tried to reach the island of stability for superheavy elements. Both predicted stability islands are presented in Figure 3.1 which shows the nuclide chart for all nowadays known elements. Currently, scientists are focusing on one of the suggested islands, namely the one with the number N = 184 or N = 196 and Z = 114.

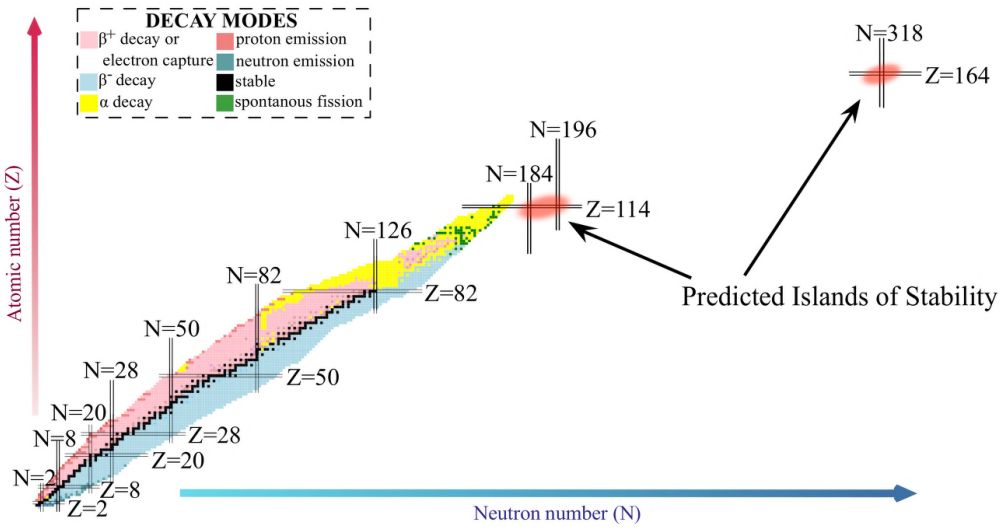

Figure 3.1: Nuclide chart for all already known elements [73].

Department of Hot Matter Physics of Jagiellonian University (UJ) with Cyclotron Institute, Texas A&M University (TAMU) in the United States instead of testing classic method (complete fusion) for SHEs production decided to study multinucleon transfer. This chapter will explain this alternative method and will present conducted experiments which caused further

development of the tested idea.

3.1 Multinucleon Transfer

Currently, scientists are struggling with many difficulties trying to obtain new SHE using traditional methods. This obstacles were described in earlier chapter (Chapter 1.2). To increase the chance of new SHEs discoveries, scientists are looking for an optional method that could be used for their production. This section will present a possible method that may open the door for further experiments.

As such alternative way of new SHEs creation can be considered a reaction using non-central collisions and both nuclear fission and the fusion itself, which at the same time is not a complete fusion anymore. This method was studied many years ago (directly and indirectly [74],[75]), but hardware limitation and electronic development significantly inhibited further research. Only about twenty years ago it gained a second life. In 2002, a group of scientists from Jagiellonian University and Texas A&M University proposed a new approach to apply this method [76]. They suggested that multinucleon transfer (MNT) can be used as a way of new heavy and superheavy element production. Three years later, in 2005, appeared new model calculations [77][78] thanks to which many more laboratories found the interest in studies of MNT as a method of SHE production.

Transfer reactions have always played an important role in nuclear physics. These allowed, for example, to study nuclear structures by providing relevant information for the shell model construction, or allowed defining reactions mechanisms from simple quasi-elastic to more sophisticated ones, like deep-inelastic or fusion [79].

Nowadays MNT is also studied as a way of searching neutron-rich heavy (and superheavy) elements. Presently all discovered superheavy nuclei are from the region of neutron-poor elements which results in their short life times and α/SF radioactivity. It is considered that the right path to reach island of stability might be creation of a neutron-rich superheavy element, and MNT method seems to be adequate for achieving that goal. For example, an experiment conducted by Sophie Heinz, substantially as she claims [80], gives a possibility for reaching elements with an atomic number higher than 100 in a reaction ^{48}Ca + ^{248}Cm. The cross section for producing neutron-rich elements around Z=102 is reaching the scope of several nanobarns. Actually, the main problem with observation MNT neutron-rich products is the lack of identification methods for this kind of elements. Normally used alpha chain method for SHE identification can not be used in case of decaying via

spontaneous fission, which is the main channel [80] of neutron-rich elements decaying. In such case Viola systematic can be helpful.

Figure 3.2 presents the visualization of MNT idea on the example of the collision Au beam on a Th target. This reaction was used during several measurements carried by UJ and TAMU collaboration during studied the MNT for SHE production. According to the reaction idea from Figure 3.2, a target containing possibly heavy nuclei, for example thorium, is bombarded with a beam ions (e.g. gold). During the reaction there is a nucleon transfer between both partners of the reaction. Nucleon transfer should be more likely for the nuclei of the target, which are easily fissile. This process may consequently lead to the formation of a superheavy nucleus accompanied by remains of the target nucleus (TLF) and several evaporated neutrons.

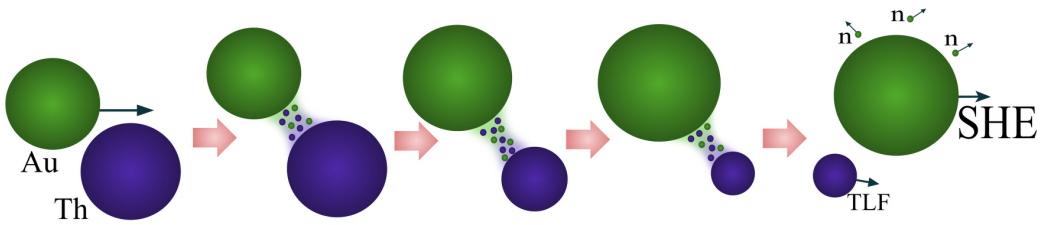

Figure 3.2: Multinucleon transfer scheme [81].

In the case of an experiment conducted in TAMU, the first step was to search superheavy elements with short life times, about few nanoseconds, decaying via α particles.

One of the important features of measurements carried at TAMU was to choose optimal energy for the collision of both reaction partners. Because of this the targets used during that experiments were relatively thick, of the order of mg/cm^2. The initial energy of the beam was set to be 7.5 AMeV, due to energy loss of ion beams in the target, beam energy is blurred. As a result wide spectrum of collision energy was obtained, down to 6 A.MeV.

The cross section for heavy elements and SHE production by MNT method is presented in Figure 3.3. Experimental data (dotted symbols) from collisions of ^{238}U beam with ^{248}Cm target confirm that neutron-rich superheavy isotopes can be produced in multinucleon transfer processes, although production cross section is low. Model calculations (solid lines) also confirm the tendency observed from the experiment. Many factors have an impact on that cross section, such as shell effects, elements used in the reaction, collision energy or excitation energy of primary fragments. It is worth remembering

that the excitation energy of the fragments has crucial importance, what can be seen also from Figure, as the orders of magnitude cross section is dropping for the residue of evaporation (SHE) [51].

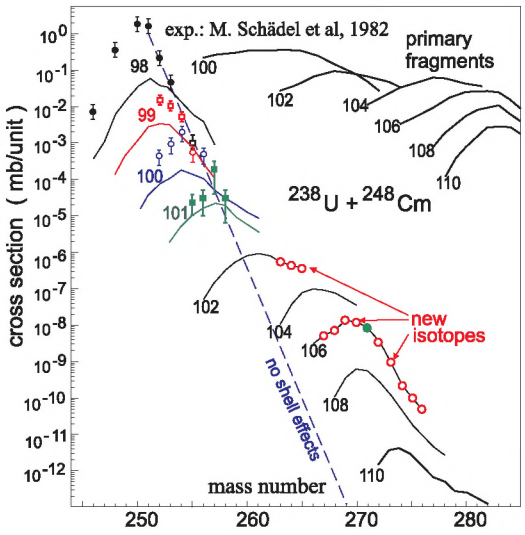

Figure 3.3: Cross section for SHE creation by MNT method. Studied reaction was ^{238}U on ^{248}Cm with a center of mass energy 750 MeV. Experimental data (dotted elements) and theoretical predictions (solid line).) [51].

3.2 Investigating of MNT method validity

3.2.1 Selection of input reaction

Collaboration with TAMU enabled access to the experimental devices adequate for conducting experiments on multinucleon transfer. The K500 cyclotron located there delivers beams of heavy ions up to the uranium, with a wide energy range. Several possible variants were tested to select the best reaction for our purpose, all of them are presented in the table 3.1. Investigated nuclear reactions of heavy projectiles on a fissile target had collision energies, near and above the Coulomb barrier. If superheavy nuclei are created during multinucleon transfer their excitation energy and angular momentum will decide on the chance of survival as SHEs. Higher chances appear when the excitation energy and angular momentum of created superheavy nuclei will be low enough. In such a case the nuclei after emission of few neutrons can become a new element(s).

Beam Ions	**Beam Energy [AMeV]**	**Target Isotope**
^{136}Xe ^{172}Yb ^{198}Pt	15	^{238}U
^{84}Kr ^{172}Yb	15	^{232}Th
^{238}U	12	^{198}Pt ^{238}U ^{232}Th
^{84}Kr	24.8	^{232}Th
^{84}Kr ^{129}Xe ^{197}Au	7.5	^{232}Th

Table 3.1: Reactions tested in the preparatory phase of the SHE program at Texas A&M University [82].

From all tested reactions the ^{197}Au (7.5 AMeV) + ^{232}Th has been chosen for further studies as the most promising one [82]. Properties of the thorium target determine three possible regions for new heavy elements creation, such as Z $\approx$ 112, Z $\approx$ 136 (for low excitation energy of Th nuclei) and Z $\approx$ 124 (for their high excitation energy). Those regions are related with two potential

ways of thorium fission process: asymmetric when it splits into two parts with Z $\approx$ 33 and Z $\approx$ 57 and symmetric one when both fission fragments have Z $\approx$ 45. Depending on which of the fragments is transferred to Au nucleus one of the mentioned SHE regions can be reached [82].

3.2.2 Beginnings of searching short-lived SHEs

Research at TAMU began around 2002 [76, 81]. From this time detection system prepared for superheavy elements production has evolved several times. At the moment we can talk about two main generations of conducted experiments that will be presented in the next sections. I joined the UJ group in 2014 which allowed me participation in the last two experiments from II generation conducted in 2015 and 2016, concept of both of them will be described below. It is important to note that results obtained from them contributed to the decision of preparation a new detection system for long-lived SHEs.

First generation of SHE detector prepared by UJ and TAMU group was focused on delivering information about time of flight (ToF) and energy losses (ΔE) of heavy reaction products to isolate produced SHEs from background events. In a classic (complete fusion) method velocities of created elements are well known, so for example Wien velocity filter, like in GSI, can be used to isolate created SHEs from other reaction products. In the case of peripheral collisions SHEs velocity spectrum can be wide and not well defined. Because of these filters with a large scope of heavy ion velocities and broad angular acceptance were required. 7 Tesla superconducting solenoid (BigSol) constructed at the Michigan State University and mounted at TAMU, was able to provide the above mentioned conditions.

Achieved by BigSol angular acceptance for reaction products was very large, the largest among devices of a similar type available in scientific centers those days, 6-14 degrees. Solenoid was producing a very large magnetic field that was parallel to the beam, so it could serve for particles separation. BigSol was a main part of the experimental setup, scheme of the whole detector is presented in Figure 3.4.

All detectors were aligned along the beam direction. To suppress ions beam and forward emitted projectile- and target-like fragments so called "Blocker" was used i.e. a metal disc placed right after the target. Size of the disc covered angular range from 0 to 6 degrees. Reaction products emitted at larger angles were reaching BigSol. Dashed lines on the scheme indicate how the solenoid curved trajectories of their flight paths and separated them spatially.

The next part in the detection setup were three parallel plate avalanche counters (PPAC, IPPAC - built in Italy, PPPAC - built in Poland, GPPAC -

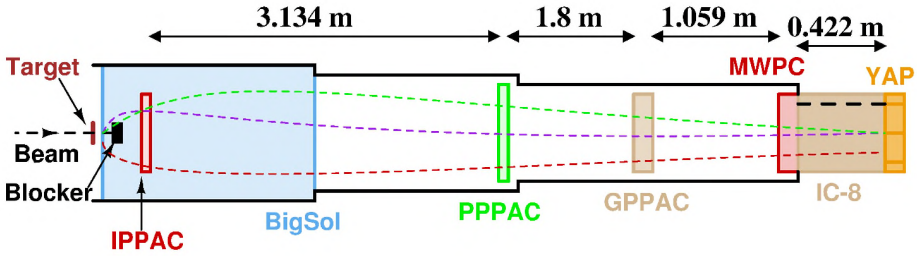

Figure 3.4: The BigSol detection system for searching superheavy elements at TAMU [81]. More detailed description is in the text.

built in Texas) which provided information about ToF and position (X,Y) on the plane perpendicular to the beam direction of passing through heavy ions. The last part of the detectors system was composed of a multiwire proportional counter (MWPC), ionization chamber (IC-8) and yttrium aluminum pervoskite (YAP) scintillator. MWPC was a subsequent detector that delivered information about ToF, position X,Y and also about energy loss ΔE_M of passing ion. This detector was also a trigger for acquisition.

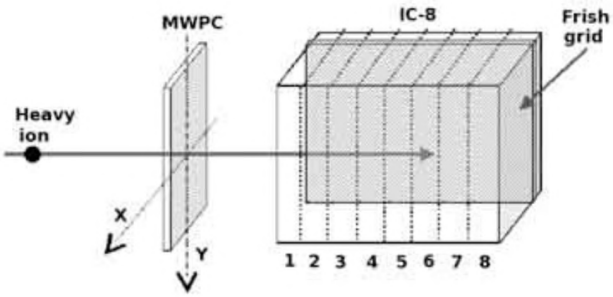

Figure 3.5: Schematics of ionization chamber IC-8, built of eight segments. All segments were closed in aluminium tube and filled with isobutane (30 mbar) [82].

The penultimate detector in this system, the IC-8, is a second detector which returns information about heavy ion energy loss ΔE_{ICi} in consecutive segments (i=1...8) of the chamber, Figure 3.5. Each segment has 4.65 cm length and it has anode mounted at the left side wall to generate an electric field perpendicular to heavy ion direction. Collected by anodes charges correspond to heavy ion energy losses in each segment. Frish grid placed next to the anodes provides independence of pulse heights, produced by anodes, on ions position in the chamber. Energy loss pulses from each segment were recorded as waveforms with help of flash ADC. YAP detectors as the last ones were placed just behind the IC-8 for the measurement of ions residual energy. YAPs are inorganic scintillators which were used also in more re-

cent experiments. This material will be described in more detail in the next sections of my dissertation. All detectors were filled with isobutane gas.

Such a detector construction with large velocity and angle acceptance enabled a high counting rate, about 200 counts per second, which led to big statistic accumulation. From over 4 million recorded events three events were classified as interesting - very heavy ions. These results are presented in Figure 3.6.

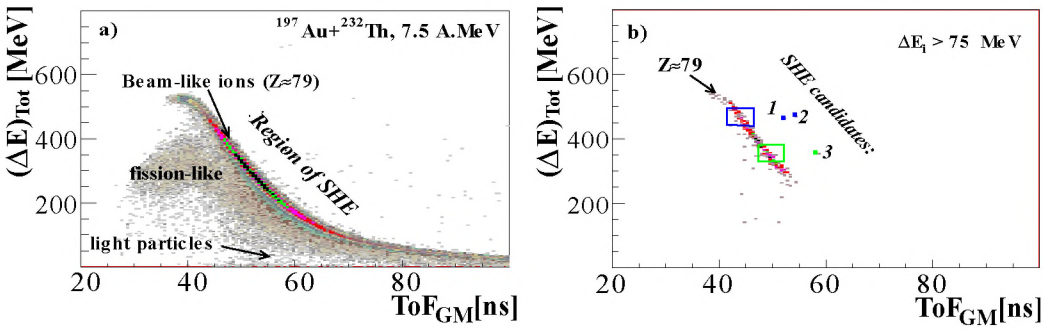

Figure 3.6: Relationship between total energy loss (sum over all ΔE_{ICi}) and registered time of flight between GPPAC and MWPC. Panel a) represents spectrum for all events collected in GPPAC-MWPC and IC-8 detectors after pileups elimination (generated because of high counting rate). Panel b) shows how additional condition on ΔE values for one of IC-8 segments can reduce number of background events. Threshold for those ΔE values to receive only interesting events was established on as greater then 75 MeV. In the region of expected SHEs remains three interesting events [81].

Preliminary analysis has shown that pulse shapes distribution for heavy ions recorded in consecutive segments of the ionization chamber was noticeable different than in case of pulses recognized as background events e.g. beam-like ions. Especially amplitude of pulses from the heavy ions was higher in the first segment of the IC-8 and then it was falling much faster in consecutive segments comparing to the pulses amplitude of beam-like ions. The same behavior of pulses amplitude was observed for the isolated SHE candidates marked on the picture 3.6b). The cross section for their production was estimated as 50 nb. The Z resolution of the IC-8 detector was rather low (on a level of 10%). Obtained results together with those published in [82] guaranteed further studies. Unfortunately, leak of He gas in the BigSol, which occurred during the experiment caused necessity for a new detector construction.

The second generation of experiments has begun a whole new chapter of searching SHEs by UJ and TAMU groups and it has several editions with a constant idea. The new detection system consisted of two walls of detectors: a backward wall of IC-Si modules and a forward wall of active catcher (AC)

modules. This system was focusing on the implantation of heavy reaction products in the AC modules and collection information about α particles or fission fragments emitted from an implanted SHE. The example arrangement of this setup is presented in Figure 3.7.

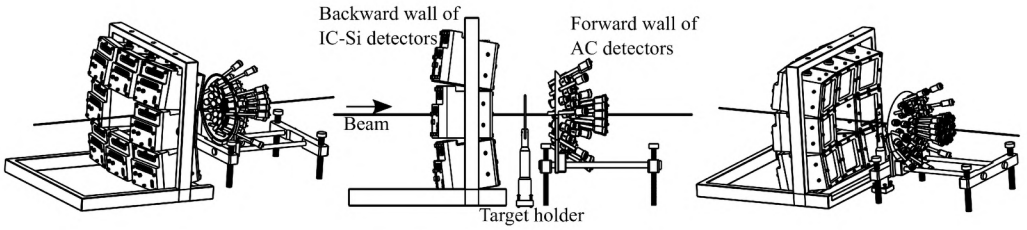

Figure 3.7: View of II generation BC-418 detector system from experiments conducted in 2015 seen from various angles.

Active catcher itself evolved during the years of experiments and finally had two forms. The first form consisted of 63 modules with Polyvinyltoluene BC-418 Saint-Gobain Crystals scintillators while the second one was based on 40 modules with Yttrium Aluminium Perovskite (YAP) scintillators. First AC type with BC-418 fast scintillator together with dedicated triggering logic was constructed by Jagiellonian University group and was used in several experiments until year 2016. By using fast scintillators we were able to search for very short lived elements - in ns range of lifetime. Second form of AC was prepared for improving the energy resolution of the detector and ensuring access to the rough particle identification by pulse shape analysis. For this purpose, the modules of AC have been changed to YAPs.

In sections 3.2.3 and 3.2.4 both AC will be presented together with results from last conducted experiment (2016).

3.2.3 Construction of AC based on BC-418 modules

First active catcher (last time used in 2015) was located 10 cm behind the target and its hemisphere was covering the range of angles from 3° to 60° with respect to the beam axis, it was built of 63 modules (see Figure 3.7 and 3.8).

Beam provided by the cyclotron was operated in two modes: beam switched on/beam switched off - with two on/off time settings: 30/20 ms and 300/200 ms for respective modes. During beam on mode the beam bursts of the order of ns were applied.

Each of 63 detection modules consisted of a 0.8 mm thick plastic BC-418 scintillator, LUCITE light guide and a photomultiplier from which information goes to the electronics triggering the acquisition, and finally to the

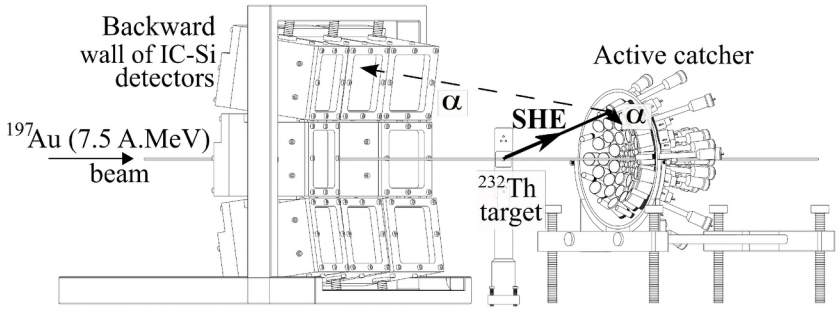

Figure 3.8: Detailed scheme of the II generation SHE nuclei detection system. The backward wall of IC-Si detectors contains gas-silicon modules while forward wall is an active catcher which is built from modules based on BC-418 scintillators. Both walls were placed 10 cm from the target. The tested reaction was ^{197}Au beam at energy 7.5 AMeV and intensity 15-50 nA on ^{232}Th target with 12 mg/cm^2 thickness.

acquisition itself. For better light collection scintillator, light guide and PMT window were connected together by optical grease, and in addition the side surface of the light guide and the front of the scintillator were covered with a thin aluminum foil. All those parts were placed in an aluminum cylindrical tube (see central part of Figure 3.9).

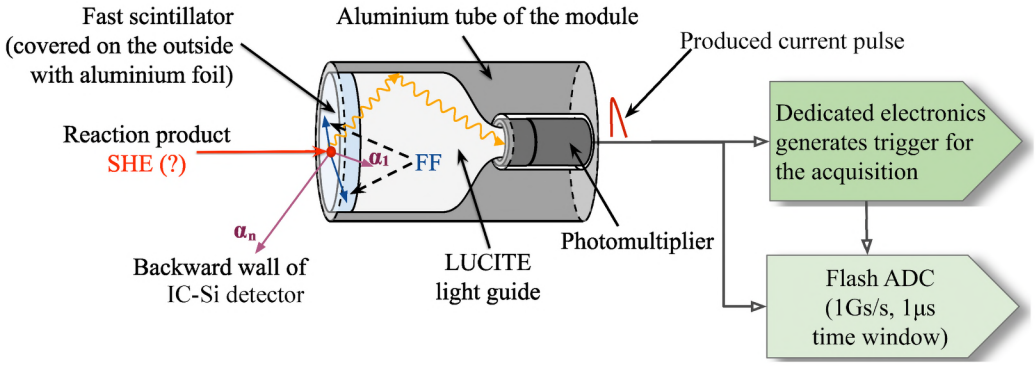

Figure 3.9: Scheme of the AC single module based on BC-418 scintillators with presentation of superheavy element decaying process.

The principle of operation of such a module is as follows: in the first step reaction product is implanted inside the scintillator. If the implanted product was superheavy element then it could decay, after some time, via two channels: by α particle or fission fragments emission. Scintillator thanks to absorbing the energy from ionizing radiation (this could be SHE, α or FF) reveals its luminescence properties by light emission. This light in the second step is carried by a light guide to the photomultiplier tube (PMT). Next, PMT as a type of electron vacuum tube, which contains both a photocathode, anode and electron multiplier with at least one amplification stage

transforms the light into electric current using an external photoelectric effect and the phenomenon of secondary electron emission. So created current pulse finally leaves the detector and goes to the electronic responsible for an acquisition system. Described process is schematically presented in Figure 3.9. In Figure dark blue arrows represent potential fission fragments emitted from the decaying SHE (red dot). Purple arrows represent α particle emission. Some of the emitted particles, like α_n marked in Figure, can escape in direction of the backward wall of the IC-SI detector. Orange wavy arrows represent behaving of the light emitted by scintillator after SHE implantation. Current pulses produced by implanted SHE and products of its decay (α/FF) are directed to the triggering and recording electronics.

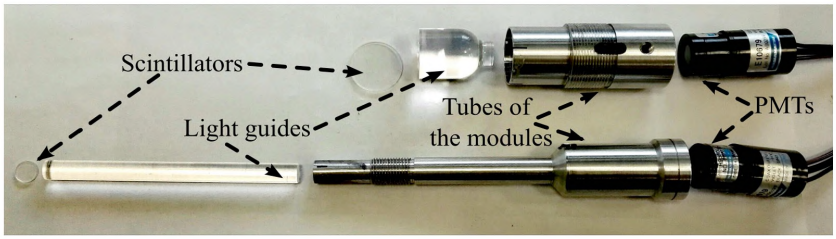

Figure 3.10: Photo of elements forming both sizes of AC modules. Modules were disassembled to show all of the components. See text for details.

During those experiments two sizes of scintillators were used, larger and smaller ones. They are presented in Figure 3.10. Upper part of Figure presents module with a larger scintillator which has a diameter of 2 cm and a light guide 2,7 cm long, while the bottom part is showing module with a smaller scintillator of 0,8 cm diameter and light guide 8,8 cm long. Such scintillator sizes were chosen for two reasons: first, to obtain maximum compactness of the AC detector and second, to ensure good granulation of modules at small angles with respect to the beam axis, where is a very large cross-section for elastic scattering.

Modules prepared in such a way required dedicated triggering logic which will allow to improve chances of MNT products selection. Such logic was prepared by scientists from Jagiellonian University [83] and its detailed description once can be found below.

Pulse outgoing from PMT was split into two signals. One of them was guided straight to the flash ADC acquisition system (ACQ), where was waiting for acquiescence from triggering logic. The second pulse was directed to electronic logic responsible for producing a trigger to record awaiting in ACQ signal. First stage of trigger production was converting analog PMT pulse into the fast (2 ns long) logical signal. The procedure begins on a comparator, where it is checked whether the PMT signal has exceeded the

established voltage threshold. If this condition was fulfilled, then the signal was sent to the splitter which produced two logical pulses on the exit. Both pulses were guided to the D type flip-flop, one on the clock (CLK) entry, and second via delay line (DL) to the reset (R) entry. Thanks to the delay line on the exit from flip-flop fast logical signal was created. That logic operation was repeated for all 63 AC modules. Scheme of this process is presented in Figure 3.11.

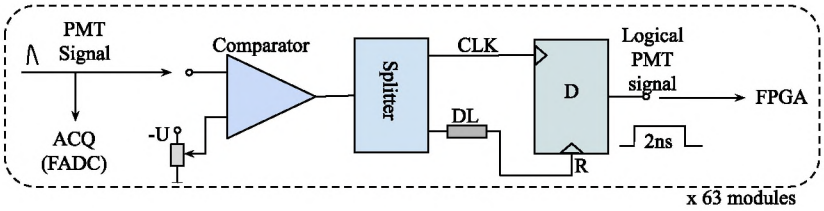

Figure 3.11: Scheme of electronics used for conversion of PMT signals to fast logical signals.

So created logical signals were sent to one of two FPGAs (on each FPGA can be plugged in only 32 channels). If the information about registered pulse appeared in any channel on the FPGAs then in the next step triggering logic was starting to use also cyclotron logical radio frequency (RF) signal in final trigger construction. Scheme of the beam structure and corresponding logical RF is shown in Figure 3.12. To improve chances of recording only MNT products acquisition was running only between beam bursts for 50 ns while every 5 ns of the beam duration was blocked. In 50 ns interval logical RF signal adopted logical "1", while for 5 ns it was "0".

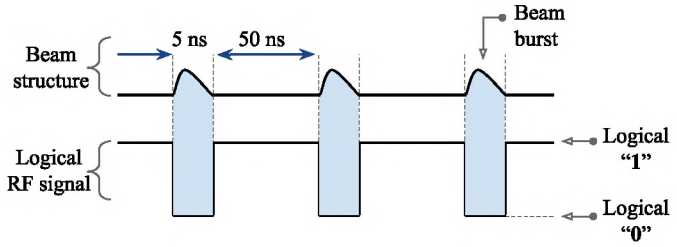

Figure 3.12: Logical RF signal is converted from the original RF signal in sinus form. During beam bursts (for 5 ns) it assumes "0" value, while between beam bursts (for 50 ns) it is "1".

When pulse was detected and the logical RF returned "1", last step of trigger creation was to check if IC-Si detector registered anything. Thanks to OR gate it was possible to produce ACQ trigger alike for pulse detected in AC modules and in IC-Si detector. Trigger described above started an

acquisition process, information from all modules was read out and written on HDD drive.

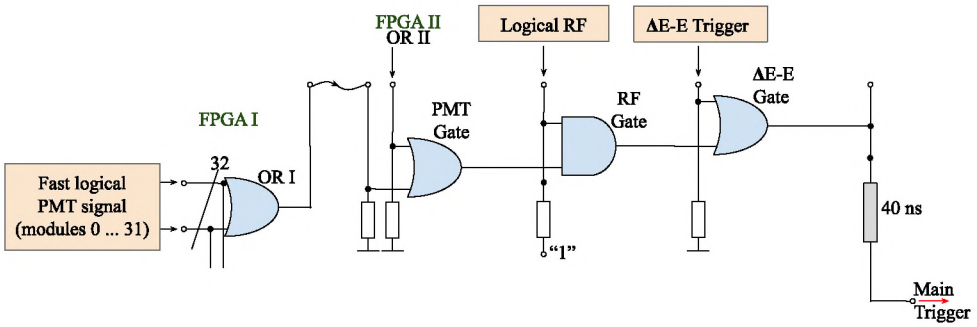

Figure 3.13: Scheme of next step of trigger logic production.

Last experiment in the setup described above took place in 2015. The data collected at that time were analyzed for a long time and focused mainly on the search for events that may have been considered as the beginning of a SHE decay chain. It was based on searching events where at least two pulses were recorded in 1 μs time window of a single module. Data analysis was concentrated on the time correlation between recorded pulses. Unfortunately, any analysis based only on the amplitude of the recorded pulses was not sufficiently reliable because of BC-418 scintillators poor energy resolution.

Obtained results were promising, these have shown that with MNT method it is possible to produce heavy (or superheavy) element with short lifetime on the level of 1 μs (details of the conducted analysis can be found in publication [84]). This apparatus also proved that it is able to observe decay reactions by α particle emission. However, due to weak energy resolution of the used scintillators material further work with active catcher required its improvement. For the next experiment, a modified AC version was used, where for newly constructed AC modules different type of scintillators were mounted. This experiment is described in the next section.

3.2.4 Experimental results

In July 2016 new experiment at TAMU was conducted. Examined reaction was testing two beams, ^{197}Au or ^{238}U AMeV, on 11mg/cm^2 ^{232}Th target The main idea of tests remained the same, only the AC system modules were changed. Texas group built an AC detector based on yttrium aluminum perovskite (YAP) scintillators. This kind of scintillation material was chosen because of its energy resolution and time properties. Figure 3.14 shows a

comparison of amplitude spectra for both types of detectors, based on BC-418 and YAP scintillators. Measurements were made with a ^{252}Cf source, and it is easy to notice that the amplitude spectrum from the YAP detector gives slightly better particle separation i.e. α particles from FF. Second mentioned

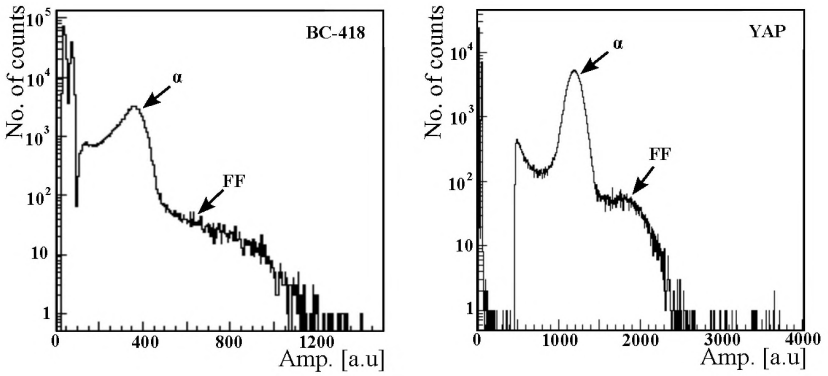

Figure 3.14: Comparison of amplitude spectra for BC-418 based detector (left panel) with YAP based detector (right panel) prepared with use of a ^{252}Cf source [85].

reason to choose YAPs scintillators was their time properties, extended decay time (~140 ns) and extended rise time (~14 ns) comparing to BC-418 scintillators. This feature together with better energy resolution facilitates the identification of a particle by analyzing the pulse shape. However, it is worth note that 14 ns is still a fast rise time, which means that the possibility to search for very short lived elements has not been completely lost.

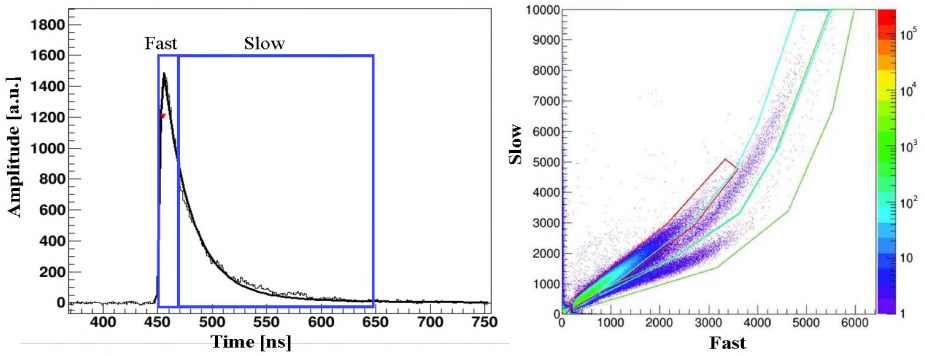

Figure 3.15: Left panel: Example of the pulse registered by the YAP detector with marked region of fast and slow component used during pulse shape analysis (PSA). Right panel: Separation of the particles based on PSA method. From left to right are located α particles, FF, beam and heavy recoils [85, 86].

An example of such pulse discrimination is presented in Figure 3.15. In the right panel of the figure it is shown integral of the Slow versus Fast

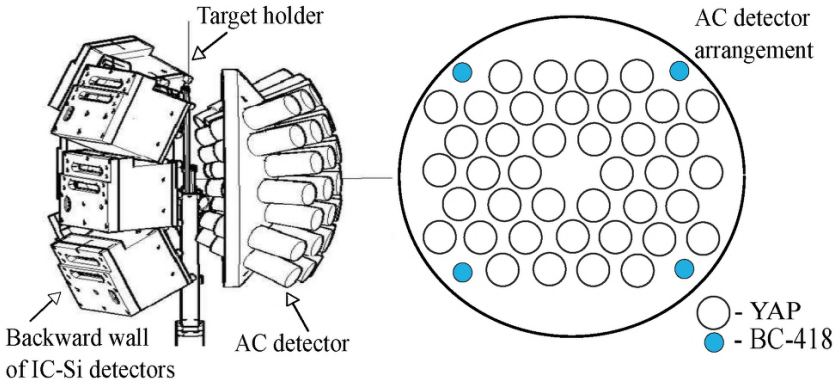

Figure 3.16: Scheme of detection setup used during experiment in 2016 year. Left panel presents realistic view of backward wall of IC-Si detectors, AC detector and target holder (similar to the one from 2015 - Fig. 3.8)[86]. Right panel shows arrangement of 40 YAP based modules and 4 additional BC-418 modules of the active catcher.

component, which are defined in the left panel, of the pulses recorded by flash ADCs. It is clear that α particles are separated from fission fragments. YAP based modules were placed on the array in a similar way as the previous AC modules, see Figure 3.16. The main differences in their assembly were related to their size and number. There were 40 AC modules with YAP scintillators discs each of them with a diameter of 2.8 cm.

In addition to the AC modules presented above, a set of four BC-418 detectors was also installed. Their arrangement is shown in Figure 3.16 by blue circles.

The results obtained from both types of detectors will be discussed in the two following subsections.

Analysis results from data collected by YAP detectors

The YAP detector was developed in Texas based on the experience gained from the AC detector built at UJ. Most analyses of data collected from YAP detectors were made by the TAMU group, and results obtained from this experiment were one of the reasons for undertaking later research on long-lived SHEs at Jagiellonian University.

YAP scintillator was placed in the single module via the Lucite light guide to the Hamamatsu R1355 photomultiplier. PMT was mounted on a custom made active base which increased the ability to handle about a hundred times more events per second, than standard passive Hamamatsu base. Because of YAPs light time decay properties for that modules it was adapting commercially available Struck SIS3316 250 MHz Flash ADC to provide adjustable acquisition triggering.

Due to constructed electronic setup experiment could be conducted in a similar way as the previous one. It means it was possible to carry it out with a suitable beam on/beam off modes time (100 ms/30 ms or 30 ms/30 ms). Triggers were generated by IC-Si wall and AC modules. To avoid an enormous amount of beam-like events forward wall of AC detector was triggering only in beam off mode, while IC-Si backward wall could have triggered acquisition all the time. Both walls were synchronized, if anything interesting appears in any detector acquisition was saving information from both walls. The angle of reaction products collection was from 7 to 60 degrees.

The triggering process was split into three fractions: BeamOn, BeamOff, HighEnergy trigger. BeamOn trigger mode was used while the beam was present, the IC-Si detectors had priority of triggering acquisition. At the same time YAP detectors were set to work in slave mode. During BeamOff mode, when the beam was turned off, both walls of the detector were triggering equally with additional condition for YAPs. Namely, if low counting Si detectors returned information about particle registration, the YAP detectors were switching into slave mode again. This logic was a result of the assumptions for that particular ΔE-E system. The last trigger mode, HighEnergy, were used all the time (during beam on and off). It was set to stop the beam for 20 s if there appears a signal in the IC-Si detectors that overcomes the threshold of 8-8.5 MeV. For such events FADC storage time ranges were also extended to 160 μs, while normally it was set for 2 μs.

The experiment was focused on searching for high-energy α particles that come from heavy elements. The cases selected in this way were placed in Figure 3.17, where they were compared with other experimental and theoretical data. This picture presents a relationship between half-life times ($t_{1/2}$) and kinetic energies of α particles, where by red solid circles data from experiment at TAMU were placed.

Blue empty circles represents first group of experimental data published by Brookhaven National Laboratory (BNL) for identified particles with Z number $\leq$ 101 [87].

Second group is marked by solid green triangles, which also represents already existing experimental data for isotopes with atomic number Z $>$ 101. Thus data were taken not only from the BNL website but also from Nuclear Reactions Video (NRV) Low Energy Nuclear Knowledge Base supported by Russian Foundation for Basic Research [87, 88].

The third group marked by solid black squares linked together by line indicates theoretical values calculated for partial alpha decay half-lives for even even isotopes with atomic number Z $\in$ [98, 130] and neutron number N $\in$ [172, 196]. That values were calculated using PC-PK1 covariant energy density functional [89, 90] and Viola-Seaborg formula [91, 92].

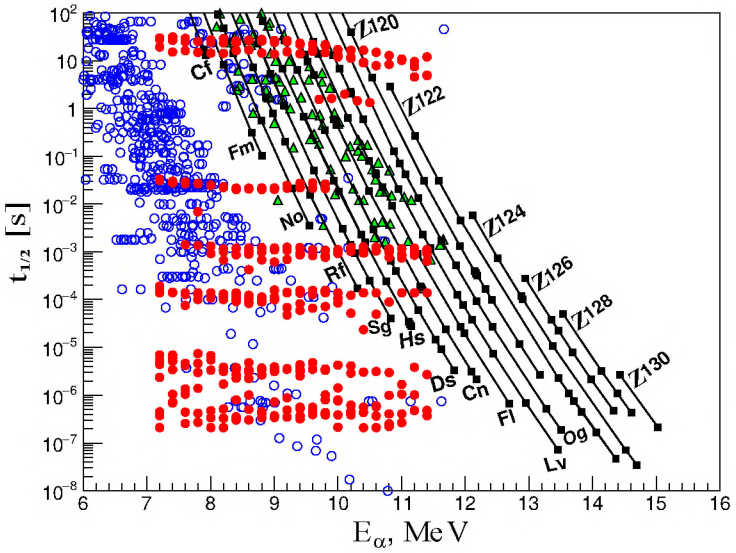

Figure 3.17: Dependence of isotopes half-lifes ($t_{1/2}$ [s]) vs kinetic energy of emitted α particle (E_α [MeV])[86]. This figure presents different data and theoretical prediction such as BNL and NRV data or already discovered isotopes, Viola-Seaborg formula calculation (also for not discovered yet elements with Z $\in$ {120, 122, 124, 126, 128 and 130}) and data from the experiment at TAMU - for details see text.

In order to identify potentially observed elements, the search area had to be narrowed down to events fulfilling the parent-daughter condition. For searching such relations the energy-energy correlation methods were used [93]. TAMU group prepared a special program which was searching two peaks in one time window, see [86] for details. This process was difficult because of the high rates of alpha decay in a single AC module and energy resolution. Despite these circumstances in events collected during the 20 s time interval of the beam off modes were found several candidates worth further analysis. Half-lives of the daughters could be calculated thanks to the recording them by flash ADC and calculated time difference between both correlated events. During this experiment, several cases were found in which daughters half-life times reached 1 $\sim$ 2 s for α particle with kinetic energy from 9.3 to 10.3 MeV. Those mentioned events are listed in the Tab.3.2 and marked in Figure 3.18 (where they were also compared with theoretical calculation and data previously published in different articles).

In comparison with theoretical predictions [90, 94, 95], it is seen that the results of the experiment do not overlap well with the calculations. Especially when it comes to calculations of the Staszczak group. Calculations that take into account not only α decays but also their competition with spontaneous fission processes for even-even nuclei indicate a severe reduction in lifetime

Emission α			Spontaneous Fission	
Parent α energy [MeV]	**Daughter α energy [MeV]**	**Daughter $t_{1/2}$ [s]**	**Parent α energy [MeV]**	**Fission $t_{1/2}$ [s]**
9.26	9.12	1.49 ± 0.32	8.15	1.86 ± 0.28
9.63	9.45	1.16 ± 0.36	8.45	1.28 ± 0.17
9.75	9.12	1.35 ± 0.38	8.97	0.74 ± 0.35
9.88	9.72	1.20 ± 0.21	9.19	1.22 ± 0.27
9.92	9.36	0.96 ± 0.26	9.45	2.18 ± 0.37
10.04	9.09	0.99 ± 0.55	10.05	1.83 ± 1.08
10.14	9.88	0.99 ± 0.32		
10.26	9.51	1.13 ± 1.18		

Table 3.2: Energies and half-lives for correlated pairs in parent-daughter relation. Note: ± 0.15 MeV standard deviation on α energies. Data from experiment conducted at TAMU in 2016 [86].

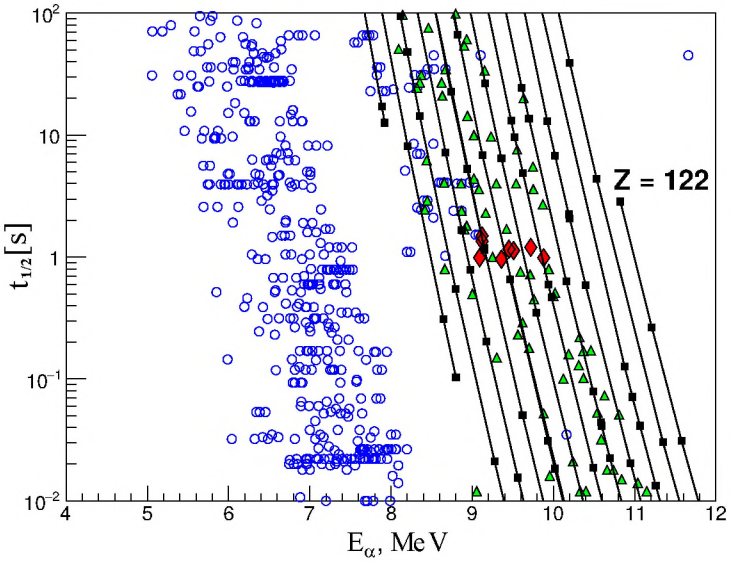

Figure 3.18: Correlated pairs in relation parent-daughter selected from experimental data (red solid diamonds) are compared with BNL and NRV data (blue circles for Z ≤ 101, green solid triangles for Z > 101) and with teoretical prediction of Viola-Seaborg formula (black lines with solid squares)[86].

expectancy. Even of many orders of magnitude. The biggest differences between theoretical predictions and experimental data occur precisely in the 8-10 MeV energy area, where an increased branching ratio to spontaneous fission is also expected.

Nevertheless obtained from our experiment data are well corresponding with other experimental data and with Viola-Saeborg calculation too. So if even-even nuclei were obtained during this experiment then observed elements were from the region of Z $\in$ [106, 114]. It should be remembered that recorded pulses correspond to daughter nuclei and the α particle accompanying it, which means that the parent nuclei would have Z number 2 units higher.

In the case of odd-odd, even-odd or odd-even nuclei the half-lives could be extended even from 2 to 10 times.

Analysis results from data collected by BC-418 detectors

During the experiment described above besides YAP detectors also four BC-418 modules were mounted on the AC holder. Analysis of this data has been fully carried out by the UJ group. All used modules were those short ones with scintillator diameter 2 cm. To operate them the ACQ and electronic setup from 2015 were also used. It made it possible to record pulse shapes of particles implanted in scintillators and to adjust the acquisition time window. Because of small amount of used detectors, there was an opportunity to split signal incoming from AC modules into two and plugged them both on two FADC channels.

This step extended the final time window almost two times. In one channel the triggering pulse was placed at the beginning of the ACQ time window, while in the second one it was moved on the end of it. Such placement created possibility of recording anything that appeared almost 1 μs before and 1 μs after recorded triggering pulse. FADCs which were used during the experiment enabled also switching between to ways of recording, with a sampling 1 Gs/s or 5 Gs/s. Depending on the mode that was used during the specific run it was possible to record from 200 ns to 1 μs time windows, which effectively gives from 400 ns to 2 μs time range for one module. During this experiment, thanks to not occupated FADC and electronic system channels, beam radio frequency (RF) signal and RC response could be registered. Data from both of these supplementary records were helpful in conducting the analysis.

Rest conditions of conducting the experiment remain the same as it was described in the paragraph concerning YAP detectors. For the record, measurements were conducted in two beam on/beam off modes (100 ms/30 ms and 30 ms/30 ms) what was taken into account during data processing. The main analysis was focused on searching for fragments of the α chain, precisely on searching for events with minimum two pulses registered in one time window.

For events selection from beam off mode there was no need for any extra conditions. During 30 ms of beam off mode there were no beam-like background events, all recorded events during this mode must come from reaction products. For example, from over 70 thousand events collected from runs in mode beam off = 30 ms there were only 19 two-peaks cases found.

An example of such an event is presented on a top raw of Figure 3.19. Probability of random coincidence of two pulses shows that in one time window during two hours of measurements with counting rate on a level 10 events/s it is possible to find 0.14 two-peak events. Such a result suggests that observed cases are from the decay chain. By specifying that the observed pulses originate from particles, it was possible to go to the next step of analysis by checking the time distance between both pulses (Δt_{12}) in all 19 events. Obtained results are presented in the middle row of Figure 3.19. A half-life time of obtained results is on a level $T_{1/2}$ = 59 ns. The bottom panel of this figure presents amplitude dependence between both registered pulses (the triggered one and its companion). Unfortunately because of low energy resolution of BC-418 there is no possibility to use amplitude for any particle identification. Contrariwise is in the case of lifetime considerations, the half-life could have been calculated thanks to extremely fast scintillators. Potentially observed chains could be found as one of those presented below (reaction 3.1).

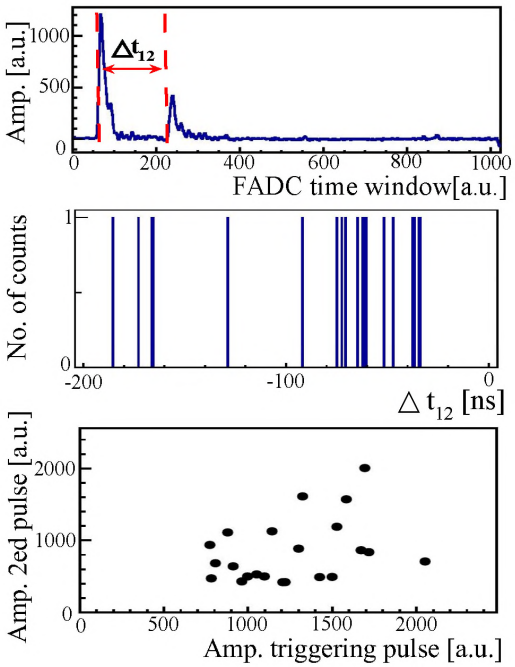

Figure 3.19: Top panel: example of interesting pulses with visualization of Δt_{12} calculation method. Middle panel: Spectrum of the time distance between two pulses registered in one time window. Bottom panel: amplitude dependence between triggering pulse and the second one registered in one time window.

$$
\begin{aligned}
^{220}Ac(T_{1/2} = 26ms) &\longrightarrow ^{216}Fr(T_{1/2} = 0.7\mu s) \\
^{219}Ra(T_{1/2} = 10ms) &\longrightarrow ^{215}Rn(T_{1/2} = 2.3\mu s) \\
^{221}Th(T_{1/2} = 1.7ms) &\longrightarrow ^{217}Ra(T_{1/2} = 1.6\mu s)
\end{aligned}
\tag{3.1}
$$

It has to be remembered that particles that were recorded during beam off mode had to be implanted in the scintillator at least a few ms earlier

and this what is observed on the histograms are actually related with decays products of element registered during beam on mode.

The same analysis was repeated for events recorded during beam on mode. For insurance that observed double-peaks events are from real particles again the probability of random coincidence was calculated. The result was as follows, after two hours of measurements with counting rate ~ 370 events/s it is possible to find an average 195.57 events with random coincidence between both registered pulses in one time window. Meanwhile, from data collected during experiment 638 cases were found. It is determining that the selected events originate from particles, and further steps in the analysis could be taken.

During beam on mode certainty that pulses recognized as interesting ones came between beam bursts were needed. For this purpose the more advanced analysis was made. Thanks to the RF recording by the ACQ system, it was possible to calculate the time of flight (Tof) of observed pulses. In the top panel of Figure 3.20 are presented results of comparison of time distance between two pulses (Δt_{12}) and the Tof of non-triggering pulse. The observed repeated structure is related to the time of beam burst dependent from the RF period. Events located between this structure, marked by frame, are located between the beam burst and they are recognized as interesting ones. From over 2,6 million of all events from the beam on mode considered during this analysis only 18 located between beam burst were found.

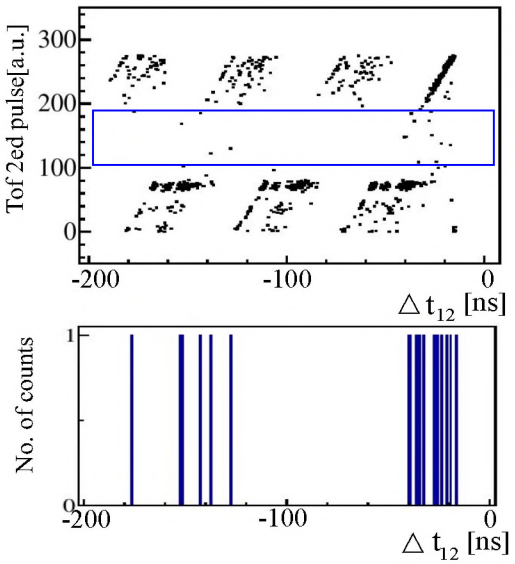

Figure 3.20: Top panel: Dependants of time distance between two pulses registered in one time window during beam on mode (Δt_{12}), on the time of flight of the second pulse from the pair (non-triggering pulse). Bottom panel: spectrum of Δt_{12} time values.

In the bottom panel of Figure 3.20, for those 18 interesting events, is presented a spectrum of time distance between both pulses. Half life estimated from this spectrum is on the level $T_{1/2} = 47$ ns. The obtained value matches the $T_{1/2}$ of the events recorded during beam off mode. It should be remembered that in the case of beam on mode, the lifetime of the reaction product can be also in the order of several ms. This is because the mode duration is

up to 30 ms. In such case results mentioned before (reactions 3.1) can also fit those events. Of course, another possibility is that an implanted heavy ion has a lifetime shorter than 1 ms.

Consider all described above results it can be said that we observed short-lived α decays. Unfortunately, because of scintillators properties it was not possible to conduct certain identification processes of implanted inside detectors elements.

Any further experiments for searching short-lived SHEs with the use of the AC detector should provide covering a bigger angle area than in the case of four BC-418 modules. An enlarged time window of the acquisition together with RF and RC signals recording should be provided. These appear to be very helpful during post-runs analysis. BC-418 has very good timing resolution but to ensure also better energy resolution replacement them by different modules should be considered. Results from YAPs were very promising but also single crystal diamond detectors (SDD) were tested in this direction and its preliminary results (presented in appendix A.3) looked optimistic.

Results from all experiments conducted during UJ and TAMU groups collaboration which were examined method of multinucleon transfer allow us to believe in sense of the further research in this direction of SHE creation. What is more, those data ushered in a new direction of experiments, concerning searching for long-lived superheavy elements, which concept will be introduced in the next chapters.

4 | Use of the MNT reactions for searching long-lived SHEs

This part of work is devoted to the search for long-lived superheavy elements with a lifetime of several years. As is well known (and what can be read from appendix A.2), all superheavy elements discovered so far have lifetimes from the range of few microseconds to several hours. The area of nanosecond lifetimes is also currently studied, and as the research of UJ and TAMU groups has shown in the previous part of this dissertation, there are indications for the existence of superheavy elements with such short lifetimes. Scientists were also studying meteors or terrestrial matter, such as rocks, in the purpose of searching SHEs with a lifetime of millions or even billions of years [96, 97]. However, the area of several years long lifetimes has never been thoroughly well studied and the attempts made so far have failed [98].

When experiments at TAMU have ended UJ group obtained the possibility of precisely studied this lifetime window. In this purpose, ACs modules that were irradiated during experiments in 2015 and 2016 year at TAMU were used. What is more, examination of scintillators from these modules allowed us to look closer on a long-lived SHEs created (if it was so) by multinucleon transfer reactions.

Figure 4.1 is giving an outline of accessible range of life times for interesting events. In this figure two plots were placed, the main one is showing the probability of α and FF decay of the long-lived SHEs (P(τ)) in life time scale (τ) started after t_{init} years after irradiation and with measurement lasting at least 2 months (Δt). This probability was calculated according to the equation eq. 4.1 for five cases: for t_{init} equal 1 (rarely dotted line), 2 (dotted line), 3 (solid line), 4 (dashed line) and 5 (dotted-dashed line) years.

$$P(\tau) = e^{-\frac{t_{init}}{\tau}} - e^{-\frac{t_{init}+\Delta t}{\tau}} \tag{4.1}$$

Formula 4.1 was obtained from the standard equation 4.2 for the probability

of surviving t time by random element.

$$P(t) = Ae^{-\lambda t} \tag{4.2}$$

Where A is normalizing factor equal λ and λ itself is a decay constant equal $\frac{1}{\tau}$. Calculating integral 4.3 on the interval t_{init} to $t_{init} + \Delta t$ resulted with desired equation.

$$\begin{aligned} P(\tau) &= \int_{t_{init}}^{t_{init}+\Delta t} \lambda e^{-\lambda t} dt \\ &= \lambda \int_{t_{init}}^{t_{init}+\Delta t} e^{-\lambda t} dt \\ &= -\frac{1}{\tau}\tau e^{-\frac{t}{\tau}} \Big|_{t_{init}}^{t_{init}+\Delta t} \\ &= e^{-\frac{t_{init}}{\tau}} - e^{-\frac{t_{init}+\Delta t}{\tau}} \end{aligned} \tag{4.3}$$

The horizontal gray line in this figure is representing the threshold of decay probability (0.01). It helps to determine possible life time range of long-lived elements (τ_{ae}) which can be detected for different t_{init} values. This relationship is shown in the upper right panel of the Figure 4.1.

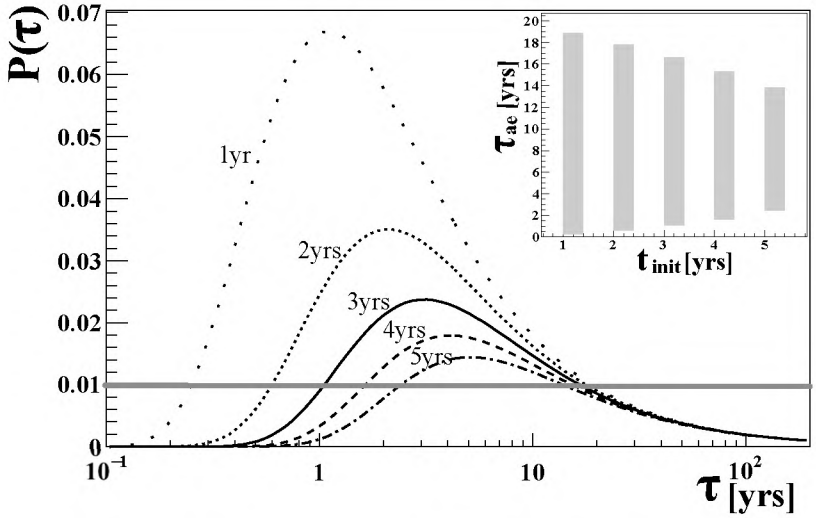

Figure 4.1: *Main plot:* Probability of α and FF decay as a function of life time for t_{init} from 1 to 5 years. *Upper right panel:* Range of life times of elements possible to examine after time t_{init} years [99].

Measurements presented in this work are corresponding with t_{init} equal 3 years (represented by black solid line and third bar). It can be easily seen

that after such time from plastic scintillators (BC-418) irradiation, lifetime of possible to observe elements are from the region of 0.8 to 18 years. The most likely to be observed are SHEs with $\tau = 2.2$ years.

4.1 Experiment setup

In 2018 we had started project focused on searching long-lived SHEs at irradiated plastic scintillators, used during experiments at TAMU [100]. The main idea was to place two active catcher detectors opposite each other in a way presented in Figure 4.2A. One of such detector should contain a scintillator irradiated by MNT reactions products in 2015 (and 2016). While the second detector in pair, should contain clean - never used before BC-418. For further convenience I will use the following notation: NACT - for not activated/new scintillators and ACT - for activated/irradiated scintillators.

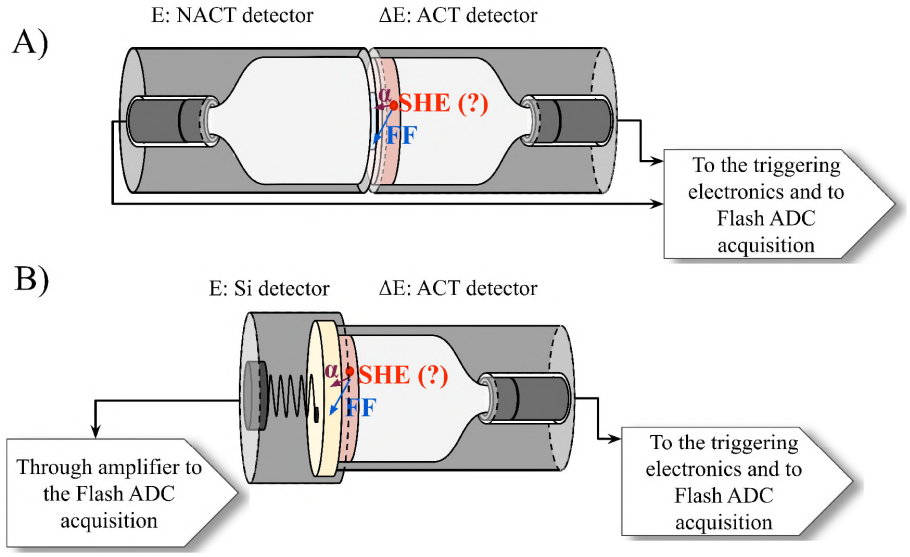

Figure 4.2: Scheme of both types ΔE-E detectors. A) Pair with NACT E detector. Scintillator used here is clean, but also is smaller and thinner than original ACT one mounted on ΔE module. B) Pair with Si E detector.

Such configuration creates a typical ΔE-E detector. If any SHE deposited in ACT scintillator decays via α particles or FF in direction of NACT detector, it will leave some of its energy (ΔE) in the activated module, while the rest energy will be deposited inside NACT detector (E). In both cases, as can be seen from the figure, short active catcher modules were used.

This idea has evolved during preparation and it was decided to add second type of ΔE-E pairs. ACT detectors still function as ΔE, but some number of NACT (E detectors) were replaced by the lithium drifted Si modules. Scheme of this assembly is presented in Figure 4.2B).

With such an idea, we proceeded to realization. The first step was to build a new holder for detector pairs. Designed rack consists of two walls enabling installation of 16 pairs of the ΔE-E detectors (8 with Si E detectors and 8 with NACT E detectors). Scheme of complete ΔE-E detector arrangement is presented in Figure 4.3. ΔE wall has been made with 8 rectangular flanges that can be easily pulled out and rotated. This mechanism enables easy exchange of ACT modules between E detectors. Consecutively this allows for an effectively longer measurement of one ACT module and obtaining feedback for each irradiated scintillators from two different types of E detectors (see Figure 4.3A). Such procedure is possible because wall of E detectors contain two rows of modules: on the upper row are mounted Si detectors and on the bottom the NACT detectors. What is more, this wall is mounted on the stable stand with two rails, which allows adjusting distance between ΔE and E detectors from about 10 cm to almost complete contact - less than 1 mm distance between them (see Figure 4.3B). The default assembled detector is shown in Figure 4.3C. The detector prepared in this way was placed in a tightly closed aluminum box. And the destination experiment was carried out in the air.

After preparing the holder, it was necessary to take care of the appropriate trigger and acquisition system for interesting events. Prepared mechanism of trigger formation for both types of ΔE-E pairs is presented in Figure 4.4. It allows to record in the acquisition information from all modules simultaneously if anything interesting will appear in any of the mounted modules.

Figure 4.4A is showing path of current pulse created in NACT E or ACT ΔE module as a result of α/FF (or other element) observation. In the first stage such pulse is split into two signals. One part is sent to the acquisition, where is waiting for a response from the trigger making mechanism. Second part is going through a threshold logical converter where it is initially checked whether pulse has exceeded the required threshold (50 mV), and then if this condition is met, it is converted into a short logic signal. The next stop on this way is an FPGA, where are located 8 "or" gates. At this stage it is checked if any of the given 8 detectors registered anything. If it is so, then logical signal is going through 40 ns delay line to the Caen v925 Fan-in Fan-out (Fin-Fout), where also signal from the second module of NACT - ACT detector pair is leaded. There finally after passing the discriminator the triggering logical signal is created. The last stage is to send it to the ACQ for trigger pulse recording.

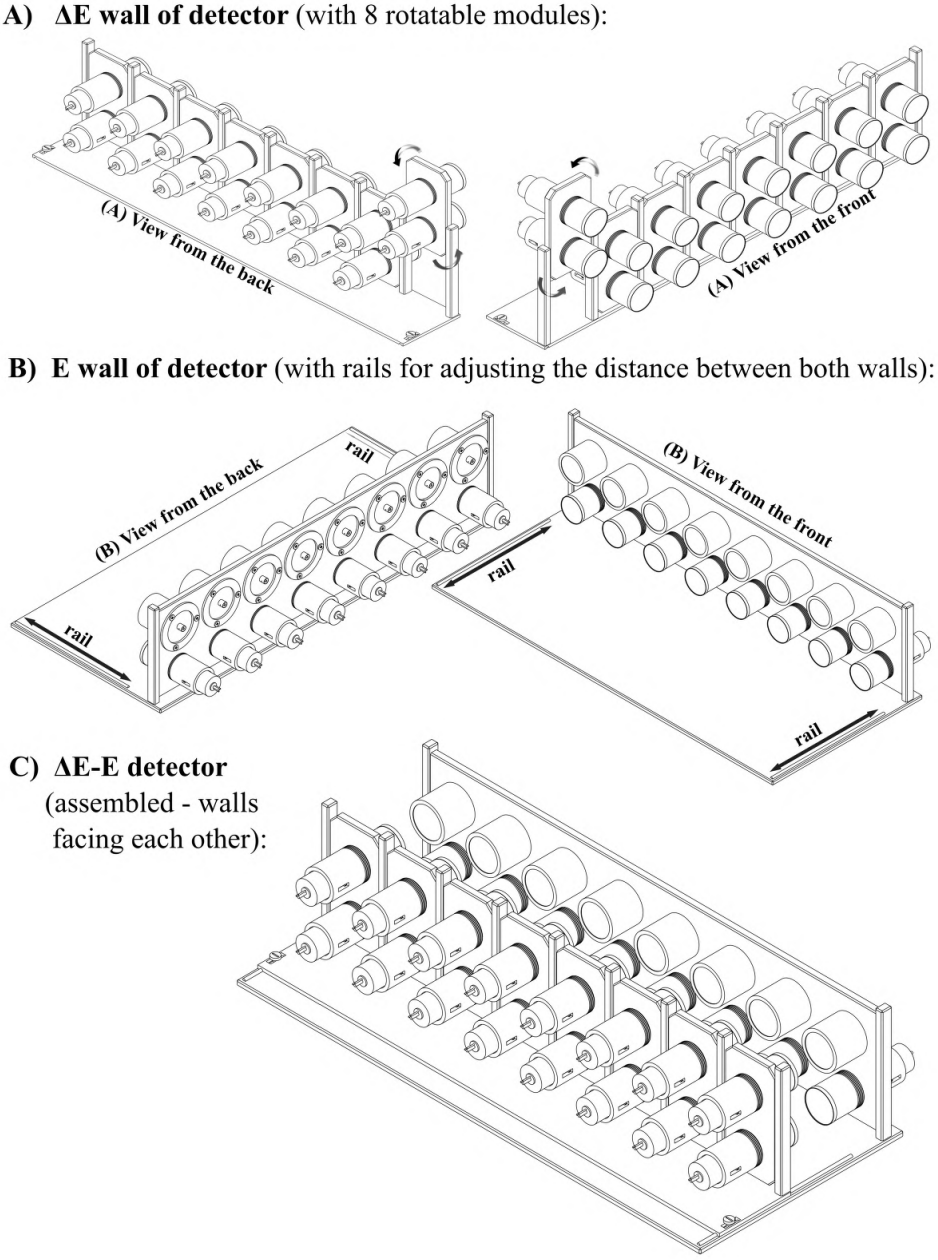

Figure 4.3: Scheme of ΔE-E detector for searching long-lived SHE. A) Wall of ΔE modules seen from two angles. B) Wall of E modules also seen from two angles. C) Walls arranged in such a way that they form a whole setup. For details see text.

In the case of ΔE-E pairs with Si detectors this path looks similar, see Figure 4.4B. The process for ACT detector remains the same. Only path for Si is slightly different. First stage for event registered by Si E detector is crossing through the preamplifier. Such a processed charge pulse is split

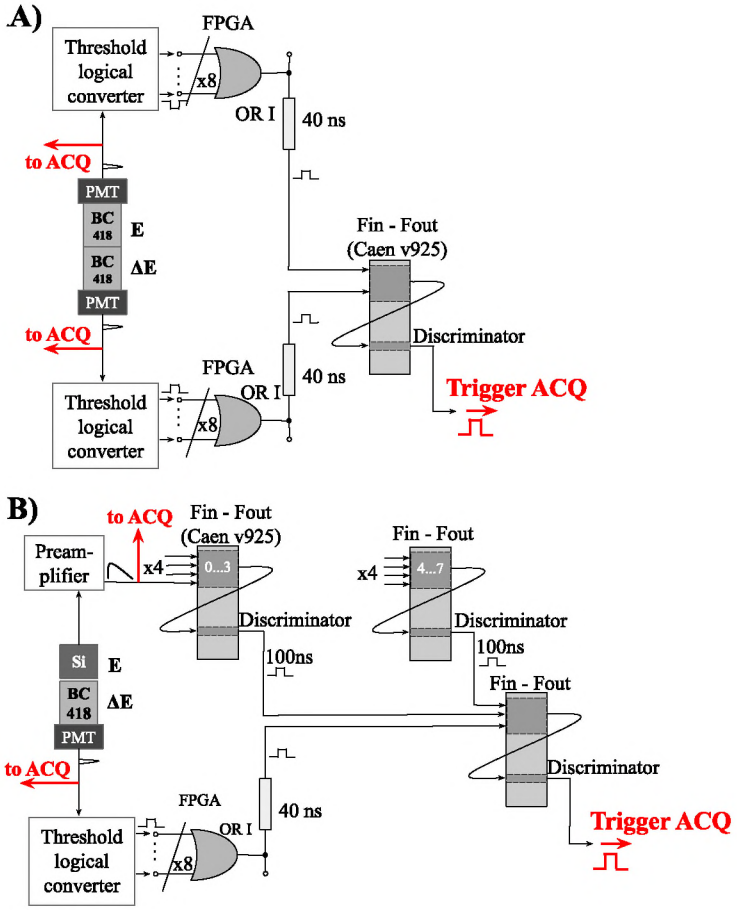

Figure 4.4: Scheme of trigger formation for A) NACT-ACT pair, B) Si-ACT pair.

into two signals, likewise previously. But this time when first signal is going to the ACQ, second one is led directly to Fan-in Fan-out. Because of Caen V925 Quad Linear FAN-IN FAN-OUT model which houses three 4 In / 4 Out sections, there have to be used two of them for processing signals from 8 Si detectors. And here again, if anywhere an appropriate signal (overcoming 70 mV threshold) has been observed the logical signal is created. This logical signal together with information from the ACT module is reaching the last Fan-in Fan-out section, where the final triggering logical signal is created.

This logic makes it possible to trigger acquisitions with any module of the 32 possible.

4.2 Background effect

Before destination tests will start, one should look at the background present during all the measurements. It is an inseparable element of every conducted run and has an influence on the analysis and results. To check its direct impact on events recording, two types of measurements were carried out with use of the active catcher detector modules. First one was conducted on the earth surface in UJ laboratory while second was made underground in salt mine Sieroszowice (about $\sim$ 930 m underground).

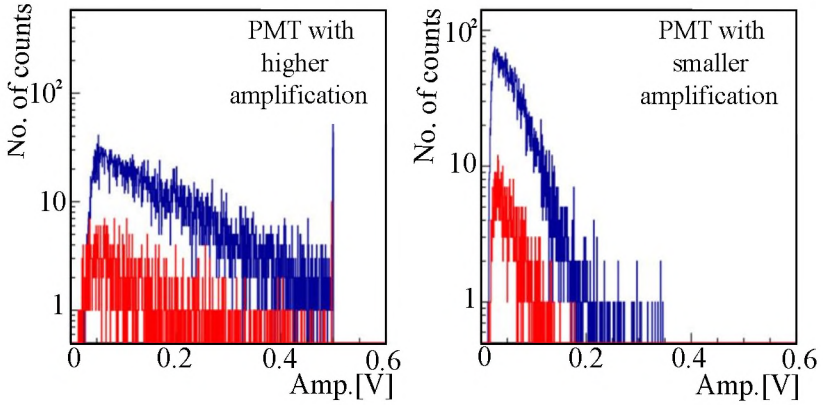

Figure 4.5: Background amplitude spectra for active catcher modules from measurements conducted on the earth surface (blue color) and underground (red color).

The measurements were made for two detectors in which photomultipliers with different amplification were mounted (such selection was made because of the properties of used PMTs). Measurements lasted 16 hours, and its results can be seen in Figure 4.5. Background obtained on the earth's surface is marked by blue color, while this from salt main is colored red. The estimated counting rate for background events in the laboratory was 7.5 events/minute while for underground measurements it was 0.71 events/minute. In conclusion, even almost 1 km of rocks, soil and salt did not eliminate natural radiation at a level higher than 10 times. Moreover, raw results from the laboratory show that working without any extra shielding causes collection of background events from larger amplitude range (region covers area of 5-6 MeV αs and FF).

In the next section there will be presented method used to narrowed background influence on data originating from searching for long-lived SHEs experiments.

4.3 Selection & calibration of setup components.

Silicon detector selection

As it was presented at the beginning of this chapter in experiment searching long-lived SHEs two types of E detectors were used and one of these types was considered Si modules. Due to their good separation properties, selecting 8 modules was not difficult. Their calibration runs were conducted in vacuum chamber with use of the complex ^{241}Am, ^{239}Pu and ^{244}Cm source placed 1.5 cm before the detection surface of the module. Results of obtained amplitude spectra can be seen in Figure 4.6, where the mentioned above separation between three different α energies coming from the source are well visualized. First peak on the left (~56.6 mV) represents the α from ^{239}Pu (5.150 MeV), peak in the middle (~60 mV) corresponds to the α from ^{241}Am (5.482 MeV), and the last on the right site (~63.5 mV) is connected with α from ^{244}Cm (5.790 MeV).

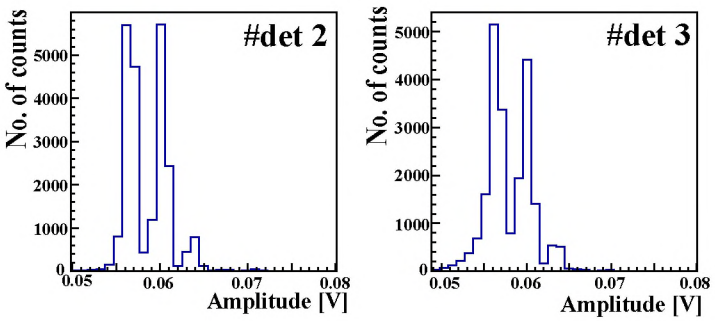

Figure 4.6: Example amplitude spectrum for pulses collected during calibration run with complex ^{241}Am, ^{239}Pu and ^{244}Cm source, in two selected silicon E detectors (detector no.2 and no. 3).

Calibration results for each Si module are presented in Table 4.1. If these data would be applied on the histogram which compares the height of the registered pulse in the Si detector and energy of corresponding it α particles, then the linear functions can be easily fitted to those data (Figure 4.2). Parameters of this energy calibration functions for five Si detectors used in the further part of analysis are presented in the Table 4.3. It could be observed that with increasing energy of the recorded particles its pulses amplitudes are also increasing. In this case it can be expected that the pulses coming from the 10 MeV α particles will have amplitude on a level of from 105 to 115 mV, depending on the detector.

Promising outcomes from the silicon detectors allows to think that analysis based on ΔE-E energy maps should give reliable results and facilitate further attempts of SHEs selection. Procedures of selection and calibration BC-418 scintillators are described in the next section.

E det No.	**Position of 5.150 MeV α [mV]**	**Position of 5.482 MeV α [mV]**	**Position of 5.790 MeV α [mV]**
0	57.8	61.6	65.3
1	54.5	57.8	61.2
2	56.5	60.2	63.5
3	56.4	59.8	63.5
4	58.4	62.2	65.5
5	56.9	60.6	64.1
6	58.4	62.3	65.7
7	57.2	60.7	64.2

Table 4.1: Position of α particles from complex ^{241}Am, ^{239}Pu and ^{244}Cm source with three different energies on amplitude spectra for Si E detectors.

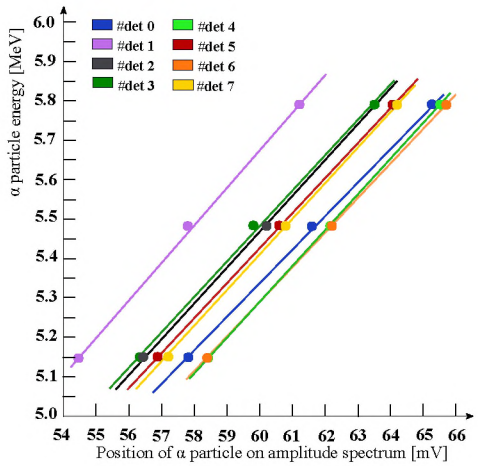

Table 4.2: Energy calibration for α particles in Si detector.

Si No.	Transformation function
det 0.	$E[a] = 85.34 \cdot a + 0.22$
det 1.	$E[a] = 95.49 \cdot a - 0.049$
det 2.	$E[a] = 91.39 \cdot a - 0.015$
det 5.	$E[a] = 88.89 \cdot a + 0.093$
det 6.	$E[a] = 87.61 \cdot a + 0.031$

Table 4.3: Energy calibration functions for five Si detectors: $E[a] = z_1 a + z_2$, where $E[a]$ corresponds to energy, a is amplitude value and z_i are parameters established by use of the data from calibration run with complex ^{241}Am, ^{239}Pu and ^{244}Cm.

Background reduction & scintillators selection

Selection of BC-418 detectors contributed two steps, selection of scintillators for NACT E modules and photomultipliers for both NACT and ACT detectors. First step, described in this section, was strictly related to the attempt

of a reduction amount of background events. Choosing only appropriate thresholds for the trigger was not a favorable solution because background events cover amplitude area of high energy α particles and reach FF energies. This situation is well presented on the energy spectrum in Figure 4.7 and marked with a dark blue color.

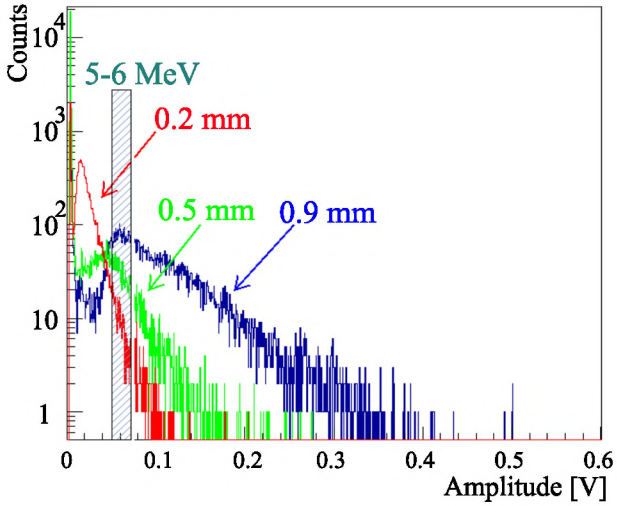

Figure 4.7: Background registered by E detector in function of the thickness of the plastic NACT scintillator. Dashed box is showing localization of 5-6 MeV α particles.

To deal with this problem, it was decided to test different scintillator thicknesses. Figure 4.7 shows background amplitude spectra for three BC-418 thickness. Where 0.9 mm is size of the scintillator used in previous experiments at TAMU, 0.5 mm is a first attempt of making scintillator thinner and 0.2 mm is the final thickness that was selected for use in NACT E detectors. As can be seen, selected thickness narrows the range of the background in the amplitude spectrum almost four times. That should ensure better possibilities for separating particles from background events. Unfortunately, thinner scintillators could not be used in NACT modules, even if their background reduction would be much better. It should be remembered that those plastics are E detectors and the particles emitted from the ACT modules should be stopped inside the NACT scintillator. Too thin scintillator may cause escape of high-energy α, and thus may falsify results. Note that this type of background elimination cannot be performed on ACT scintillators. These are not only a ΔE detectors but also a source of SHEs produced during examination of the multinucleon transfer method.

Photomultipliers & amplification selection.

To improve work on subsequent analysis, it was necessary to select photomultipliers, for both types of detectors (NACT E and ACT ΔE), whose characteristics would be similar. And if necessary, adjust the appropriate voltages for each of them so that they do not differ from each other in amplification. Despite common producer and the same model, each of PMTs differed from the others.

Process of PMT selection and adjusting their voltage supply was based on amplitude spectra prepared for the same complex ^{241}Am, ^{239}Pu and ^{244}Cm source as in the case of Si detectors. Prepared measuring setup was using standard active catcher module with clean BC-418 and it was facing complex ^{241}Am, ^{239}Pu and ^{244}Cm source. After testing a single PMT, it was changed to the next one (along with its socket assembly), meanwhile, the whole module setting together with source placement remained unchanged.

During a single test, a set of 2-3 measurements were performed to check the behavior of the pulse mean amplitude value according to different high voltage (HV) required for PMT supplying. Then the exponential function with two parameters ($f(x) = exp(p_0 + p_1 x)$) was fitted to the collected data, see Figure 4.8A). Several dozen photomultipliers were tested in this way, in Figure 4.8 only small sample of them is presented.

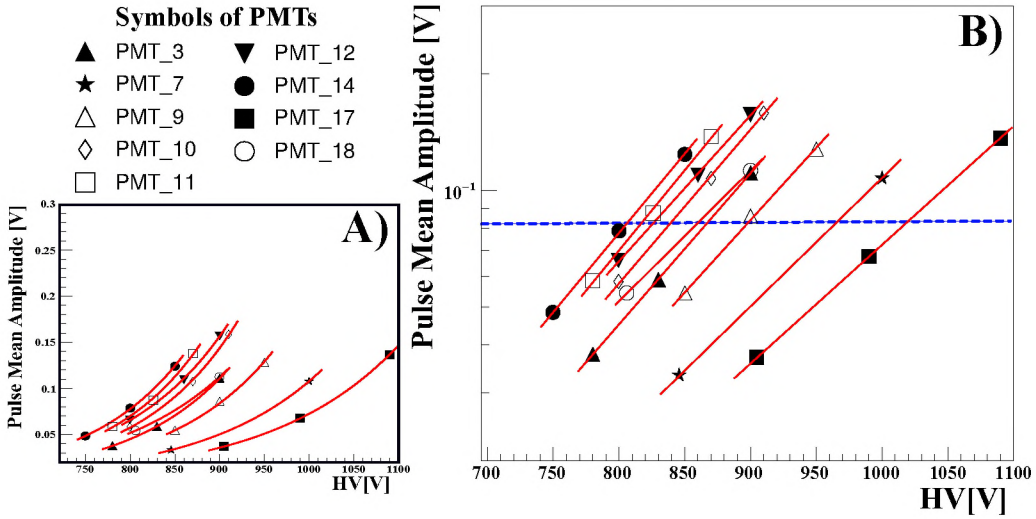

Figure 4.8: Dependence of the pulse mean amplitude value for 5-6 MeV α particles according to different HV values adjusted to nine PMTs. Results are presented on a linear (A) and logarithmic (B) scale. Dashed line indicates the level of gain desired for the experiment. Note: The photomultiplier numeration on the legend concerns entire PMT collection owned by our laboratory, not to detector itself.

On the histogram prepared in this way the Y-axis was transformed to the logarithmic view and then the common gain level was determined by choosing the desired pulse mean amplitude value. Level of the gain has been set to about 0.08 V (dashed line in a Figure 4.8B)). The next step was to determine the intersection point of the line corresponding with given photomultiplier and line fixing the gain so the voltage value could be read from the horizontal axis (X coordinate).

In this way, 24 photomultipliers with similar amplification were selected for the NACT E and ACT ΔE modules and the appropriate voltages were adjusted to them.

For PMT from ΔE detectors (with numeration from 16 to 31) first approach values of high voltage have been established according to the blue line from the figure discussed earlier, as shown in Table 4.4.

With this setting, the first calibration measurements in vacuum were made using the complex ^{241}Am, ^{239}Pu and ^{244}Cm source again. The spectrum of amplitudes obtained from them turned out to be too narrow, and its maximum was in the area of background events. Used complex ^{241}Am, ^{239}Pu and ^{244}Cm source decaying via 5-6 MeV αs and it had to be remembered that during experiment in ΔE detector only a small part of α energy will be deposited - on the level of 1-3 MeV. To avoid further hindrance during analysis the gain for all ΔE detectors was increased. The finally chosen voltages for selected PMTs are presented in Table 4.5, and Figure 4.9 shows examples of the amplitude spectra after applying new gain.

ΔE det No.	16	17	18	19	20	21	22	23
HV [V]	803.8	853.4	831.3	926	889	933.2	1049	956
ΔE det No.	24	25	26	27	28	29	30	31
HV [V]	832.5	876	799.1	849	999	879.9	918	1009.5

Table 4.4: First approach HV values for PMTs mounted on ΔE detectors.

ΔE det No.	16	17	18	19	20	21	22	23
HV [V]	875.5	910	920	1018	968	997	1049	1062
ΔE det No.	24	25	26	27	28	29	30	31
HV [V]	909.9	942	910	932.6	1056	962.7	1020	960

Table 4.5: Final established HV values for PMTs mounted on ΔE detectors.

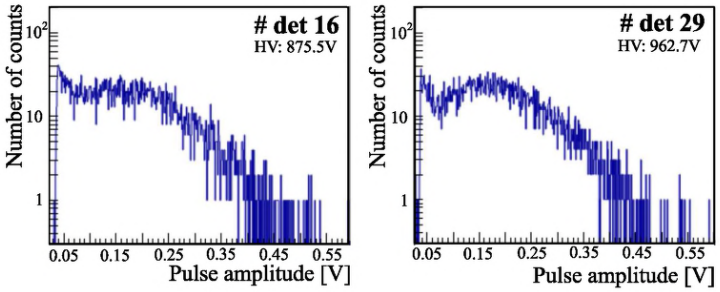

Figure 4.9: Example amplitude spectrum for pulses collected during calibration run with complex ^{241}Am, ^{239}Pu and ^{244}Cm source, in two selected ΔE detectors (detector no. 16 and no. 29) after final HV establishing.

Same process of HV for PMT adjusting and detectors calibration was made for E detectors. Values of selected voltages for photomultiplier mounted on E detectors (with numeration 8 to 15) are presented in Table 4.6 and example amplitude spectra are also presented in Figure 4.10. This time, low energies are not a problem, in fact experiment is focusing on searching events in E detector with pulses corresponded to the energies on a level 10 MeV or higher.

E det No.	8	9	10	11	12	13	14	15
HV [V]	710	790	790	780	762	821	786	791

Table 4.6: Established HV values for PMTs mounted on E detectors.

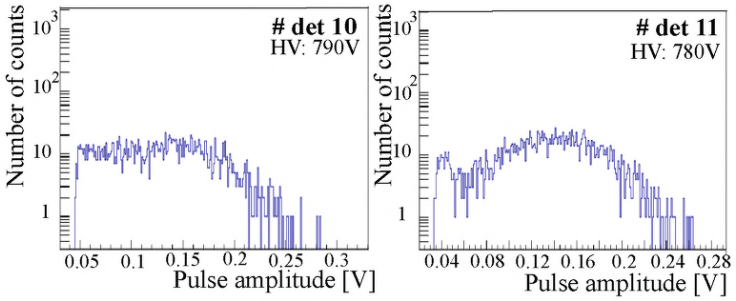

Figure 4.10: Example amplitude spectrum for pulses collected during calibration run with complex ^{241}Am, ^{239}Pu and ^{244}Cm source, in two selected E detectors based on PMTs (detector no.10 and no. 11) after HV establishing.

Preliminary monitored parameters

After adjusting proper voltages and initial background elimination it was time to check how the detection system behaves during longer measurements. A set of histograms showing example parameters observed online during conducted measurements is presented below.

In Figure 4.11 is shown an example of obtained baselines for the Si E module and for the NACT E module (left panel) together with cumulative counting rate for all modules of the ΔE-E detector (right panel) during 7 days of continuous measurements.

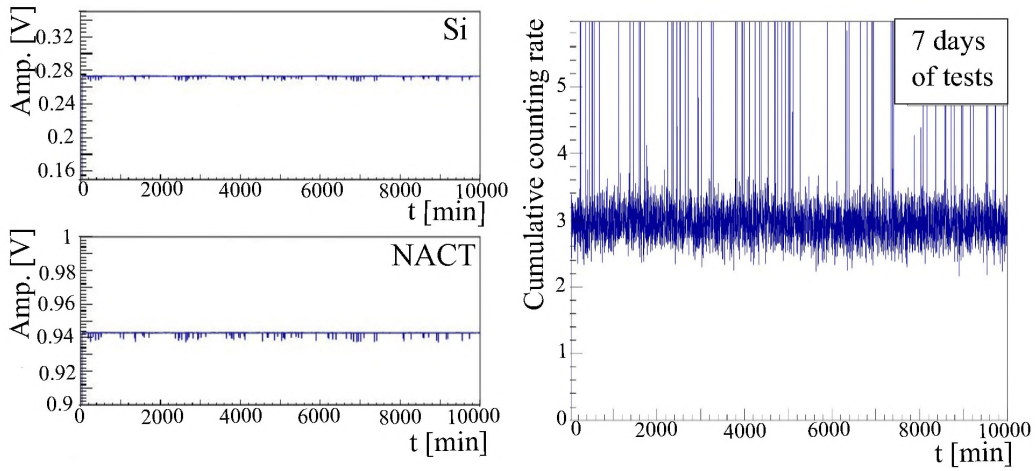

Figure 4.11: Left panel: baseline amplitude for Si (top row) and NACT (bottom row) E module over 7 days of measurements. Right panel: cumulative counting rate for all detectors in the same time of measurement.

It is visible that work of the detector is stable both in terms of baselines and the counting rate itself. The counting rate is on a level of 3 cts/minute, all deviations from the norm are associated with the self-triggering of electronics that appeared from time to time. Such cases are however relatively rare and the events recorded at that time can be easily rejected from analyzed cases.

Figure 4.12 shows typical amplitude spectra in the same time range of measurements as for previous histograms. On the left panel are located histograms for one pair of ΔE-E detector, which contains NACT module as E detector, while on the right panel are histograms for pair with Si module as E detector (top row). Corresponding to them amplitude spectra from ACT modules of ΔE detectors were placed in the bottom row.

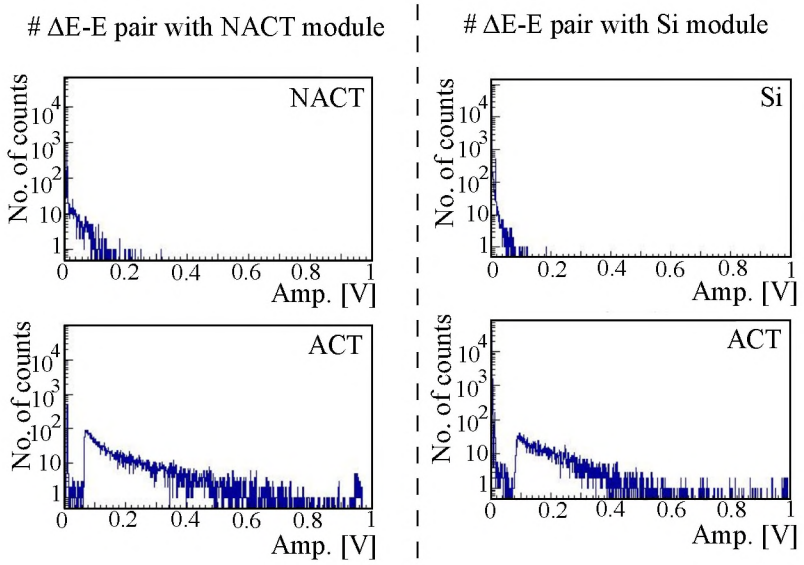

Figure 4.12: Example amplitude spectra for two pairs of ΔE-E modules.

Thanks to online monitoring, measurements can be controlled 24 hours a day, and very preliminary results can be observed, e.g. ΔE-E maps for each pair of detectors. Of course, the main analysis is done later in offline mode.

5 Use of DSP methods in pulse shape analysis

Thanks to used FADCs during experiments it was possible to record digital signals from all detectors (from AC modules in Texas A&M experiments and ACT, NACT and Si modules from the current experiment). They allowed to carry out a digital signal processing (DSP) with pulse shapes analysis of recorded events. This chapter will describe taken steps and used DSP methods during the analysis of data collected in the experiment of searching long-lived SHEs.

5.1 Pulse preparation

To conduct digital pulse shape analysis (DPSA) it is necessary to prepare recorded pulses accurately. The first step of such preparation is to calculate the baseline value (b_l) for each module of the detector. This step is required because baselines are usual slightly moved from 0 V value, like in case of Si modules - for about 0.2 to 0.3 V. What in this particular case is interfering with final pulses amplitudes that are expected for interesting events from E detectors. For this purpose mean value of first 100 bins ($a_1, a_2, ..., a_{100}$, values in a given bin) from 1024 bins covered by FADC time window is calculated (eq. 5.1).

$$b_l = \frac{\sum_{t=1}^{100} a_t}{100} \tag{5.1}$$

Those a_t bins are located before the recorded pulse. Next step in this procedure is to subtract the baseline value (b_l) for all 1024 channels, $i = [0, 1023]$ (eq. 5.2).

$$a_i^c = a_i - b_l \tag{5.2}$$

On the pulse proceeded in this way, with corrected values (a_i^c) for all channels, searching for the amplitude of the recorded pulse (equivalent to the energy

deposited in the detector) can be started. In this case can be used the simplest method of searching the highest value (amplitude) recorded in a given time window - checking bin after bin if a^c_{i+1} have a higher value then a^c_i. The last value fulfilling this condition is considered as the amplitude of the whole pulse.

For a fast scintillator, searching for the pulse amplitude and determining its time position is clear while pulse shape analysis seems very uncertain. This limitation appears due to the fact that pulses from BC-418 are extremely short, with a full width at half maximum (FWHM) on a level of 5-25 ns (depending on amplitude pulse value), contrary to the Si detectors. For them typical rise time is from the range of 80 - 300 ns. Unfortunately because of the short ACQ time window (1 μs) it is possible to record only a fragment of Si pulse: full rising scope, amplitude and only a small portion of a falling scope. However, this information allows the transition from charge Si pulse into a current pulse with FWHM on a level of 80 - 300 ns. Although to perform such transformation there are needed some digital filters which will smooth the original pulse or even directly transform it from charge to current one. The smoothing process is especially required because of different noise levels occurring on registered pulses. Examples of different types of original pulses recorded during the experiment are presented in Figure 5.1. In the next section tested filters will be discussed.

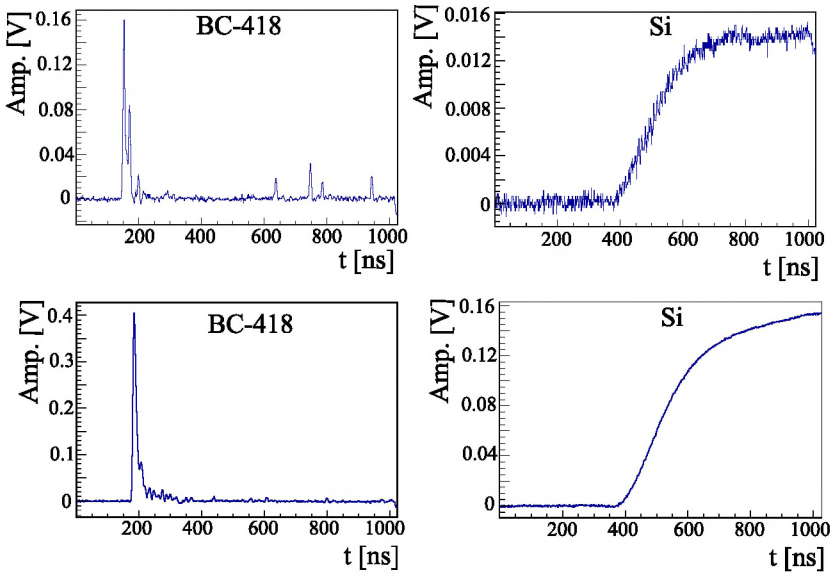

Figure 5.1: Example of different input pulse shapes recorded from Si and BC-418 detector.

5.2 Digital filters

Digital filters (DF), one of the most popular digital signal processing method, are used mainly for cleaning signals from any interference like noises, crosstalks or overlapping with other signals. Digital filters are also often used in the purpose of reconstruction partly destroyed signals, which could be caused by bad quality apparatus or some unpredictable accidents during measurements. What is more, such DF can be used also for transforming one type of pulse into another.

Digital signal processing is an operation on the original signal (raw pulse - R(t)) conducted with use of the filter to eliminate unwanted components, such as electronic contribution or other random noises. Filter F(t) is a mathematical transformation that is making all desired convolutions and returns processed signal P(t).

$$R(t) \xrightarrow{F(t)} P(t) \tag{5.3}$$

DSP can be considered as a sum of the discrete signals sequences. In such approach discrete transformed signal P[t] will have values like this presented in equation 5.4. Where R[t] is the input signal, t is sample number (in SHE experiment case it is time), N+1 is a filter size and h[k] is a filter coefficients as response for a single impulse in k point (for simplifying in further part of the work h[k] will be called a kernel of the filter) [101].

$$P[t] = \sum_{k=0}^{N} h[k]R[t-k] \tag{5.4}$$

This equation can be easily extended to the form presented below:

$$P[t] = \underbrace{h[0]R[t] + h[1]R[t-1] + \cdots + h[N]R[t-N]}_{N+1} \tag{5.5}$$

Kernel itself can be written as:

$$h = \Big[\underbrace{h[0], h[1], \ldots, h[N]}_{N+1}\Big] \tag{5.6}$$

A detailed explanation of the above mentioned formula will be shown on the example of a moving average filter, which is one of the most common filters in DSP.

5.2.1 Moving Average Filter

Moving average filter is one of the most popular and simplest in use and in the understanding digital filter. It is mainly used to reduce different types of noises from registered input signals.

This filter to produce a new smoother processed signal (output) is using the average of the number of points coming from the raw original signal (input signal).

Lets consider a filter which output signal P[t] is the average of the 3 points from the input signal R[t]:

$$P[t] = 1/3(R[t] + R[t-1] + R[t-2]) \tag{5.7}$$

Now equation 5.7 can be expanded to the form of:

$$P[t] = 1/3R[t] + 1/3R[t-1] + 1/3R[t-2] \tag{5.8}$$

In next step above presented equation 5.8 can be compared with sum 5.4. Kernel h in this particular case take form:

$$h = \left[1/3, 1/3, 1/3\right] \tag{5.9}$$

In moving average filter kernel size and its values are depending on considered number of points for calculating average itself. For general description of averaging by M points the kernel h will have M size with values $1/M$.

$$h = \left[\underbrace{1/M, \ldots, 1/M}_{\mathrm{M}}\right] \tag{5.10}$$

It happens like this because for M number of averaging points equation 5.8 will look as follow:

$$P[t] = \underbrace{1/MR[t] + 1/MR[t-1] + \cdots + 1/MR[t-M-1]}_{M} \tag{5.11}$$

Therefore general representation of moving average filter is presented below, by equation 5.12, with kernel h[t] values equal to $1/M$.

$$P[t] = 1/M \sum_{k=0}^{M-1} R[t-k] \tag{5.12}$$

The selection of proper kernel size is very important because the amount of noise reduction is depending on them. The square root of M number gives a factor of its reduction, e.g. for M = 100, noises will be reduced by factor 10. It could lead to insufficient or excessive smoothing [101].

5.2.2 Trapezoidal & Triangular Filters

Another quite common filters used in DSP are trapezoidal filters. This kind of DF can be used for several purposes. Mostly they are used to achieve easy access to amplitude values of the input signal, because of their skill of pileup elimination and smoothing properties by eliminating any unwanted noises. Nevertheless, a special type of this filter can be used also for the time determination of incoming original signals, which also can be helpful in case of calculation time distance between pulses. This special type of filter is a triangular filter, and it has also more usable function. It allows to transform charge impulse into the current one, that trick is often applied in the electronic systems for easier establishing triggering thresholds for experiments acquisition.

Once it has been established in the previous sections that work of each filter depends on its kernel now it can be considered a kernel for trapezoidal filters. Trapezoidal filter kernels are based on three components which are considering different samples sizes: positive - with L number of samples, gap - with G samples and negative - again with L samples. For pulses from preamplifiers positive and negative parts of the kernel are using averaging. Like it is presented in the equation 5.13. Size of the gap part is not depending on L values, but its size has an impact on the outcome signals.

$$h = \Big[\underbrace{{}^{1}/_{L}, \ldots, {}^{1}/_{L}}_{\times \mathrm{L}}, \underbrace{0, \ldots, 0}_{\times \mathrm{G}}, \underbrace{-{}^{1}/_{L}, \ldots, -{}^{1}/_{L}}_{\times \mathrm{L}}\Big] \tag{5.13}$$

Lets consider trapezoidal filter for preamplifiers with L = 10 and G = 5. Impact of this filter is presented on the left panel of Figure 5.2. Simplified example input signal from the preamplifier (marked by red) was treated with filter returned trapezoidal shaped output signal. The rising and falling slopes of the output are corresponding to the size of L component of the kernel, while the width in the maximum amplitude of the impulse is equal to the G size. How can be easily perceive the response of the filter returned signal with no baseline. Establishing of the real pulse amplitude is here much easier to do. It can be also seen how this filter has moved a peaking time (δt). User applying it during DPSA must be keeping in mind, that from processed response there is no possibility to read real time of the recorded pulse.

For this purpose there will be much better to use a triangular filter, which is nothing more then trapezoidal one with G = 0.

Example response of the triangular filter is presented on the right panel of Figure 5.2. The charge pulse of the input signal is transformed into the

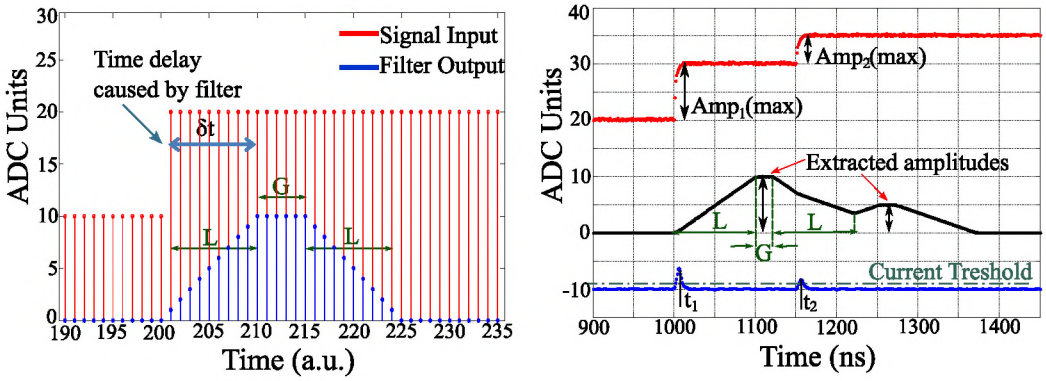

Figure 5.2: Left panel is showing pulse shape of the output as a reaction on trapezoidal filter (with L = 10, and G = 5) used on preamplifier input signal. Right panel is presenting impact of trapezoidal and triangular filters on a raw signal. Red signal represents the original input with a pileup pulse. Black signal is an output after use of the trapezoidal filter (with L = 100 and G = 20), while blue signal is an output from triangular filter (with L = 5 and G = 0) [102]. For more details look at the text.

current one which allows to adjust triggering thresholds on the electronics. However, it should be remembered that the amplitude of the obtained pulse has been scaled up, and the use of the filter itself caused the baseline to shift to negative values. Nevertheless, after the preparation of the output signal for the use of triggering electronics, this is not an insurmountable problem. The figure is also well showing that a triangular filter is returning precise information about the time of the recorded signals, which is helpful in DPSA e.g. for calculating time distance between pulses recorded at pileups.

5.2.3 Least Squares Filter

It is also common to use iteration filters instead of using those based on kernels. An example of such an iteration filter is method of least squares (LSF). This is the standard method of approximation solution of the overdetermined systems, what are mathematical systems of equation with more equations than unknowns. Mostly used in regression analysis during fitting line to the set of data.

In the simplest situation to any set of data with at least two variables like time on the axis X and amplitude on the axis Y in the coordinate system, a straight line can be fitted defined by equation 5.14.

$$y = ax + b \tag{5.14}$$

where a and b are unknown parameters. The search for parameters is based on minimizing the sum from equation 5.15.

$$S(a,b) = \sum_{i=1}^{n}[y_i - y(x_i)]^2 = \sum_{i=1}^{n}[y_i - (ax_i + b)]^2 \tag{5.15}$$

where n is number of data, y(x_i) are the y coordinate values calculated from the linear equation for the x_i data. The differences between the exact values of y_i and the values calculated from the linear equation are squared to avoid possibility that they will cancel each other due to the difference in characters. For this reason, the presented method is called the least squares method. The process of searching for parameters a and b can be simplified by using the formulas listed below (eq. 5.16 -5.20).

$$S = \sum_{i=1}^{n}\frac{1}{\sigma_i^2} \tag{5.16}$$

$$S_x = \sum_{i=1}^{n}\frac{x_i}{\sigma_i^2} \tag{5.17}$$

$$S_y = \sum_{i=1}^{n}\frac{y_i}{\sigma_i^2} \tag{5.18}$$

$$S_{xx} = \sum_{i=1}^{n}\frac{x_i^2}{\sigma_i^2} \tag{5.19}$$

$$S_{xy} = \sum_{i=1}^{n}\frac{x_i y_i}{\sigma_i^2} \tag{5.20}$$

Where σ_i is a standard deviation and its square can be negligible when the standard deviation for all measuring points is the same. In such case, the classic regression can be considered and above mentioned equations receive form like those from eq. 5.22 - 5.26.

$$S = \sum_{i=1}^{n} 1 = n \tag{5.22}$$

$$S_x = \sum_{i=1}^{n} x_i \tag{5.23}$$

$$S_y = \sum_{i=1}^{n} y_i \tag{5.24}$$

$$S_{xx} = \sum_{i=1}^{n} x_i^2 \tag{5.25}$$

$$S_{xy} = \sum_{i=1}^{n} x_i y_i \tag{5.26}$$

The parameters a and b can be given by formulas 5.28 and 5.29:

$$a = \frac{S \cdot S_{xy} - S_x \cdot Sy}{\Delta} \tag{5.28}$$

$$b = \frac{S_{xx} \cdot S_y - S_x \cdot Sxy}{\Delta} \tag{5.29}$$

Where $\Delta = S \cdot S_{xx} - S_x^2$. Now their values can be entered into the linear equation 5.14 as follow:

$$y = \left(\frac{S \cdot S_{xy} - S_x \cdot Sy}{\Delta}\right)x + \left(\frac{S_{xx} \cdot S_y - S_x \cdot Sxy}{\Delta}\right) \tag{5.30}$$

The equation obtained in this way is extremely useful when it will be realized that having it in the form of a mathematical formula allows to carry out further mathematical operations on it. Such an operation could be calculating of the derivative. If DPSA consider charge pulses where consecutive q(t) values can be described by equation 5.30, i.e. when t corresponds to x values and q(t) is equal y, then calculating of the derivative $\frac{dq}{dt}$ will give the current signal values i(t), like in the equation 5.31. In this very simple way charge input signal can be transformed into the current one.

$$i(t) = \left(\frac{S \cdot S_{xy} - S_x \cdot Sy}{\Delta}\right) \tag{5.31}$$

5.3 Process of filters selection

In this section process of matching digital filters for current analysis needs will be presented. Each of those described above filters can find application in pulse shape analysis for both types of signals recorded from detectors ΔE and E (Si and BC-418 modules).

5.3.1 Filters for Si detectors

One of the goals of DSP in this analysis was to transform charge pulse from the Si detector into the current pulse. This step required a filter that will smooth the input signal since the transformed pulse is more reliable when it is made from the noise-free signal.

The First attempt was focused on testing moving average filters.

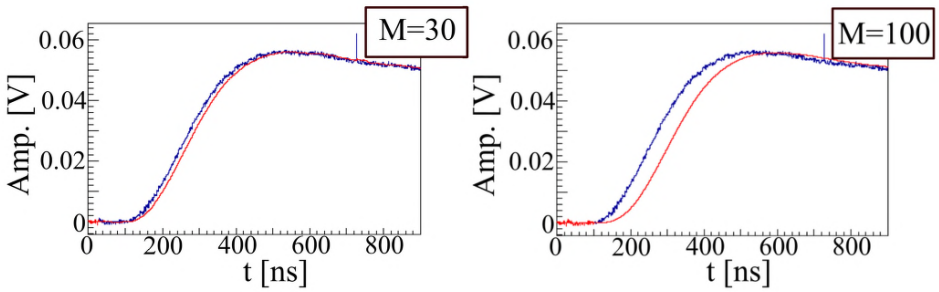

Figure 5.3: Impact of moving average filters on pulse recorded from Si detector. Marking: blue line - input signal, red line - output from the filter, M - filter size.

In Figure 5.3 is presented comparisons of the original charge pulse (blue line) with output signals from moving average filters with different kernels sizes (red line). Filter with M = 30 meets the condition of pulse smoothing but is starting modifying output signal shape by changing slightly angle of the slope, which is much better visible on the example with M = 100. Small filter size is mapping the amplitude and slope of the input signal well, but it doesn't eliminate the noise enough. On the other hand to high filter size (M>100) is also changing amplitude value and caused shifted of the beginning point for the smoothing process.

During searching the best method for pulse smoothing the triangular and trapezoidal filters were also tested. Triangular filter with L < 150 transforms shape of the input signal instead of smoothing it. Unfortunately increasing L size (e.g. tested L = 350) also does not help with noise reduction.

For trapezoidal filters different configurations of L and G values were examined. It appears that level of smoothing is dependent mainly on the L value while the range of smoothing is related to G values. Choosing the right parameters required however testing many combinations of both L and G values. During selection it was checked dozens of cases with L size from 0 to 350, and with G range from 0 to 500.

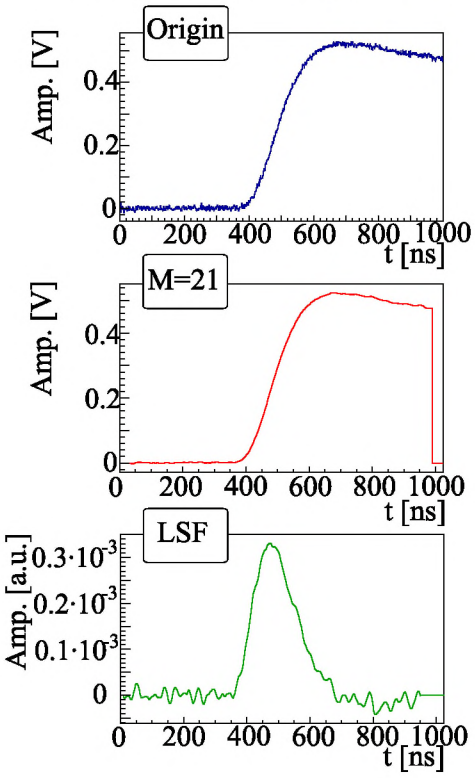

Figure 5.4: Impact of moving average filters with M = 21 (middle panel) on original charge pulse from Si detector (top panel). Result of use of the least squares filter for transforming charge signals into current (bottom panel).

Essentially from all tested smoothing methods in further DSP they were used three types of filters. It was two moving average filters with M = 11 and M = 21, and averaging trapezoidal filter with L = 16 and G = 250. However, all results (related with DPSA) presented in chapter 6 will be based on smoothing by moving average filter with M = 21 and least squares filter for transforming charge signals into current ones. Their impact on typical charge pulse from Si detector is presented in the Figure 5.4.

6 | Analysis & Results

The analysis of collected data is focusing on searching events related with decay of the superheavy elements implanted in scintillator material. Due to roughly estimated depth of potential SHE implantation inside of the ACT scintillators, on the level of several microns, it was possible to establish energy range where high energetic alpha particles related with superheavy elements are expected to be found. Procedure of this area selection together with results obtained from analysis will be described in this chapter. Additionally, thanks to the good energy resolution of Si detectors it was possible to conduct pulse shape discrimination analysis of silicon current signals. The studied DSP moments showed the potential in the process of separating interesting events from fission events. Results from this analysis also will be presented in this chapter.

6.1 Definition of the energy area on the $Amp_{\Delta E}$-E maps for search SHEs candidates

Having made sure that the acquisition process is working correctly, the question *Which events are interesting in the aspect of searching for long-lived super-heavy elements?* can be finally asked.

It is important to note that if any SHE was implanted in BC-418 ACT scintillator during experiments tested multinucleon transfer at TAMU it was implanted very shallow, on the level of several microns. This property allows to approximate localization of such an event on the $Amp_{\Delta E}$ - E map. Namely, due to the depth of implantation, a small portion of α energy (typically 1-3 MeV) will be deposited in the ΔE module, while the remaining part (more than 10 MeV) will be deposited in the E detector, what is well seen especially on the ΔE-E map presented in the Figure 6.1. This map is showing simulated by SRIM energy localization of alpha particles with three different values of its total energy and emitted under different angles and depths from particle implanted in the ACT scintillator. By circles were marked situations when α

was emitted at 50μm depth: by full circles when it was emitted perpendicularly to the ΔE detector surface, and by empty circles when emission was at 45° to this surface. Star symbol corresponds to case where α particles were emitted perpendicularly to the ΔE detector surface, but from the element implanted in ACT scintillator at 20μm depth. Calculations were made for α particles with total energy 15 MeV (blue color), 18 MeV (green color) and 20 MeV (orange color).

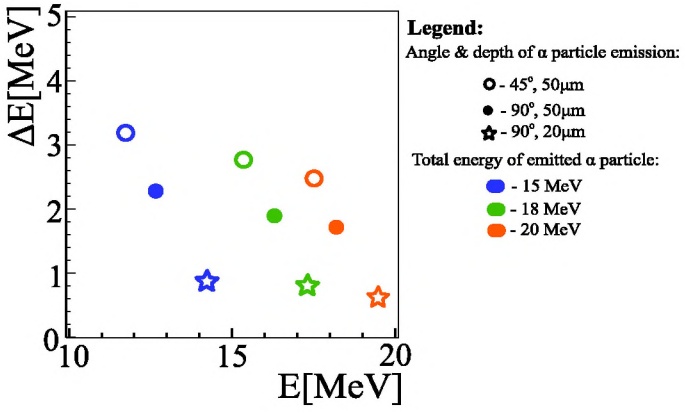

Figure 6.1: ΔE-E map for high-energetic α particles emitted from scintillator material under different angles, from different depth, and with different total energies. Obtained results originate from SRIM simulations [103].

Figure 6.2 presents Amp$_{\Delta E}$ - E map for background measurement on a pair with Si 0 E module. For creating this map used ΔE scintillator was new (not activated in any experiment before). Left panel represents the whole obtained energy spectrum while the right panel is showing zoom of the area marked by black dashed rectangular on the left side. The same map was also prepared for the detector pair based on NACT scintillator, Figure 6.3.

The region marked with a red dotted frame is an area where particles originating from long-lived superheavy elements should be located. Boundaries of this area for Si E detectors were possible to established on 10 - 20 MeV, thanks to use of the energy calibration functions described in the section 4.3 and presented in Table 4.3. For detectors based on scintillators (E and ΔE modules) selecting proper range was more complicated.

To establish boundaries for NACT E detectors as 10 - 20 MeV it was necessary to find energy calibration functions. Due to scintillators non-liner characteristic and not good energy resolution it was decided to parameterize those detectors according to the Si energy spectra. For the same environment conditions and same set of examined particles the energy spectra should look consistent for both types of E detectors.

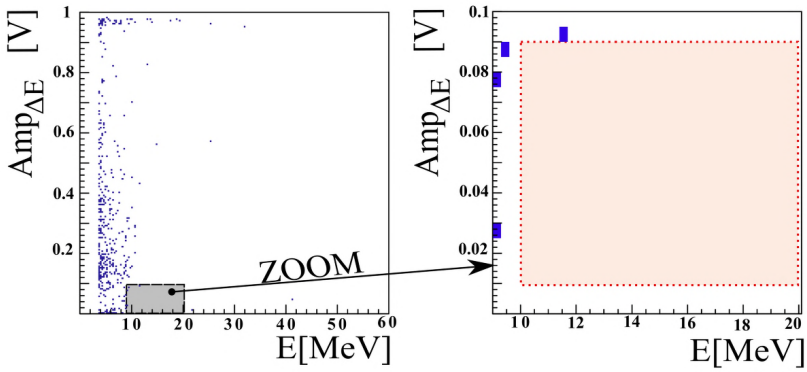

Figure 6.2: Background Amp$_{\Delta E}$ - E map for detector pair with Si No. 0. Left panel: map for whole amplitude and energy spectrum. Right panel: zoomed area from the left histogram. Map prepared for 39 days lasting run with clean ΔE scintillator.

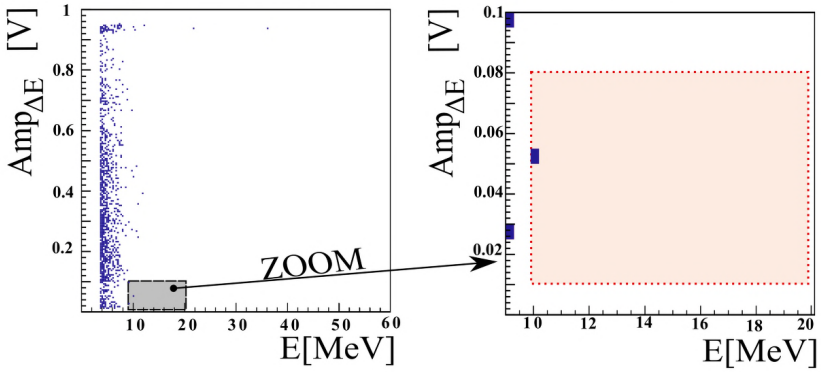

Figure 6.3: Background Amp$_{\Delta E}$ - E map for pair with NACT No. 11. Left panel: map for whole amplitude and energy spectrum. Right panel: zoomed area from the left histogram. Map prepared for 39 days lasting run with clean ΔE scintillator.

First step was to prepare energy spectra for Si detectors to check their shape and compare if actually, it looks uniformly. Figure 6.4 presents energy spectra for all Si detectors used in the farther analysis. Figure was prepared for 87 day long measurement run with irradiated ACT scintillators with normalization to the field under the histograms area for single module. The next step was to find energy calibration function for NACT E detectors, which at the same time adjust the shape of this spectrum to the Si detectors energy spectra shape. The selected function has the form of third degree polynomial presented in the equation 6.1, where a corresponds to amplitude value in V and $E[a]$ is energy in MeV.

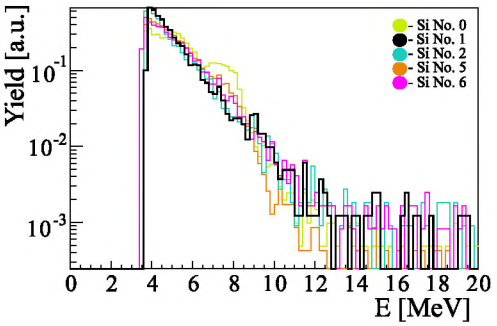

Figure 6.4: Energy spectra for Si E detectors made for run with irradiated during MNT scintilators.

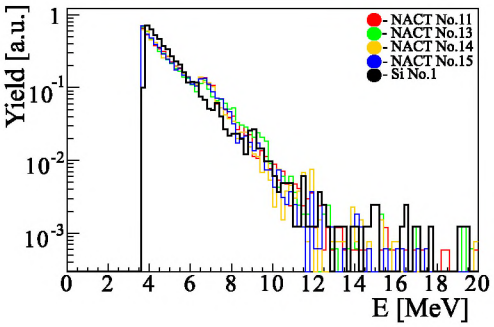

Figure 6.5: Energy spectra for NACT E detectors with additional energy spectrum of Si no. 5 for comparison, made for run with irradiated during MNT scintilators.

$$E[a] = \begin{cases} x_1 a & \text{for } a \leq a_0, \\ x_1 a + x_2(a-a_0) + x_3(a-a_0)^2 + x_4(a-a_0)^3 & \text{for } a > a_0; \end{cases}$$

where:

$$x_1 = 36, \qquad x_3 = -19.3045, \qquad a_0 = 0.18V,$$
$$x_2 = -14.7717, \qquad x_4 = 54.7708,$$

(6.1)

Results obtained thanks to it use are presented in Figure 6.5. Additionally, the spectrum from silicon detector no. 1 (black line) has been added in this figure for a better comparison of the results.

The ΔE detectors required a different approach. Having no reference ΔE detector whose good energy calibration could be used to establish the energy calibration function, it was decided to use for upper limitation instead of energy range the amplitude (Amp$_{\Delta E}$) corresponding to the 5-6 MeV αs. Values of this amplitudes were chosen as a maximum of the amplitude spectra prepared for individual detectors with use of the complex ^{241}Am, ^{239}Pu and ^{244}Cm source. Example of such amplitude spectra was presented in the Figure 4.9 in section 4.3, while limitations for modules used in this analysis are presented in Table 6.1. For bottom limitation 0.01 V was established as a potential noise reducer.

With knowledge how range of interesting events were defined data presented in the Figures 6.2 and 6.3 can be more carefully considered.

After this lasted 39 days background measurement with clean scintilla-

ACT's E pair no.:	Si 0	Si 1	Si 2	Si 5	Si 6
ACT's ΔE amplitudes [V]:	0.09	0.08	0.13	0.07	0.09
ACT's E pair no.:	NACT 11	NACT 13	NACT 14	NACT 15	
ACT's ΔE amplitudes [V]:	0.08	0.075	0.075	0.16	

Table 6.1: Upper limitation for region of searching interesting events for ΔE detectors represented by amplitudes values in the maximum of the amplitude spectrum for calibration run with complex ^{241}Am, ^{239}Pu and ^{244}Cm source.

tors ΔE instead ACT ones there were no background events registered in considered red rectangular area for Si pair (called in the further part of the work as 'area/region of interest'), and only one event for NACT pair was found. Those results can be treated as encouragement for conducting further research.

As a generating $Amp_{\Delta E}$ - E maps for data collected during main experiment is the first step in the analysis, it is done for all detector pairs - with Si and NACT E modules. In the Figures 6.6 and 6.7 are presented maps for pair with Si E detector number 0 and for pair with NACT E scintillator number 11. Considered run was 87 days long (more than twice time long as for Figures 6.2 and 6.3) and was testing irradiated by reactions products ACT scintillators. On the left panel again has been placed map for the full available energy spectrum while on the right panel zoom of the shadowed black rectangular was attached.

In both figures (6.6 and 6.7) the right panels contain also red rectangular areas were interesting events should be located. How it can be seen for both modules there appear several events that can be considered as interesting ones. Nevertheless on these maps still can be found background events and random coincidences related to noise or just badly recorded pulse shapes. To eliminate noises and cases inadequate for analyzing all events from the region of interest were checked by eye and for further analysis, only particle-related events, like those presented in Figures 6.8 and 6.9, were selected.

The upper panels of those figures present pulse shapes from E detectors while the bottom panels correspond to pulse shapes recorded from ΔE modules. Both events from Figure 6.8 originate from pair with Si No. 0. In column **A)** is presented event with total energy above 12 MeV, while in column **B)** recorded event is overcoming 17 MeV. Events from Figure 6.9 were taken from pair with NACT scintillator No. 11. In column **A)** is shown event with total energy higher then 13 MeV, while event from column **B)** is overcoming 11 MeV. All these cases may be related to α particles from superheavy elements.

Examples of rejected events from region of interest (chosen from Si pair for same 87 day long run) are presented in Figure 6.10. In the column **A)** is

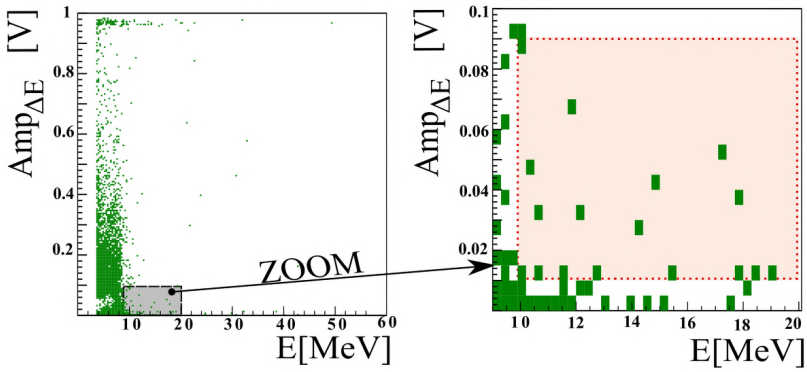

Figure 6.6: Amp$_{\Delta E}$ - E map for pair with Si No. 0. Left panel: map for whole amplitude and energy spectrum. Right panel: zoomed area highlighted by rectangular on the left histogram. Map prepared for 87 days lasting run.

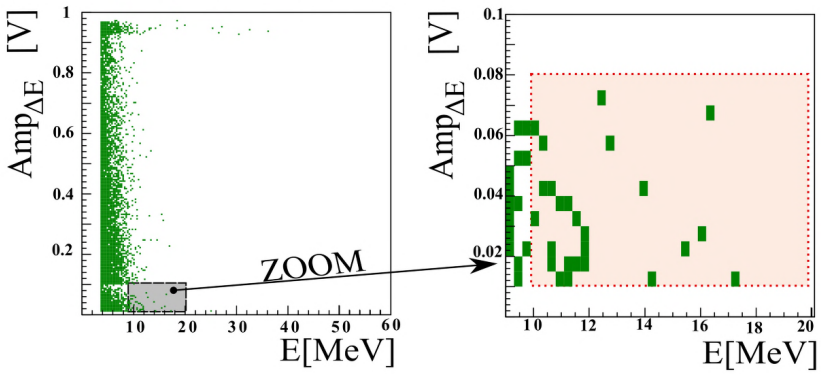

Figure 6.7: Amp$_{\Delta E}$ - E map for pair with NACT No. 11. Left panel: map for whole energy spectrum. Right panel: zoomed area highlighted by rectangular on the left histogram. Map prepared for 87 days lasting run.

shown example of event which could be considered as interesting one but due to not fully recorded Si pulse shape in the acquisition time window must be omitted in further analysis (it disallow proper DPSA). For 87 long run and for five Si modules pairs only several such events in energy area of interest were found, and this one was recorded in Si No 2. In the column **B)** is presented example of typical noise recorded from ACT ΔE module during measurement. Presented event originate from pair Si No. 0.

In Figure 6.11 are presented two rejected cases for pair with Si 0 E detector, because of their high energy values (from region above of the red rectangular). In the column **A)** is presented a case which can originate from natural radiation as an example of an event with total energy on the level higher than 15 MeV, with amplitude of the pulse from ΔE detector slightly above the considered area of interest. In column **B)** is presented a very en-

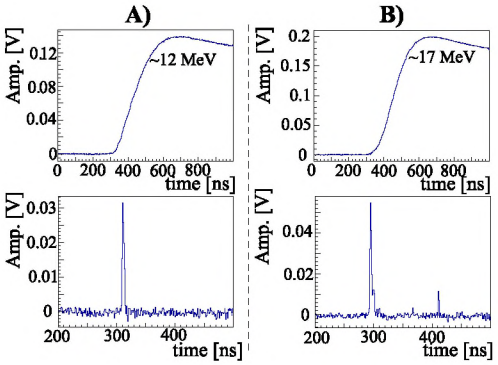

Figure 6.8: Example of two coincidence events from energy region of interests for pair with Si module. Top panels shows pulses registered for this events from E detector while bottom panels presents corresponded to them response of the ΔE modules.

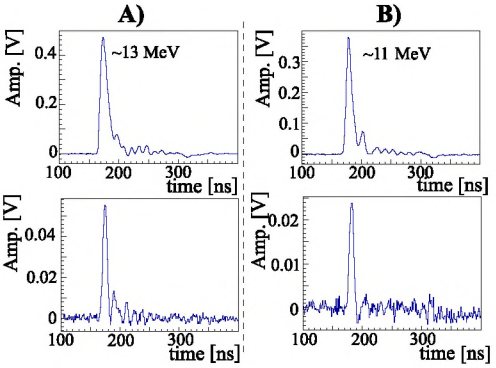

Figure 6.9: Example of two coincidence events from NACT pair with energy from region of interests. Top panels presents pulses registered for this events in E detector while bottom panels shows corresponded to them response of the ΔE modules.

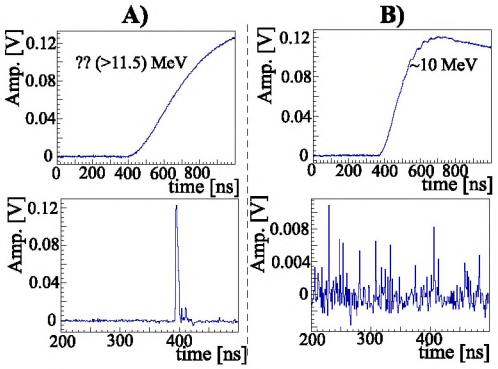

Figure 6.10: Example of two rejected coincidence events from Si module pair with energy from area of interest. Top panels shows pulses registered from E detector while bottom panels corresponds to their response from the ΔE modules.

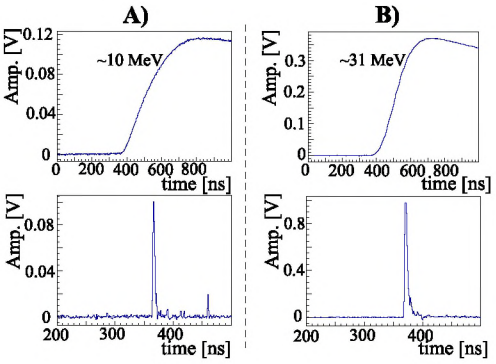

Figure 6.11: Example of two rejected coincidence event from Si pair with energy above area of interest. Top panels shows pulse registered from E detector while bottom panels corresponds to their response from the ΔE modules.

ergetic example with total energy above 31 MeV which may correspond with γs produced during decaying of some radioactive element occurring in the detector (Si or scintillator) or with high energetic cosmic originate particles.

In all ΔE-E detector pairs inside of the featured area for high energy αs can find some events. Further steps required conducting more advanced analysis, for example, a digital pulse shape analysis methods (DPSA), which seems more approachable especially in the case of detector pairs based on

the Si modules. In the next sections these methods will be described and explained. Results from its application on selected interesting events will be also discussed.

6.2 Pulse shape discrimination of silicon detector current signals

After testing various methods of digital identification of elements due to their Z and A values, it was decided to check the moment method used by S. Barlini group for pulse shape discrimination of silicon detector current signals [104]. It is a method of estimation of population parameters in statistics and it is based on the expected value E(X) of X random variables. There are two types of moments, standard one (commonly use for m_1 calculation) and central moment (mostly used for higher orders of moments calculation). Both of them can be used for a random variable with a discrete or continuous distribution, formulas for moment (m_k) of order k prepared for each case are presented on equations 6.2 and 6.3.

Standard moment:

$$m_k = E(X^k) \begin{cases} \sum_i x_i^k p_i & \text{- discrete distribution} \\ \int_{-\infty}^{\infty} x^k f(x) dx & \text{- continuous distribution} \end{cases} \tag{6.2}$$

Central moment:

$$m_k = E[X - E(X)]^k \begin{cases} \sum_i [x_i - E(X)]^k p_i & \text{- discrete distribution} \\ \int_{-\infty}^{\infty} [x - E(X)]^k f(x) dx & \text{- continuous distribution} \end{cases} \tag{6.3}$$

By p is marked probability function and by f density function. Different moments order are corresponding with different statistical parameters, their examples are presented in the table 6.2.

Starting with formulas presented in table 6.2 Barlini group prepared own equations (6.4, 6.5, 6.6) perfect for calculating three moments for obtained current pulses. For this purpose, they had to rescaled signals to start the calculation with the first sample and to make more compact scale they also extracted k root from each considered moment.

$$m_0 = \sum_{i=i_{start}}^{i_{stop}} f[i] \tag{6.4}$$

Moment ordinal	**Parameter name**	**Example formula**	**According to equation number:**
m_1	mean value *or* expected value	E(X)	eq. 6.2
m_2	variance	$\sum_i [x_i - E(X)]^2 p_i = = \sum_i [x_i - m_1]^2 p_i$	eq. 6.3
m_3	skewness *or* asymmetry	$\sum_i [x_i - E(X)]^3 p_i = = \sum_i [x_i - m_1]^3 p_i$	eq. 6.3

Table 6.2: Commonly used moments formulas.

$$m_1 = \sum_{i=i_{start}}^{i_{stop}} \frac{f[i](i - i_{start})}{m_0} \tag{6.5}$$

$$m_k = \Big| \sum_{i=i_{start}}^{i_{stop}} \frac{f[i][(i - i_{start}) - m_1]^k}{m_0} \Big|^{1/k} \tag{6.6}$$

Here $f[i]$ is a current signal obtained from smoothed charge silicon output signal after baseline elimination and i is ith sampling point. Summing is made on the time interval of sampling points between first (i_{start}) and last (i_{stop}) point fulfilled condition of threshold overcoming, which defines area of pulse occurrence.

$$m_2 = \Big| \sum_{i=i_{start}}^{i_{stop}} \frac{f[i][(i - i_{start}) - m_1]^2}{m_0} \Big|^{1/2} \tag{6.7}$$

$$m_3 = \Big| \sum_{i=i_{start}}^{i_{stop}} \frac{f[i][(i - i_{start}) - m_1]^3}{m_0} \Big|^{1/3} \tag{6.8}$$

Calculation of moment m_2 and m_3 (eq.6.7 and eq.6.8) helped Barlini group separate two isotopes of argon element how it is presented on the left panel of Figure 6.12. More efficient separation was made by their group by projecting plot along a perpendicular direction to the two major-axes of the

moments distributions - x' marked on left panel of Figure 6.12 and defined by equation 6.9.

$$x' = (m_2 - x_0)cos\theta + (m_3 - y_0)sin\theta \tag{6.9}$$

Where θ is a rotation angel between new reference system (x', y') and old one(m_2, m_3). Right panel of the Figure 6.12 is showing results obtained by making above transformation.

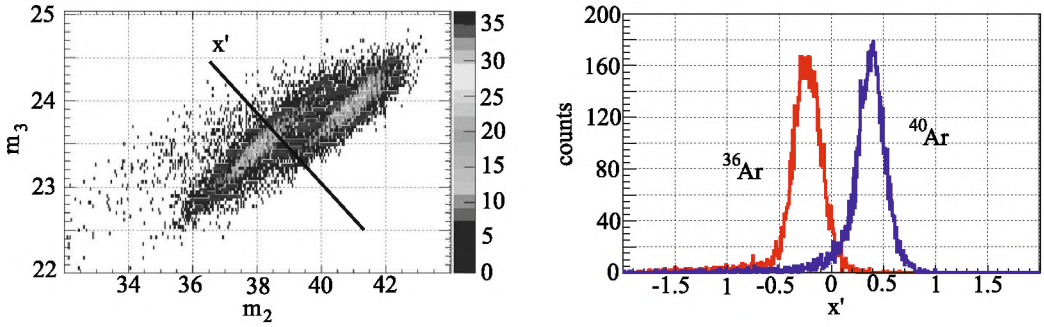

Figure 6.12: ^{36}Ar and ^{40}Ar isotopes separation by using moments m_2 and m_3, details about both panels are presented in the text [104].

Separation presented above encouraged to attempt a similar pulse shape discrimination test on data collected from Si detectors during the experiment to which this work relates.

6.3 Results of data analysis

In this section, five parameters obtained from digital pulse shape analysis for pairs with Si modules will be compared. The correlation shown on the figures contains a comparison of two amplitudes values: amplitude of the charge silicon pulse Amp_q and amplitude of current pulse Amp_i obtained from transformed original Si output signal with use of the least square filter. It is also comparing two moments, second m_2 and third m_3, which were calculated with use of the formulas 6.7 and 6.8 proposed by Barlini group and presented in the previous section. The final examined parameter is a rise time: $\mathrm{RiseT}_{1-99\%}$ calculated on the distance from 1% to 99% of pulse amplitude high.

6.3.1 α, FF & cosmic originate particles localization

Each of presented below Figures (6.13-6.19) contains set of four panels described as **A**, **B**, **C** or **D**. Maps there presented are prepared from events detected and recorded by a single silicon detector (Si 0). On the panels **A** of each figure data collected from open Cf source placed between ΔE and E modules, are presented. The highest density of counts marked by circles is representing 6.1 MeV α localization. On the panels **B** are located data from the same run (using open Cf source) with the additional condition of selection only events with coincidence between ΔE and E detector. This requirement allows determining the fission fragments localization on each of the considered maps. On the **C** panels are located data collected from the experiment - a coincidences events with ACT scintillator as a source of potential SHEs. The last **D** panels are showing localization of the background with high energetic cosmic originate particles. Measurements of them were conducted with a 1 mm thick aluminum layer between both walls of the detectors what provided elimination of coincidence between activated ΔE scintillators and E modules.

On the all presented here figures separation between 6.1 MeV α and fission fragments is quite well visible. The problem appears with cosmic radiation elimination. Best cosmic originate particle discrimination is visible in figures with m_2 and m_3 parameters, especially in one which compares them both (Figure 6.13). Most of the data collected during the experiment are gathered around α particles region but also in the area of the cosmic radiation. The number of cosmic originate particles observed in data is a result of long measurement conducted with detectors ΔE-E faced each other. Nevertheless because of similar measurement duration time for data presented on **C** and **D** panels (over a dozen days) amount of collected cases suggest that events registered in this region do not all came from cosmic radiation, so it can not be definitely eliminated in an analytic way.

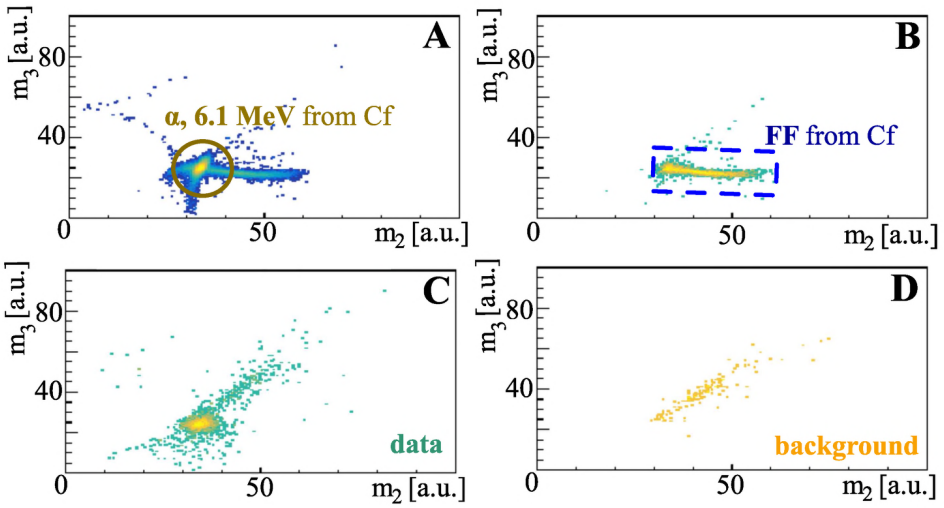

Figure 6.13: Maps of moments m_2 vs m_3 correlation for pair with Si module. Panel **A** is showing localization of 6.1 MeV α particles from Cf source, panel **B** is showing localization of FF from Cf source. Panel **C** is a map for typical data collected during experiment. Panel **D** is showing localization of background (especially high energetic comics) events. For more details see text.

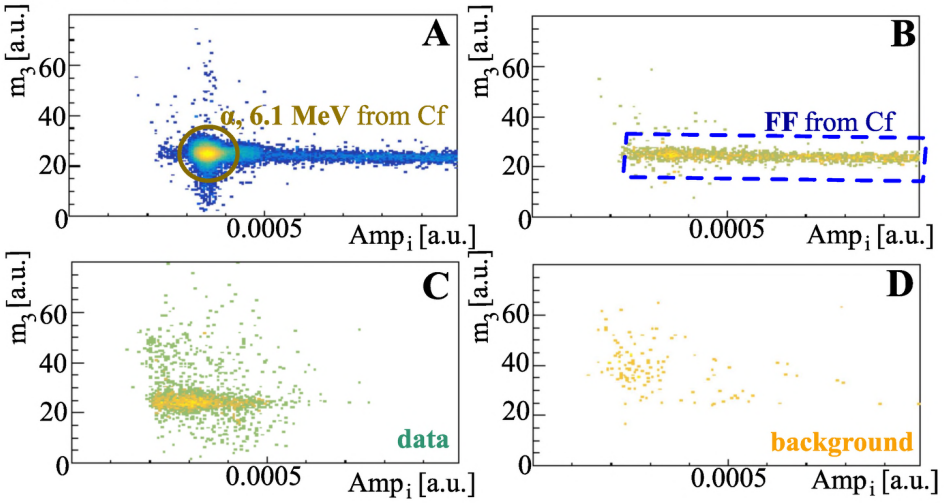

Figure 6.14: Maps of correlation between m_3 and Amp_i value for pair with Si module. Panel **A** is showing localization of 6.1 MeV α particles from Cf source, panel **B** is showing localization of FF from Cf source. Panel **C** is a map for typical data collected during experiment. Panel **D** is showing localization of background (especially high energetic comics) events. For more details see text.

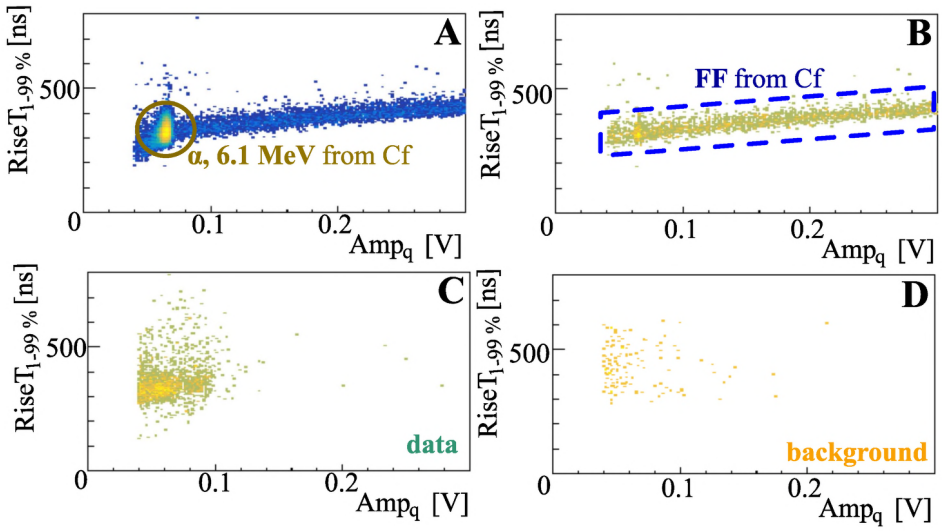

Figure 6.15: Maps of $RiseT_{1-99\%}$ and Amp_q values correlation for pair with Si module. Panel **A** is showing localization of 6.1 MeV α particles from Cf source, panel **B** is showing localization of FF from Cf source. Panel **C** is a map for typical data collected during experiment. Panel **D** is showing localization of background (especially high energetic comics) events. For more details see text.

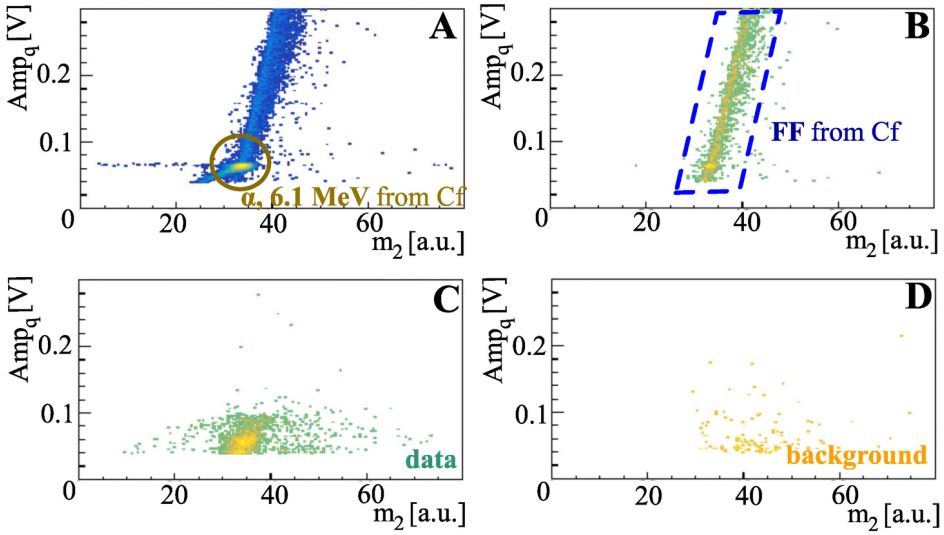

Figure 6.16: Maps of correlation between Amp_q and m_2 values for pair with Si module. Panel **A** is showing localization of 6.1 MeV α particles from Cf source, panel **B** is showing localization of FF from Cf source. Panel **C** is a map for typical data collected during experiment. Panel **D** is showing localization of background (especially high energetic comics) events. For more details see text.

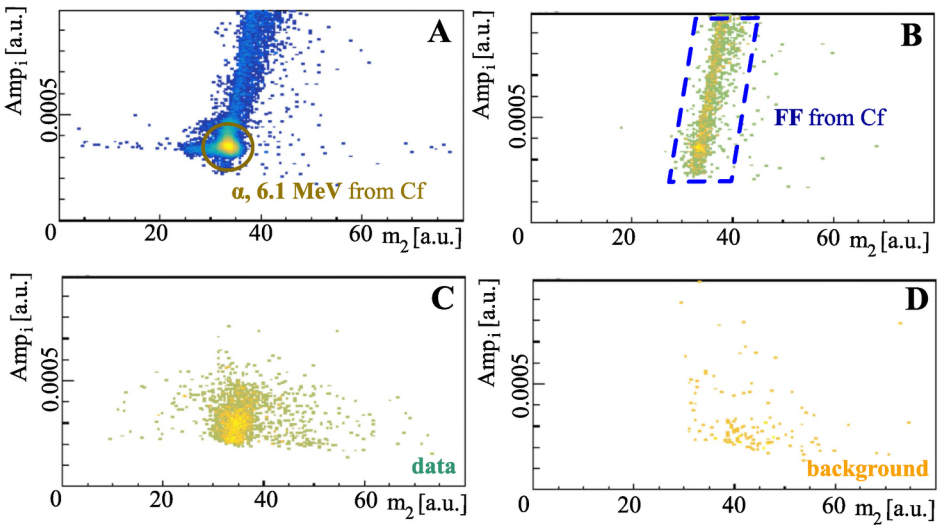

Figure 6.17: Maps of correlation between Amp_i and m_2 values for pair with Si module. Panel **A** is showing localization of 6.1 MeV α particles from Cf source, panel **B** is showing localization of FF from Cf source. Panel **C** is a map for typical data collected during experiment. Panel **D** is showing localization of background (especially high energetic comics) events. For more details see text.

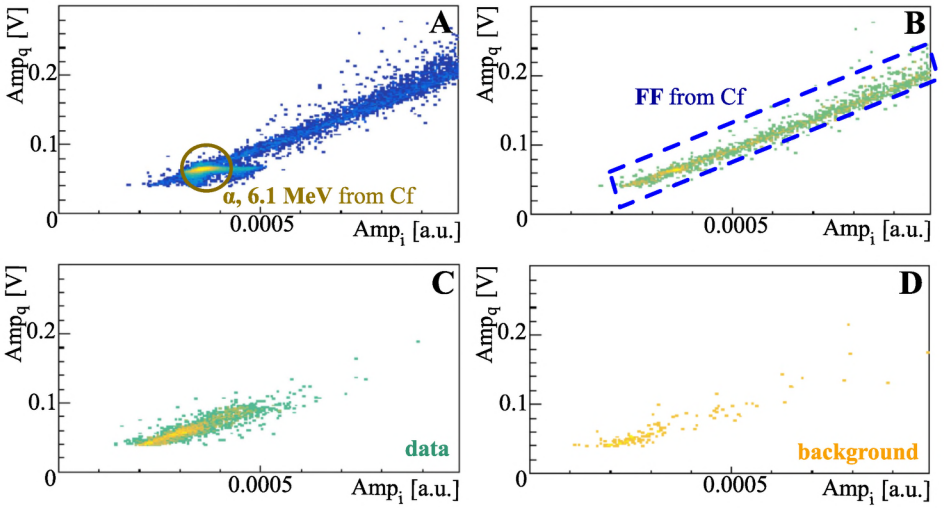

Figure 6.18: Maps of correlation between values of the Amp_q and Amp_i for pair with Si module. Panel **A** is showing localization of 6.1 MeV α particles from Cf source, panel **B** is showing localization of FF from Cf source. Panel **C** is a map for typical data collected during experiment. Panel **D** is showing localization of background (especially high energetic comics) events. For more details see text.

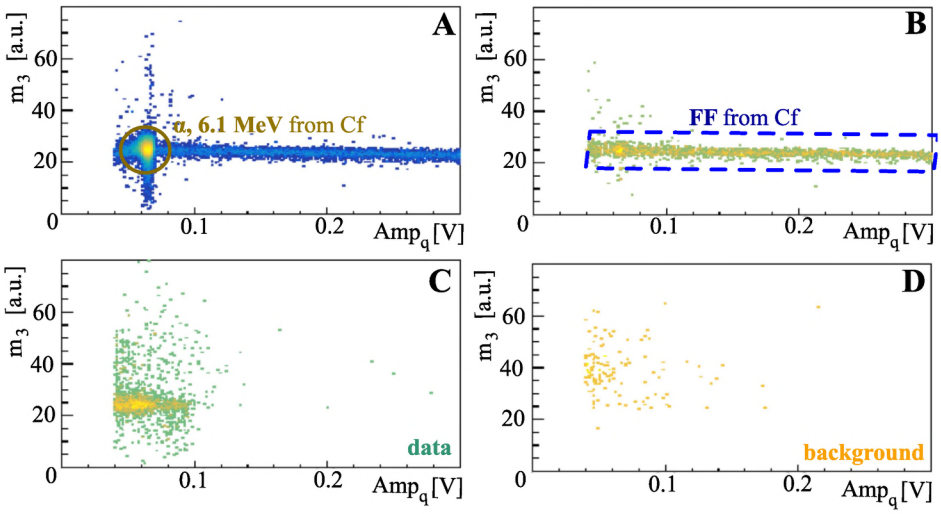

Figure 6.19: Maps of Amp_q and m_3 values correlation for pair with Si module. Panel **A** is showing localization of 6.1 MeV α particles from Cf source, panel **B** is showing localization of FF from Cf source. Panel **C** is a map for typical data collected during experiment. Panel **D** is showing localization of background (especially high energetic comics) events. For more details see text.

6.3.2 Searching for α particles candidates

The most effective method of searching pulses related with α particles or FF emitted from heavy element deposited inside ACT scintillator of the ΔE detector is to combine interesting events form $\mathrm{Amp}_{\Delta E}$ - E maps with a different combination of maps presented in the previous section.

As a reminder, interesting events are considered to be a coincidence for which low pulses were registered in the ΔE detector (according to the table 6.1), and high energy (i.e. from range 10 MeV - 20 MeV) was detected in E detector. During the experiment, there were found several events in Si pairs and over fifty cases in pairs with NACT scintillator which fulfilled this condition.

In silicon pairs from measurement lasting 87 days 26 such events were selected, where 9 of them were found in Si 0. Due to problem with distinguishing α particles, fission fragments or cosmic originating particles only by recorded energy next step of the analysis was comparing described before parameters (m_2, m_3, Amp_i, Amp_q, $RiseT_{1-99\%}$) for those events with DSP maps prepared with use of the open Cf source like in case of **A** panels in a set of figures from the previous section (Figures 6.13-6.19). The effects of this juxtaposition are showed in Figure 6.20.

Mentioned above nine interesting events are marked in Figure 6.20 by orange dots. Despite their localization on the maps close to the region of fission fragments it can be said that we have a distinction between FF and particles considered as interesting. This is because all fission-like events with above described energy conditions are situated on the main FF tail on all of presented here panels while interesting events are above them in three considered panels. Special attention requires a group of six events marked by dashed circle with E energy on the level of 10 - 14 MeV. Their are located on panels **A)**, **C)** and **F)**, in an area slightly different from that for low-energy αs, FFs, or cosmic originate particles and other background events. What actually may suggest that observed events correspond to high energy α particles and m_3 can be used as a discrimination parameter.

The approximate values of energy, amplitudes (current and charge), moments (m_2 and m_3) and the rise time (in range of 1% to 99% of registered pulse high) calculated for these 9 events together with another 17 cases recorded in tested run from the remaining Si pairs are presented in the table 6.3.

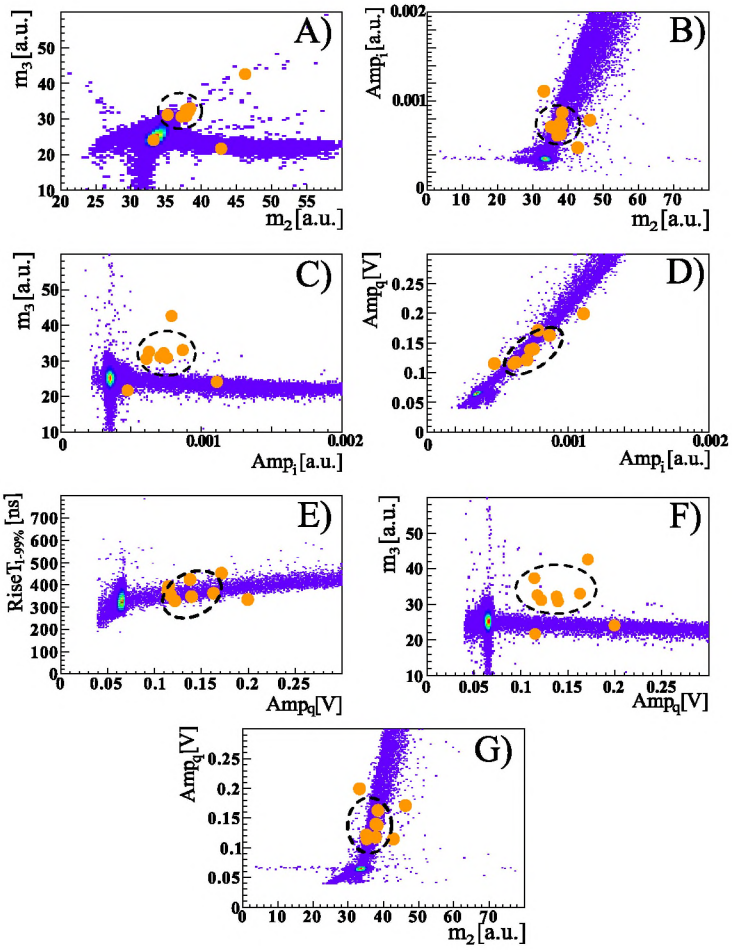

Figure 6.20: Comparison of 9 interesting events from the Si 0 detector (orange dots) with ^{252}Cf source decays map on the seven types of DSP maps [99].

To compare if considered events are origin form α particles from SHE decay the same tables of data (with the same energetic condition) were prepared for two types of background measurement.

In table 6.4 are presented 3 cases of background events selected from cosmic originate particles measuring run after 17 days of measurement with 1 mm thick Al layer between ΔE and E wall, while in table 6.5 are shown 3 background events from 39 day lasting run with clean ΔE scintillators. How it can be seen in both cases there are detectors where no background events from interesting energy areas were registered.

Si No.	m_2 [a.u.]	m_3 [a.u.]	Amp_q [V]	Amp_i [a.u.]	RiseT [ns]	E [MeV]	$Amp_{\Delta E}$ [V]
Si 0	35.1947	31.1724	0.1217	7.0961×10^{-4}	328	10.6073	0.0336
	37.8271	32.514	0.1173	6.2844×10^{-4}	354	10.2335	0.0456
	33.1976	24.0408	0.1994	11.1089×10^{-4}	334	17.2403	0.0290
	37.8815	30.7737	0.1394	7.561×10^{-4}	348	12.1203	0.0688
	46.2292	42.5986	0.1713	7.8829×10^{-4}	452	14.8416	0.0546
	38.4095	33.0103	0.163	8.6846×10^{-4}	362	14.1309	0.0314
	38.2546	32.1789	0.1378	7.3351×10^{-4}	424	11.9809	0.0146
	42.8077	21.6628	0.1151	4.7729×10^{-4}	393	10.0439	0.0417
	37.2773	30.7692	0.1151	6.0058×10^{-4}	367	10.0408	0.0883
Si 1	69.397	74.9545	0.1133	3.5309×10^{-4}	717	10.772	0.0428
	71.4702	56.639	0.1148	4.7013×10^{-4}	634	10.9104	0.0651
	93.4745	65.2817	0.1227	2.3463×10^{-4}	830	11.6681	0.0457
Si 2	62.9807	51.1299	0.1552	4.6483×10^{-4}	641	14.1705	0.0409
	74.2709	63.5351	0.2018	5.2352×10^{-4}	730	18.4261	0.0469
	61.4852	44.3829	0.1507	4.4167×10^{-4}	559	13.7551	0.1011
	76.7207	62.078	0.1106	2.7169×10^{-4}	724	10.0966	0.0773
	76.3821	64.9541	0.1372	3.5902×10^{-4}	753	12.5268	0.0199
	76.9055	74.0931	0.1117	3.2321×10^{-4}	755	10.1896	0.0395
Si 5	20.3239	65.3646	0.1176	6.3854×10^{-4}	559	10.5456	0.0550
Si 6	51.4288	42.2145	0.1147	4.4277×10^{-4}	551	10.0835	0.0748
	48.066	39.3185	0.1226	5.0838×10^{-4}	430	10.722	0.0653
	40.1174	33.107	0.1245	5.8745×10^{-4}	395	10.9384	0.0826
	38.5592	31.6852	0.1379	6.7626×10^{-4}	371	12.1148	0.0849
	40.0821	35.9396	0.1701	8.9065×10^{-4}	410	14.9341	0.0708
	37.3014	30.441	0.1386	6.9653×10^{-4}	375	12.1775	0.0788
	57.2825	61.1146	0.132	5.2264×10^{-4}	706	11.5959	0.0317

Table 6.3: Parameters of 26 interesting events chosen from area of interest for Si pairs in 87 days long run with irradiated ACT scintillators.

Si No.	m_2 [a.u.]	m_3 [a.u.]	Amp_q [V]	Amp_i [a.u.]	RiseT [ns]	E [MeV]	$Amp_{\Delta E}$ [V]
Si 0	36.622	34.1639	0.1348	7.7883×10^{-4}	361	11.7251	0.0172
Si 2	78.7546	68.671	0.1657	4.6672×10^{-4}	737	15.132	0.0474
Si 6	80.371	61.298	0.1369	3.1852×10^{-4}	722	12.0299	0.0611
In Si: 1, 5 - events not found							

Table 6.4: Parameters of background events for cosmic originate particles measurements chosen for five Si pairs from area of interest.

Si No.	m_2 [a.u.]	m_3 [a.u.]	Amp_q [V]	Amp_i [a.u.]	RiseT [ns]	E [MeV]	$Amp_{\Delta E}$ [V]
Si 1	85.867	77.9353	0.1185	4.4942×10^{-4}	781	11.2711	0.0675
	79.3107	71.6395	0.1133	3.0064×10^{-4}	812	10.7734	0.0668
Si 6	36.7646	24.5269	0.1168	6.4254×10^{-4}	404	10.2644	0.0286
In Si: 0, 2, 5 - events not found							

Table 6.5: Parameters of background events collected in run with clean scintillators and chosen for five Si pairs from area of interest.

For pairs with NACT scintillators were made selection based on amplitude and energy analysis. From 87 day long run measuring irradiated scintillators in area of interest 53 events were found. Their parameters can be found in Table 6.6. From tests conducted for background measurement statistics were as fallow: for 17 days long run with Al wall it was 2 events, and for 39 days long run with clean ΔE scintillators it was 13 events. Parameters of those cases can be found in the tables, Table 6.7 and Table 6.8. Presented data were obtained from four pairs with NACT scintillators (the other four were out of order). The number of selected data from this type of detector pairs is strongly dependent on amplitude into energy transformation function for E detector. The number of counts could be even lower if the adjusted function would be even more precise.

E $[MeV]$	**Amp**$_{\Delta E}$ $[V]$
NACT No. 11	
11.2257	0.0174
10.9494	0.0386
15.9134	0.0287
11.8381	0.0215
11.4759	0.0340
14.3523	0.0123
10.5363	0.0238
15.4728	0.0230
16.4326	0.0686
12.6112	0.0552
10.4926	0.0439
10.3011	0.0596
12.5723	0.0721
13.8322	0.0408
11.3265	0.0384
11.9648	0.0279
10.0698	0.0641
11.8808	0.0208
11.5182	0.0165
11.2989	0.0111
10.6489	0.0411
12.7500	0.0593
10.6306	0.0175

E $[MeV]$	**Amp**$_{\Delta E}$ $[V]$
NACT No. 13	
11.4175	0.0598
10.6855	0.0173
10.6277	0.0685
11.2914	0.0436
11.1436	0.0362
10.3245	0.0637
17.1732	0.0182
10.4185	0.0210

E $[MeV]$	**Amp**$_{\Delta E}$ $[V]$
NACT No. 14	
11.0789	0.0358
10.7126	0.0436
11.3611	0.0162
11.4307	0.0285
11.5806	0.0694
10.3733	0.0326
11.4011	0.0116
11.9291	0.0300

E $[MeV]$	**Amp**$_{\Delta E}$ $[V]$
NACT No. 15	
12.4999	0.1071
16.3865	0.1599
10.5050	0.1587
17.1368	0.1245
10.8807	0.0139
10.1996	0.0456
10.0386	0.0123
11.5868	0.0304
10.8275	0.1172
12.0119	0.1406
11.2021	0.1204
10.5942	0.1560
10.0878	0.1416
10.0013	0.1208
14.1789	0.1565

Table 6.6: Energies of pulses registered by NACT E detectors and amplitudes of pulses saved in ΔE ACT detector. Data were collected for run with irradiated scintillators and chosen for four ACT - NACT pairs from area of interest.

E $[MeV]$	**Amp**$_{\Delta E}$ $[V]$
NACT No. 11	
10.0207	0.0520

E $[MeV]$	**Amp**$_{\Delta E}$ $[V]$
NACT No. 13	
11.8955	0.0207
14.1020	0.0217
12.1373	0.0141
13.7037	0.0600

E $[MeV]$	**Amp**$_{\Delta E}$ $[V]$
NACT No. 14	
10.0258	0.0185
12.0119	0.0543

E $[MeV]$	**Amp**$_{\Delta E}$ $[V]$
NACT No. 15	
12.6511	0.1057
11.5316	0.1174
11.5036	0.0307
10.6157	0.0248
10.2465	0.0371
11.7340	0.0368

Table 6.7: Table of energies of pulses registered by NACT E detectors and amplitudes of pulses saved in ΔE ACT detector. Data were collected for clean ΔE scintillators and chosen for four ACT - NACT pairs from area of interest.

Due to different run times to compare the number of counts from considered energy areas another table was prepared. It contains information about

E $[MeV]$	**Amp**$_{\Delta E}$ $[V]$
NACT No. 11	
no events found	

E $[MeV]$	**Amp**$_{\Delta E}$ $[V]$
NACT No. 13	
no events found	

E $[MeV]$	**Amp**$_{\Delta E}$ $[V]$
NACT No. 14	
13.7247	0.0493

E $[MeV]$	**Amp**$_{\Delta E}$ $[V]$
NACT No. 15	
10.8139	0.0178

Table 6.8: Table of energies of pulses registered by NACT E detectors and amplitudes of pulses saved in ΔE ACT detector. Data were collected in run with Al wall between ΔE and E modules and chosen for four ACT - NACT pairs from area of interests.

the number of events detected in the individual detector pair with its normalized counting rate per day. The upper part of the Table 6.9 was prepared for pairs with Si E detector, while the bottom one contains information for pairs with NACT E scintillators.

		Cosmics measurements with Al wall - 17 days long		**Background measurements with clean scintillators - 39 days long**		**Measurements with irradiated scintillators - 87 days long**	
Si No.		***Coinc.***	***Int. Evt.***	***Coinc.***	***Int. Evt.***	***Coinc.***	***Int. Evt.***
Si 0:	***cts***	142	1	451	0	10244	9
	cts/d	8.354	0.059	11.564	0	117.747	0.103
Si 1:	***cts***	66	0	330	2	4109	3
	cts/d	3.882	0	8.462	0.051	47.229	0.034
Si 2:	***cts***	102	1	377	0	5518	6
	cts/d	6	0.059	9.667	0	63.425	0.069
Si 5:	***cts***	95	0	230	0	11709	1
	cts/d	5.588	0	5.897	0	134.586	0.012
Si 6:	***cts***	148	1	412	1	6090	7
	cts/d	8.706	0.059	10.564	0.026	70	0.08
NACT No.		***Coinc.***	***Int. Evt.***	***Coinc.***	***Int. Evt.***	***Coinc.***	***Int. Evt.***
NACT 11:	***cts***	495	0	1218	1	7768	23
	cts/d	29.118	0	31.231	0.026	89.287	0.264
NACT 13:	***cts***	540	0	1048	4	7273	8
	cts/d	31.765	0	26.872	0.103	83.598	0.092
NACT 14:	***cts***	428	1	1139	2	5951	8
	cts/d	25.176	0.059	29.205	0.051	68.402	0.092
NACT 15:	***cts***	380	1	1373	6	7369	15
	cts/d	22.353	0.059	35.205	0.154	84.701	0.174

Table 6.9: Number of counts (cts) and counts per day (cts/d) for examined detector pairs: five with Si and four with NACT E detectors. In this table are presented two groups of collected events: total number of coincidence in one detector pair (Coinc.) and events selected for those pairs as interesting ones (Int. Evt.).

From Table 6.9, it is well seen that for both types of pairs counting rate per day for the full number of coincidences from measurement conducted

with use of the irradiated ACT scintillators is higher than in the case of background measurement with clean ΔE scintillators. It means that after use of the MNT reactions some long-lived elements may be deposited inside of the ACT scintillators. What is more, it seems that high energetic cosmic originate particles or γs from natural radiation do not constitute a significant part of the collected data, which is visible in the counting rate calculated for interesting events selected with considered energy condition. Obtained counting rates differ little for each module, it is especially well seen in the comparison of counting rate for pairs with Si and NACT scintillators.

Because of the discrepancy between all modules and different types of detector pairs for those three kinds of measurement figures with normalized counting rate per day calculated over single pair were prepared. Figure 6.21 presents the normalized counting rate per day calculated for single pair over five tested Si ΔE-E detectors, while Figure 6.22 was prepared for calculation over four NACT E pairs. By orange squares are marked calculations for interesting events, by blue squares are presented calculations for background events from run with clean scintillators, and green squares corespondents to calculations for background from cosmic radiation measurement.

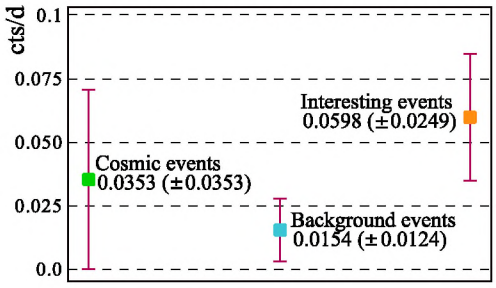

Figure 6.21: Normalized count rate per day (with statistical error over number of counts) for single Si pair calculated for events selected from region of interest.

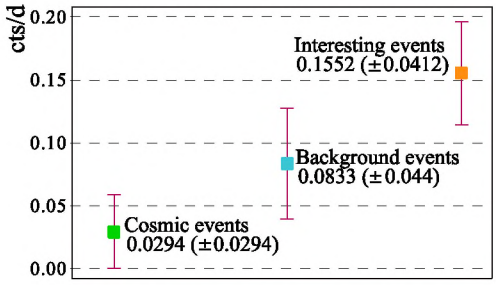

Figure 6.22: Normalized count rate per day (with statistical error over number of counts) for single NACT pair of detector calculated for events selected from region interest.

The difference between the counting rate for Si and NACT E pairs is a factor 3, and the possible reason for such effect is a combination of scintillators energy resolution and substantial uncertainty of the used energy calibration function. Important in this comparison is fact that even with normalized errors calculated over the number of counts in both types of detectors, with Si and with NACT scintillators counting rate for run with irradiated scintillator is higher than for both background measurements. It gives hope that the reaction of multinucleon transfer is a proper way for long-lived superheavy elements creation.

The disparity of counting rate for NACT and Si pairs may be related with inaccurate energy calibration and use of advanced pulse shape analysis for those data may improve selecting interesting events process. In the case of Si detectors use of the m_3 parameter seams to be a well chosen approach for help with of discerned selected events from fission fragments. Discrimination from background events requires further analysis. Unfortunately at the moment in this experiment there are no tools to identify collected data.

Obtained results are encouraging to prepare a new project which will conduct all tests with additional anti-coincidence detector. It may exclude all unwanted possibilities related to background influence. A good choice would be also adding control pair of modules with clean ΔE detectors to the setup, which in the same run time will measure only background impact. Without these steps occurring background events in the area of αs from SHEs can not be completely rejected, even if for most of the examined modules its counting rate is lower than for run with irradiated scintillators. Moreover, the new experiment could broaden the lifetime range of the SHEs sought. Immediately examined irradiated by products of the MNT reactions material will allow extension of the SHEs lifetime range from a several ns to several years by including all lifetimes between: several minutes, days or months.

7 | Conclusions

Research on the superheavy elements has been going on for 60 years. During this time, the complete fusion method was used for their production, which was tested in both possible variants (cold and hot fusion). Despite the very precise conditions that had to be met for the fusion to occur (central collision, adequate collision energy), it has so far been the most effective way to produce new SHEs. This efficiency was supported by technological development. Currently, however, the cross section for the production of heavier elements by the traditional method is decreasing. This happens for both hot and cold fusion. The cross section for producing an element with Z greater than 118 is estimated as 0.1 pb.

However, this is not the only obstacle standing in the way of production for heavier SHEs. The problem seems to be the lack of possibility to prepare sufficiently heavy targets and beams of appropriate intensity used in such experiments. Fusion of the element Es (from the target) with Ti (from the beam) is considered as the most promising reaction to produce the next SHE. ORNL, the only laboratory producing targets for SHE experiments, is able to obtain only a small amount of Es, in the order of μg, when milligrams of it are needed. Use of the Ti beam requires also increasing its intensity to enlarge possibility for SHE creation which is related to accelerator development.

The above mentioned difficulties have led scientists to consideration of other possible method for new superheavy nuclei production, multinucleon transfer reactions. MNT does not require central collisions, because transfer of many nucleons can appear after the peripheral collision of the projectile with target nuclei, which gives it an advantage over complete fusion. It also may open a pathway for creation neutron-reach elements, which can lead to obtaining nuclei from the island of stability.

Conducted during my PhD studies researches had pilot character and this doctoral dissertation was meant to introduce multinucleon transfer as an alternative path for SHEs creation. It was focused on presenting two types of detector systems prepared for searching short- and long-lived SHEs. In both cases, the obtained results suggest that the tested method is hope for the production of new superheavy elements. In both cases also, received data has shown the necessity of detectors development, especially the scintillator-based modules. Their inability to obtain better energy information for registered particles is presently the biggest difficulty in post-measurement analysis.

Searching for short-lived superheavy elements by the Jagiellonian Univer-

sity group has a long history. This time factor and big collaboration with Texas A& M University allowed to conduct different updates of used detector systems. I had the opportunity to join the UJ group in 2014 for the last two experiments which allowed me to work with two different active catchers.

First SHE detector with which I was working used AC based on 63 modules with BC-418 scintillators. Results from analyzing data collected during the experiment in 2015 show that through time distance discrimination it was possible to select several events that could be classified as fragments of alpha chains. Unfortunately because of the energy resolution of the used AC modules, it was impossible to identify those elements. Nevertheless, it shows that heavy or superheavy elements with a lifetime on the level of ns can be created through a multinucleon transfer reactions. In addition, its unique construction has allowed the use of AC individual modules together with the irradiated by MNT reactions products scintillators as the base for conducting an experiment focused on long-lived SHEs.

The second AC detector, used in 2016, was made of two types of modules, built with 40 YAP and 4 BC-418 scintillators. YAP detectors were chosen because of their better energy resolution and easiness of DPSA conducting. The use of slightly slower detectors as the price of better information about the energy of the registered particles did not negatively affect the results. Also for this detection setup, it was shown that the MNT reactions can be considered as an alternative path for SHEs production. Several events recorded by acquisition were considered as superheavy elements candidates. It was even possible to estimate the region of Z values for these elements ($Z \in [106,114]$). Four BC-418 modules attached at large angles from the beam axis also provided evidence that the MNT reactions are effective. Despite the difficulties associated with their energetic properties, thanks to saving information about beam modes and RF period, the results obtained seem promising. In collected data, there were found other several events that can correspond to the short-lived SHEs. Their identification, however, can not be made due to the same reasons as in the first experiment from 2015.

Nevertheless, those promising results from all experiments related to searching short-lived nucleus were a motivation for conducting further tests on SHEs creation with a larger lifetime range.

The experiment focused on long-lived superheavy elements is novel. The new experiment required a new detection setup and dedicated for acquisition electronic system, all of it was built at UJ. Prepared detector holder enables easy adjustment of the ΔE and E walls, while used electronics system made possible recording events form all modules when only something interesting is detected. Together with the prepared program, it allowed also online monitoring of the detector work. However, the most important components

of the detection setup are irradiated in 2015 and 2016 by MNT reactions products scintillators. Those BC-418 scintillators are used as a source of a potential heavy or superheavy element with a lifetime on a level of few years.

Obtained results from analysis data presented on the $\mathrm{Amp}_{\Delta E}$ - E maps with additional use of DSP methods for smoothing and calculating variance and skewness indicate that used procedures seams to be adequate for selection interesting events from the recorded data. For both types of ΔE-E detector pairs there were found several candidates for SHEs, what is additionally indicated by higher counting rate per day for measurements conducted with irradiated scintillators than for measurements for background. Events registered in Si E detector deserve special attention due to possibility of their distinction from fission events by use of the m_3 parameter. However, their location on DSP maps could not eliminate the possibilities of its cosmic radiation origin. The best solution for improving data identification is to modify detection system by adding anti-coincidence detectors, with thick BC-400 scintillators, which will report information from possible cosmic originate particles interruption. This step should greatly improve quality of collecting data and it is opening possibility for preparing new project were SHEs with enlarged range of lifetime (full time spectrum from ns to years) could be searched. The process of upgrading the detection setup is currently underway. However, it is worth to underline that Si detectors as E modules were a good choice. They ensure the greater possibility to carry out the pulse shape analysis, thanks to which they return more information about recorded events than BC-418 scintillators. BC-418 scintillators as material for irradiation should be more carefully considered, and maybe their should be replaced by YAP detectors in next experiment.

Those promising results obtained through years of experiments on superheavy elements allows to think that the MNT reactions can be treated as real competition to the traditional way of new element creation, complete fusion. It has potential not only in the case of short-lived SHEs searches but also long-lived SHEs. In both cases, however, it required detectors development and further experiments.

Acknowledgements

First of all, I would like to thank prof. dr hab. Roman Płaneta, prof. dr hab. Zbigniew Majka and dr hab. Andrzej Wieloch without whose this thesis would not exist. I thank dr Wieloch for a warm welcome in Department of Hot Matter Physics of the Jagiellonian University seven years ago, and for years of common work on searching superheavy elements. I am grateful to prof. Majka for enabling me to join the collaboration which gave me the opportunity to meet many talented scientists and the scientific environment itself. Special thanks to my supervisor, prof. Płaneta for everything, he has done for me in the last months. I am grateful for his support, and all valuable comments and observations which allowed me to complete this thesis.

I also would like to thank Konrad Łojek and Marek Adamczyk without whose work on electronics and detectors construction none of described in this dissertation experiments would take place. I am also grateful for their positiveness and making experimental physics so vivid.

I am grateful to the whole TAMU group for giving me the opportunity of common work during the experiments and for the experience which I gained thanks to them.

Special thanks to dr hab. Janusz Brzychczyk, dr hab. Paweł Staszel, dr Marcin Misiaszek and all others form FAIS G-0 segment, for all inspiring and amusing corridor talks.

I also thank my colleagues whose presence made my PhD studies enjoyable and fulfilled with friendships. Special thanks to Natalia Niesyt, dr Irene Dedes Nonell, dr Katarzyna Sowa, Monika Pawlik-Niedźwiecka, dr Magda Skurzok, Katarzyna Kutera, Katarzyna Lipiecka, Łukasz Bodek, dr Szymon Niedźwiecki and Paweł Grądek.

Finally, I would like to thank my family for all support and love which they gave me, to my parents Ewa and Lech Zelga, to my aunt Elżbieta Hardzina and my grandparents Salomea and Józef Hardzina. Thank you for believing in me and my dreams. Grandpa, I finally did it.

I would like to end this work with full of motivation words that in every single day of the passing year encouraged me to face even most demanding challenges:

For the first time, I'm thinking past tomorrow,
And I am not throwing away my shot.

HAMILTON, Lin-Manuel Miranda

This work was supported by grants: DSC 2018 from the Ministry of Science and Higher Education 7150/E-338/M/2018, No. K/DSC/005314; DSC 2019 at WFAIS UJ, No. 2019-N17/MNS/000049; by the National Science Center in Poland, contract no. UMO-2012/04/A/ST2/00082; and by the U.S. Department of Energy under Grant No. DE-FG03-93ER40773 and by the Robert A. Welch Foundation under Grant A0330.

A | Appendixies

In section presented below additional information about selected subjects can be found. List of their content looks as follows:

A.1 Decay mode and half-life for each actinide.

Element	Decay mode	Isotope	Half-life ($t_{1/2}$)
Neptunium $_{93}$Np	α	^{225}Np	3,6 ms
		^{226}Np	35 ms
		^{227}Np	0,51 s
	EC + β^+	^{228}Np	61,4 s
	α	^{229}Np	4 min
	EC + β^+	^{230}Np	4,6 min
		^{231}Np	48,8 min
		^{232}Np	14,7 min
		^{233}Np	36,2 min
		^{234}Np	4,4 d
		^{235}Np	396,1 d
		^{236}Np	153 × 10^3 y
	α	^{237}Np	2,14 × 10^6 y
	β^-	^{238}Np	2,099 d
		^{239}Np	2,36 d
		^{240}Np	61,9 min
		^{241}Np	13, 9 min
		^{242}Np	2,2 min
		^{243}Np	1,85 min
		^{244}Np	2,29 min
Plutonium $_{94}$Pu	α	^{228}Pu	1,1 s
		^{229}Pu	90 s
		^{230}Pu	102 s
	EC + β^+	^{231}Pu	8,6 min
		^{232}Pu	33,8 min
		^{233}Pu	20,9 min
		^{234}Pu	8,8 h
		^{235}Pu	25,3 min
	α	^{236}Pu	2, 86 y
	EC + β^+	^{237}Pu	45,64 d
	α	^{238}Pu	87,7 y
		^{239}Pu	2,4 × 10^4 y
		^{240}Pu	6,56 × 10^3 y
	β^-	^{241}Pu	14,33 y
	α	^{242}Pu	3,75 × 10^5 y
	β^-	^{243}Pu	4,96 h
	α	^{244}Pu	8,13 × 10^7 y
	β^-	^{245}Pu	1,5 h
		^{246}Pu	10,84 d
		^{247}Pu	2,27 d

Element	Decay mode	Isotope	Half-life ($t_{1/2}$)
Americium $_{95}$Am	α	^{223}Am	5 ms
		^{229}Am	0,9 s
	EC + β^+	^{230}Am	31 s
		^{232}Am	79 s
	α	^{233}Am	3,2 min
	EC + β^+	^{234}Am	2,32 min
		^{235}Am	10,3 min
	α	^{236}Am	3,6 min
	EC + β^+	^{237}Am	73,6 min
		^{238}Am	98 min
		^{239}Am	11,9 h
		^{240}Am	50,8 h
	α	^{241}Am	432,6 y
	β^-	^{242}Am	16,02 h
	α	^{243}Am	7,36 × 10^3 y
	β^-	^{244}Am	10,1 h
		^{245}Am	2,05 h
		^{246}Am	39 min
		^{247}Am	23 min
	SF	^{248}Am	-
Curium $_{96}$Cm	α	^{233}Cm	ND
		^{234}Cm	51 s
	ND	^{235}Cm	ND
	α	^{236}Cm	ND
	ND	^{237}Cm	ND
	EC + β^+	^{238}Cm	2,2 h
		^{239}Cm	2,7 h
	α	^{240}Cm	27 d
	EC + β^+	^{241}Cm	32,8 d
	α	^{242}Cm	162,8 d
		^{243}Cm	29,1 y
		^{244}Cm	18,1 y
		^{245}Cm	8,42 × 10^3 y
		^{246}Cm	4,71 × 10^3 y
		^{247}Cm	1,56 × 10^7 y
		^{248}Cm	3,48 × 10^5 y
	β^-	^{249}Cm	64,15 min
	SF	^{250}Cm	8,3 × 10^3 y
	β^-	^{251}Cm	16,8 min
	ND	^{252}Cm	2 d

Element	Decay mode	Isotope	Half-life ($t_{1/2}$)
Berkelium $_{97}$Bk	α	^{233}Bk	21 s
		^{234}Bk	140 s
	EC + β^+	^{236}Bk	22 s
		^{238}Bk	144 s
		^{239}Bk	ND
	SF	^{240}Bk	4,8 min
	α	^{241}Bk	4,6 min
	EC + β^+	^{242}Bk	7 min
		^{243}Bk	4,6 h
		^{244}Bk	4,35 h
		^{245}Bk	4,95 d
		^{246}Bk	1,8 d
	α	^{247}Bk	1,38 × 10^3 y
	α	^{248}Bk	23,7 h
	EC + β^-		9 y
	β^-	^{249}Bk	330 d
		^{250}Bk	3,2 h
		^{251}Bk	55,6 min
	ND	^{252}Bk	ND
	ND	^{253}Bk	10 min
Californium $_{98}$Cf	SF	^{237}Cf	2,1 s
		^{238}Cf	21,1 ms
	α	^{239}Cf	39 s
		^{240}Cf	0,96 min
	EC + β^+	^{241}Cf	378 min
	α	^{242}Cf	3,7 min
	EC + β^+	^{243}Cf	10,7 min
	α	^{244}Cf	19,4 min
	EC + β^+	^{245}Cf	45 min
	α	^{246}Cf	35,7 h
	EC + β^+	^{247}Cf	3,11 h
	α	^{248}Cf	333,5 d
		^{249}Cf	3,51 × 10^2 y
		^{250}Cf	13,08 y
		^{251}Cf	8,98 × 10^2 y
		^{252}Cf	2,65 y
	β^-	^{253}Cf	17,81 d
	SF	^{254}Cf	60,5 d
	β^-	^{255}Cf	85 min
	SF	^{256}Cf	12,3 min

Element	Decay mode	Isotope	Half-life ($t_{1/2}$)
Eisteinium $_{99}$Es	α	^{240}Es	6 s
		^{241}Es	8 s
		^{242}Es	13,5 s
		^{243}Es	21 s
	EC + β^+	^{244}Es	37 s
		^{245}Es	1,1 min
		^{246}Es	7,5 min
	α, EC	^{247}Es	4,55 min
	EC + β^+	^{248}Es	24 min
		^{249}Es	102,2 min
		^{250}Es	8,6 h
		^{251}Es	33 h
	α	^{252}Es	471,7 d
		^{253}Es	20,47 d
		^{254}Es	275,7 d
	β^-	^{255}Es	39,8 d
		^{256}Es	25,4 min
		^{257}Es	7,7 d
Fermium $_{100}$Fm	SF	^{241}Fm	0,73 ms
		^{242}Fm	0,8 ms
	α	^{243}Fm	231 ms
	SF	^{244}Fm	3,3 ms
	α	^{245}Fm	4,2 s
		^{246}Fm	1,54 s
		^{247}Fm	31 s
		^{248}Fm	34,5 s
	EC + β^+	^{249}Fm	2,6 min
	α	^{250}Fm	30 min
	EC + β^+	^{251}Fm	5,30 h
	α	^{252}Fm	25,39 h
	EC + β^+	^{253}Fm	3 d
	α	^{254}Fm	3,24 h
		^{255}Fm	20,07 h
	SF	^{256}Fm	157,1 min
	α	^{257}Fm	100,5 d
	SF	^{258}Fm	370 μs
		^{259}Fm	1,5 s

Element	Decay mode	Isotope	Half-life ($t_{1/2}$)
Mendelevium $_{101}$Md	α	^{245}Md	0.9 ms
		^{246}Md	0.9 s
		^{247}Md	1,2 s
	EC + β^+	^{248}Md	7 s
	α	^{492}Md	21,7 s
	EC + β^+	^{250}Md	52 s
		^{251}Md	4 min
		^{252}Md	2,3 min
		^{253}Md	6 min
		^{254}Md	10 min
		^{255}Md	27 min
		^{256}Md	77,7 min
		^{257}Md	5,52 h
	α	^{258}Md	51,5 d
	SF	^{259}Md	1,6 h
		^{260}Md	31,8 d
Nobelium $_{102}$No	ND	^{248}No	2 μs
	SF	^{250}No	4,2 μs
	α	^{251}No	0,8 s
		^{252}No	2,44 s
		^{253}No	1,62 min
		^{254}No	51 s
	EC + β^+	^{255}No	3,52 min
	α	^{256}No	2,91 s
		^{257}No	24,5 s
	SF	^{258}No	1,2 ms
	α	^{259}No	58 min
	SF	^{260}No	106 ms
		^{262}No	5 ms

Element	Decay mode	Isotope	Half-life ($t_{1/2}$)
Lawrencium $_{103}$Lr	α	^{252}Lr	0,36 s
		^{253}Lr	0,57 s
		^{254}Lr	13 s
		^{255}Lr	31,1 s
		^{256}Lr	27,9 s
		^{257}Lr	4 s
		^{258}Lr	3,92 s
		^{259}Lr	6,2 s
		^{260}Lr	180 s
	SF	^{261}Lr	39 min
		^{262}Lr	4 h
		^{266}Lr	11 h

Markings :

EC - electron capture,
SF - spontaneous fission,
ND - no data,
h - hour,
d - day,
y - year.

Table A.1: Decay mode and half-life for each actinide. All data comes from the website Nuclear Data Services (*https: //www-nds.iaea.org/*).

A.2 Transactinides decay modes and half-lifes.

Element	**Decay mode**	**Isotope**	**Half-life ($t_{1/2}$)**
Rutherfordium $_{104}$Rf	SF	^{253}Rf	48 μs
		^{254}Rf	23 μs
	SF, α, EC + β^+	^{255}Rf	1,68 s
	SF, α	^{256}Rf	6,67 ms
	SF, α, EC	^{257}Rf	4,4 s
	SF, α	^{258}Rf	12 ms
	SF, α, EC	^{259}Rf	2,4 s
	SF	^{260}Rf	21 ms
	SF, α	^{261}Rf	68 s
	SF	^{262}Rf	2,3 s
	SF, α	^{263}Rf	10 min
	SF	^{265}Rf	1 min
		^{267}Rf	ND
Dubnium $_{105}$Db	SF, α	^{255}Rf	1,6 s
	SF, α,EC	^{256}Rf	1,6 s
	SF, α,	^{257}Rf	2,3 s
	α, EC + β^+	^{258}Rf	4,3 s
	α	^{259}Rf	0,51 s
	SF, α, EC	^{260}Rf	1,52 s
	SF, α	^{261}Rf	1,8 s
	SF, α EC + β^+	^{262}Rf	35 s
	SF, α	^{263}Rf	27 s
	ND	^{266}Rf	ND
	SF	^{267}Rf	ND
		^{268}Rf	32 h
	SF, α	^{270}Rf	23 h
Seaborgium $_{106}$Sg	SF, α	^{258}Sg	22,5 s
	SF, α,EC	^{259}Sg	0,29 s
	SF, α	^{260}Sg	3,6 ms
		^{261}Sg	0,23 s
		^{262}Sg	6,9 ms
		^{263}Sg	1 s
		^{264}Sg	37 ms
		^{265}Sg	14,4 s
		^{266}Sg	21 s
	α	^{269}Sg	3,1 min
	SF, α	^{271}Sg	2,4 min

Element	**Decay mode**	**Isotope**	**Half-life ($t_{1/2}$)**
Bohrium $_{107}$Bh	SF, α, EC	^{260}Bh	35 ms
	SF, α	^{261}Bh	12 ms
	α	^{262}Bh	120 ms
	ND	^{263}Bh	ND
	α	^{264}Bh	0,44 ms
	ND	^{265}Bh	ND
	α	^{266}Bh	1,7 s
		^{267}Bh	17 s
		^{270}Bh	ND
	ND	^{271}Bh	ND
	α	^{272}Bh	10 s
		^{274}Bh	54 s
Hassium $_{108}$Hs	α	^{263}Hs	ND
	SF, α	^{264}Hs	0,8 ms
		^{265}Hs	2,0 ms
		^{266}Hs	2,3 ms
		^{267}Hs	52 ms
	α	^{269}Hs	9,7 s
		^{270}Hs	3,6 s
		^{273}Hs	0,76 s
		^{275}Hs	0,15 s
	SF	^{277}Hs	3 ms
Meitnerium $_{109}$Mt	α	^{266}Mt	1,7 ms
		^{268}Mt	21 ms
		^{270}Mt	5 ms
	SF,α	^{274}Mt	0,45 s
	α	^{275}Mt	ND
		^{276}Mt	0,72 s
	SF, α	^{277}Mt	5 s
		^{278}Mt	7,6 s
Darmstadtium $_{110}$Ds	α	^{267}Ds	ND
		^{269}Ds	ND
	SF,α	^{270}Ds	0,10 ms
	α	^{271}Ds	1,63 ms
		^{273}Ds	0,17 ms
		^{277}Ds	4,1 ms
	SF, α	^{279}Ds	0,18 s
	SF	^{281}Ds	9,6 s

Element	Decay mode	Isotope	Half-life ($t_{1/2}$)
Roentgenium $_{111}$Rg	α	^{272}Rg	3,8 ms
		^{274}Rg	ND
	SF, α	^{278}Rg	4,2 ms
	α	^{279}Rg	0,17 s
		^{280}Rg	3,6 s
	SF, α	^{281}Rg	26 s
		^{282}Rg	0,5 s
Copernicium $_{112}$Cn	α	^{277}Cn	0,69 ms
		^{281}Cn	0,13 s
	SF	^{282}Cn	0,5 ms
	SF, α	^{283}Cn	4 s
	SF	^{284}Cn	101 ms
	α	^{285}Cn	34 s
Nihonium $_{113}$Nh	α	^{278}Nh	ND
		^{282}Nh	ND
		^{283}Nh	ND
		^{284}Nh	0,48 s
		^{285}Nh	5,5 s
		^{286}Nh	20 s
Flerovium $_{114}$Fl	SF	^{284}Fl	2,5 ms
	SF, α	^{286}Fl	0,16 s
	α	^{287}Fl	0,51 s
		^{288}Fl	0,80 s
		^{289}Fl	2,7 s
Moscovium $_{115}$Mc	α	^{287}Mc	ND
		^{288}Mc	ND
		^{289}Mc	0,22 s
		^{290}Mc	16 ms
Livermorium $_{116}$Lv	α	^{290}Lv	15 ms
		^{291}Lv	ND
		^{292}Lv	18 ms
		^{293}Lv	53 ms
Tennessine $_{117}$Ts	α	^{293}Ts	14 ms
		^{294}Ts	ND
Oganesson $_{118}$Og	α	^{294}Og	1,8 ms

Markings :

EC - electron capture,
SF - spontaneous fission,
ND - no data.

Table A.2: Decay mode and half-life for each transactinide. All data comes from the website Nuclear Data Services (*https*: *//www-nds.iaea.org/*).

A.3 SDD detector

To improve energy resolution of AC moduls replacement of the BC-418 scintillators by single crystal diamond detectors (SDD) was considered. Their energy resolution provides better distinguish between α particles and fission fragments, and between other heavy elements. This process can be seen on the figure A.1. Where on the left panel amplitude spectrum of background is

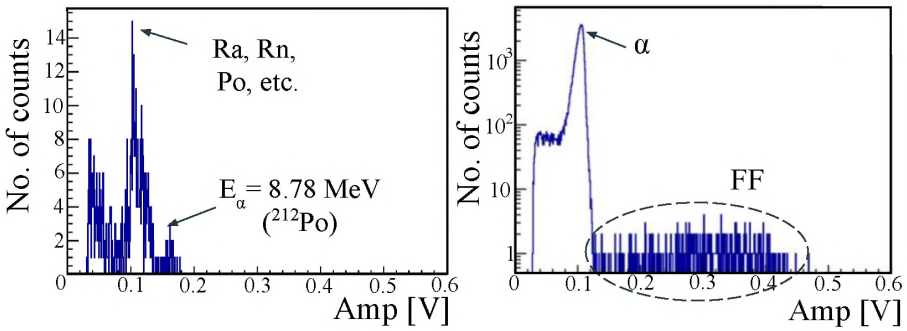

Figure A.1: Preliminary amplitude spectra for diamond detector, left panel: for background measurement, right panel: for measurements with Cf source.

presented - measurements were made five days in UJs laboratory in Kraków. It can be seen how well background events are separated. It should be also mentioned here that observed peak for α particles from ^{212}Po have energy beyond 10 MeV, while αs with energy higher then 10 MeV are interesting for searching of SHE element. Right panel of this figure is presenting short measurements (in the same lab conditions as for background) with use of the californium source. How can be see registered α particles and fission fragments are really good separated here. Such amplitude spectrum discrimination of SDD would be extremely helpful in future experiments for heavy or superheavy elements identification process.

B | Abbreviations

AC - active catcher
ACQ - acquisition system
ACT - activated scintillators

BNL - Brookhaven National Laboratory.

CN - compound nucleus

DF - digital filters.
DGFRS - Dubna gas-filled separator of recoil nuclei
DIP - deep inelastic scattering
DPSA - digital pulse shape analisys
DSP - digital signal processing

EvR - evaporation residue

FADC or flesh ADC - analog to digital converter
FF - fission fragments
FPGA - field-programmable gate array
FWHM - full width at half maximum

GARIS - gas-filled recoil ion separator
GSI - Helmholtz Centre for Heavy Ion Research

IF - immediate fission
IUPAC - International Union of Pure and Applied Chemistry
IUPAP - International Union of Pure and Applied Physics

JENDL - Japan Atomic Energy Agency Nuclear Data Center
JINR - Joint Institute of Nuclear Research at Dubna

LLNL - Lawrence Livermore National Laboratory
LNGS - Gran Sasso National Laboratory

MCP - micro channel plate

MNT - multinucleon transfer

N - neutron number
NACT - not activated scintillators
NRV - Nuclear Reactions Video (Low Energy Nuclear Knowledge Base supported by Russian Founfaation for Basic Research)

PMT - photomultiplier tube
PSD - positional strips detector

QF - quasi-fission

RF - radio frequency
RILAC - RIKEN Linear Accelerator Facility
RIKEN - Rikagaku Kenkyujyo, Nishina Center for Accelerator-Based Science

SDD - single-crystal diamond detector
SF - spontanous fission
SHE - super heavy elements
SHIP - search for hidden particles detector
SHN - super heavy nucleus

TAMU - Texas A & M University
TKE - total kinetic energy
TKEL - total kinetic energy loss
TLF - target like fragment
ToF - time of flight

YAP - yttrium aluminum perovskite

Z - atomic number

Bibliography

[1] G. Scharff-Goldhaber. Nucleonics. *Nuc. Phys.*, **15**:122, 1957.

[2] W.D. Myers, W.J. Świątecki. Nuclear masses and deformations. *Nucl. Phys.*, **81, No. 1**:1, 1966.

[3] A. Sobiczewski, F.A. Gareev, B.N. Kalinkin. Closed shells for Z > 82 and N > 126 in a diffuse potential well. *Phys. Lett.*, **22, No. 4**:500, 1966.

[4] E. Fermi. Possible Production of Elements of Atomic Number Higher than 92. *Nature*, **133**:898, 1934.

[5] A. Ghiorso, S.G. Thompson, G.H. Higgins, G.T. Seaborg, et al. New Elements Einsteinium and Fermium, Atomic Numbers 99 and 100. *Phys. Rev.*, **99**:1048, 1955.

[6] P.R. Fields, et al. Additional Properties of Isotopes of Elements 99 and 100. *Phys. Rev.*, **94**:209, 1954.

[7] G.R. Choppin, S.G. Thompson, A. Ghiorso, B.G. Harvey. Nuclear Properties of Some Isotopes of Californium, Elements 99 and 100. *Phys. Rev.*, **94**:1080, 1954.

[8] M.H. Studier, et al. Elements 99 and 100 from Pile-Irradiated Plutonium. *Phys. Rev.*, **93**:1428, 1954.

[9] B.G. Harvey, et al. Further Production of Transcurium Nuclides by Neutron Irradiation. *Phys. Rev.*, **93**:1129, 1954.

[10] S.G. Thompson, A. Ghiorso, B.G. Harvey, G.R. Choppin. Transcurium Isotopes Produced in the Neutron Irradiation of Plutonium. *Phys. Rev.*, **93**:908, 1954.

[11] E. McMillan and P. Hauge Abelson. Radioactive Element 93. *Phys. Rev.*, **57**:1185, 1940.

[12] G.T. Seaborg. The Plutonium Story. *Conference: Actinides-1981 conference, Pacific Grove, CA, USA*, 1981. LBL-13492, DE82 004551.

[13] G.T. Seaborg, R.A. James, L.O. Morgan. The New Element Americium (Atomic Number 95). *National Nuclear Energy Series, Plutonium Project Record*, **14 B The Transuranium Elements: Research Papers, Paper No. 22.1**, New York 1949. McGraw-Hill Book Co., Inc.

[14] G.T. Seaborg, R.A. James, A. Ghiorso. The New Element Americium (Atomic Number 96). *National Nuclear Energy Series, Plutonium Project Record*, **14 B The Transuranium Elements: Research Papers, Paper No. 22.2**, New York 1949. McGraw-Hill Book Co., Inc.

[15] S. G. Thompson, A. Ghiorso, G.T. Seaborg. The New Element Berkelium (Atomic Number 97). *Phys. Rev.*, **80**:781, 1950.

[16] S. G. Thompson, A. Ghiorso, G.T. Seaborg. Element 97. *Phys. Rev.*, **77**:838, 1950.

[17] S.G. Thompson, K. Street, Jr.A. Ghiorso, G. T. Seaborg. The New Element Californium (Atomic Number 98). *Phys. Rev.*, **80**:790, 1950.

[18] S.G. Thompson, K. Street, Jr.A. Ghiorso, G. T. Seaborg. Element 98. *Phys. Rev.*, **78**:298, 1950.

[19] A. Ghiorso, B.G. Harvey, G.R. Choppin, S.G. Thompson, G.T. Seaborg. New Element Mendelevium, Atomic Number 101. *Phys. Rev.*, **98**:1518, 1955.

[20] R.C. Barber, A. Z. Hrynkiewicz, D.H. Wilkinson, et al. Discovery of the transfermium elements. Part II: Introduction to discovery profiles. Part III: Discovery profiles of the transfermium elements. *PAC*, **65, issue 8**:1757, 1991.

[21] A. Ghiorso, T. Sikkeland, A.E. Larsh,R.M. Latimer. New Element, Lawrencium, Atomic Number 103. *Phys. Rev.*, **6**:473, 1961.

[22] A. S. Eddington. THE INTERNAL CONSTITUTION OF THE STARS. *The Scientific Monthly*, **11, No. 4**:297–303, 1920. https://www.jstor.org/stable/6491.

[23] A. S. Eddington. On the Radiative Equilibrium of the Stars. *Monthly Notices of the Royal Astronomical Society*, **77, No. 1**:16, 1916.

[24] M.L. Oliphant, E. Rutherford. Experiments on the transmutation of elements by protons. *Roy. Soc.*, **141, No. 843**:259, 1933.

[25] M.L. Oliphant, E. Rutherford, B.B. Kinsey. The transmutation of lithium by protons and by ions of the heavy isotope of hydrogen. *Roy. Soc.*, **141, No. 845**:722, 1933.

[26] M.L. Oliphant, E. Rutherford, P. Harteck. Transmutation effects observed with heavy hydrogen. *Roy. Soc.*, **144, No. 853**:692, 1934.

[27] M.L. Oliphant, E. Rutherford, E.S. Shire, B.M. Crowther. Separation of the isotopes of lithium and some nuclear transformations observed with them. *Roy. Soc.*, **146, No. 859**:922, 1934.

[28] G.N. Flerov, Yu.T. Oganessian, et al. Synthesis and physical identification of the isotope of element 104 with mass number 260. *Phys. Lett.*, **13, No. 1**:73, 1964.

[29] Yu.T. Oganessian, et al. Identification of the elements 102 and 104 by means of the collimation method. *Atomnaya Énergiya*, **28,No.5**:393, 1970.

[30] A. Ghiorso, M. Nurmia, J. Harris, K. Eskola, P. Eskola. Positive Identification of Two Alpha-Particle-Emitting Isotopes of Element 104. *Phys. Rev.Lett*, **22**:1317, 1969.

[31] G.N. Flerov, Yu.T. Oganessian, et al. On the synthesis of element 105. *Nucl. Phys. A*, **160, No. 1**:181, 1971.

[32] A. Ghiorso, M. Nurmia, J. Harris, K. Eskola, P. Eskola. New Element Hahnium, Atomic Number 105. *Phys. Rev. Lett*, **24**:1498, 1970.

[33] Yu.T. Oganessian, et al. Synthesis of Neutron-Deficient Isotopes of Fermium, Kurchatovium, and Element 106. *ZhETF Pis.*, **20**:580, 1974. JETP Lett. (USSR) 20, 265 (1975).

[34] A. Ghiorso,et al. Element 106. *Phys. Rev. Lett*, **33**:1490, 1974.

[35] Yu.T. Oganessian, et al. On spontaneous fission of neutron-deficient isotopes of elements 103, 105 and 107. *Nucl. Phys. A*, **273, No. 2**:505, 1976.

[36] G. Münzenberg, et al. Identification of element 107 by α correlation chains. *Z. Phys. A*, **300**:107, 1981.

[37] Yu.T. Oganessian. Some Aspects of Fusion and Fission of Heavy Nuclear Systems. *School-Seminar Heavy Ion Phys*, 1983. JINR D7-83-644 (1983)55-75.

[38] Yu.T. Oganessian, et al. Experiments on the synthesis of element 108 in the ^{226}Ra+^{48}Ca reaction. *Report in JINR*, 1978.

[39] G. Münzenberg, et al. The Identification of Element 108. *Z. Phys. A*, **317**:235, 1984.

[40] G. Münzenberg, et al. Observation of one correlated α-decay in the reaction ^{58}Fe on ^{209}Bi $\longrightarrow$ ^{267}109. *Z. Phys. A*, **309**:89, 1982.

[41] S. Hofmann, et al. Production and decay of ^{269}110. *Z. Phys. A*, **350, No. 4**:277, 1995.

[42] S. Hofmann, et al. The new element 111. *Z. Phys. A*, **350, No. 4**:281, 1995.

[43] S. Hofmann, et al. The new element 112. *Z. Phys. A*, **354, No. 3**:229, 1996.

[44] Yu.T. Oganessian, et al. Synthesis of Superheavy Nuclei in the ^{48}Ca + ^{244}Pu Reaction. *Phys. Rev. Lett.*, **83, No. 16**:3154, 1999.

[45] Yu.T. Oganessian, et al. Experiments on the synthesis of element 115 in the reaction ^{243}Am(^{48}Ca,xn)$^{291-x}$115. *Phys. Rev. C*, **69, No. 2**:021601, 2004.

[46] K. Morita, et al. Experiment on the Synthesis of Element 113 in the Reaction ^{209}Bi(^{70}Zn,n)^{278}113. *J. Phys. Soc. Jpn.*, **73**:2593, 2004.

[47] Yu.T. Oganessian, et al. Observation of the decay of ^{292}116. *Phys. Rev. C*, **63, No. 1**:011301, 2000.

[48] Yu.T. Oganessian, et al. Synthesis of a New Element with Atomic Number Z=117. *Phys. Rev. Lett.*, **104, No. 14**:142502, 2010.

[49] Yu.T. Oganessian, et al. Synthesis of the isotopes of elements 118 and 116 in the ^{249}Cf and ^{245}Cm + ^{48}Ca fusion reactions. *Phys. Rev. C*, **74, No. 4**:044602, 2006.

[50] Z-Q. Feng, et al. Production of heavy and superheavy nuclei in massive fusion reactions. *Nucl. Phys. A*, **816, No. 1-4**:33, 2009.

[51] V. Zagrebaev, et al. Future of superheavy element research: Whichnuclei could be synthesized within the next few years? *J. Phys.: Conf. Ser.*, **420**, 2013.

[52] V. Zagrebaev, W. Greiner. Cross sections for the production of superheavy nuclei. *Nucl. Phys. A*, **944**:257, 2015.

[53] J.B.Roberto, et. al. Actinide targets for the synthesis of super-heavy elements. *Nucl. Phys. A*, **944**:99, 2015.

[54] J.B.Roberto, et. al. Capabilities and priorities for transactinide research and related actinide target development at Oak Ridge National Laboratory. *4th International Conference on the Chemistry and Physics of the Transactinide Elements*, 2011 Sochi. Russia. Coference and programme website: http://tan11.jinr.ru/Final_Programme-TAN11.htm.

[55] H. Koura, T. Tachibana. How Far does the Area of Superheavy Elements Extend?: Decay Modes of Heavy and Superheavy Nuclei Predicted by a Mass Formula(Science around Superheavy Elements). *Butsuri*, **60, No. 9**:717, 2005.

[56] H. Koura. Decay modes and a limit of existence of nuclei. *4th International Conference on the Chemistry and Physics of the Transactinide Elements, (TAN'11)*, 5-11 Se 2011, Sochi, Russia.

[57] M.Bender, et. al. Self-consistent mean-field models for nuclear structure. *Rev. Mod. Phys.*, **75**:121, 2003.

[58] M. Bender, P-H. Heenen. Structure of superheavy nuclei. *J. Phys.: Conf. Ser.*, **420**, 2013.

[59] S. Ćwok, et. al. Structure of Odd-N Superheavy Elements. *Phys. Rev. Lett.*, **83, Number 6**:1108, 1999.

[60] S. Ćwok, et. al. Shell structure of the superheavy elements. *Nucl. Phys. A*, **611, No. 2-3**:211, 1996.

[61] J.Terasaki, et. al. Superdeformed rotational bands with density dependent pairing interactions. *Nucl. Phys. A*, **593, No. 1**:1, 1995.

[62] M. Samyn, et. al. A Hartree–Fock–Bogoliubov mass formula. *Nucl. Phys. A*, **700, No. 1-2**:142, 2002.

[63] M.Bender. α-decay chains of $^{289}_{175}114$ and $^{293}_{175}118$ in the relativistic mean-field model. *Phys. Rev. C*, **61**:031302, 2000.

[64] M.Bender, et. al. Shell structure of superheavy nuclei in self-consistent mean-field models. *Phys. Rev. C*, **60**:034304, 1999.

[65] Ch. Qi. R.J.Liotta, R. Wyss. Generalization of the Geiger-Nuttall law and alpha clustering in heavy nuclei. *J. Phys.: Conf. Ser.*, **381**, 2012.

[66] K. Grotowski, Z. Majka, R. Płaneta, and M. Szczodrak. Symmetric splitting ofvery light systems. *Phys. Rev. C*, **30, No. 4**:1214, 1984.

[67] D.C.Hoffman, M.R.Lane. Spontaneous Fission. *Radiochimica Acta*, **70**:135, 1995.

[68] D.C.Hoffman, M.R.Lane, T.M.Hamilton In: D.N.Poenaru & editors. Spontaneous Fission. *Handbook of Decay Modes*. Boca Raton, Florida: CRC Press.

[69] V. E. Viola, K. Kwiatkowski, M. Walker. Systematics of fission fragment total kinetic energy release. *Phys. Rev. C*, **31, No. 4**:1550, 1985.

[70] Yu.Ts. Oganessian, et. al. Heaviest nuclei from ^{48}Ca-induced reactions. *J. Phys. G: Nucl. Part. Phys.* , **34**:R165, 2007.

[71] K.Morita, et al. Production and decay of the isotope ^{271}Ds (Z = 110). *The European Physical Journal A - Hadrons and Nuclei*, **21**:257, 2004.

[72] K.Morita. SHE research at RIKEN/GARIS. *Nucl. Phys. A*, **944**:30, 2015.

[73] http://people.physics.anu.edu.au/∼ecs103/chart/.

[74] R. Płaneta, et. al. Nucleon exchange properties of the E/A=8.5 MeV ^{74}Ge + ^{165}Ho reaction. *Phys. Rev. C*, **41, No. 3**:942, 1990.

[75] R. Płaneta, et. al. N/Z equilibration in damped collisions induced by E/A=8.5 MeV ^{58}Ni and ^{64}Ni on ^{238}U. *Phys. Rev. C*, **38, No. 1**:195, 1988.

[76] T. Materna, et. al. Exploring New Ways to Produce Heavy and Superheavy Nuclei with BigSol. *Progress in Research, April 1, 2003–March 31, 2004, Cyclotron Institute Annual Reports, Texas A&M University*, pages **pp. II–17**.

[77] G.G. Adamian, N.V. Antonenko, and A.S. Zubov. Production of unknown transactinides in asymmetry - exit - channel quasifission reactions. *Phys. Rev. C*, **71, No. 3**, 2005.

[78] Yu.E. Penionzhkevich, G.G. Adamian, N.V. Antonenko. Towards neutron drip line via transfer - type reactions. *Phys. Lett. B*, **621, No. 1-2**:119, 2005.

[79] L. Corradi, et al. Multinucleon transfer processes in heavy-ion reactions. *J. Phys. G: Nucl. Part. Phys.*, **36**, 2009.

[80] S. Heinz. Multinucleon transfer reaction - a pathway to new heavy and superheavy nuclei? *J.Phys.: Conf. Ser.*, **1014**:012005, 2018.

[81] Z. Majka, et al. Experimental Search for Super and Hyper Heavy Nuclei at Cyclotron Institute Texas A & M University. *Acta Phys. Pol B*, **45, No. 2**:279, 2014.

[82] M. Barbui, et. al. New experimental approach for heavy and superheavy elements production. *Int. J. Mod. Phys. E*, **18, No.4**:1036, 2009.

[83] K. Zelga in: A. Wieloch, et. al. A novel approach to the island of stability of super-heavy elements search. *EPJ Web of Conferences*, **117**, 2016.

[84] K. Zelga in: Z. Majka, et. al. A novel experimental setup for rare events selection and its potential application to super-heavy elements search. *Acta Phys. Pol. B*, **49, No. 10**:1801, 2018.

[85] S. Wuenschel, et. al. *Collaboration meetings.*

[86] K. Zelga in S. Wuenschel, et. al. An experimental survey of the production of alpha decaying heavy elements in the reactions of ^{238}U +^{232}Th at 7.5-6.1 MeV/nucleon. *Phys. Rev. C*, **97, Iss. 6**:064602, 2018.

[87] BrookHaven National Laboratory. https://www.bnl.gov/NST/NNDC.php.

[88] Nuclear Reactions Video Low Energy Nuclear Knowledge Base supported by Russian Foundation for Basic Research. http://nrv.jinr.ru/.

[89] P.W. Zhao, Z.P. Li, J.M. Yao, J. Meng. New parametrization for the nuclear covariant energy density functional with point-coupling interaction. *Phys.Rev.C*, **82**:054319, 2010.

[90] S.E. Agbemava, A.V. Afanasjev, T. Nakatsukasa, P. Ring. Covariant density functional theory: Reexamining the structure of superheavy nuclei. *Phys.Rev.C*, **92**:054310, 2015.

[91] V.E.Viola Jr., G.T.Seaborg. Nuclear systematics of the heavy elements—II Lifetimes for alpha, beta and spontaneous fission decay. *J. Inorg. Nucl. Chem.*, **28, Iss. 3**:741, 1966.

[92] Yu.T. Oganessian. Heaviest Nuclei from ^{48}Ca-induced Reactions. *J. Phys. G: Nucl. Part. Phys*, **34**:R165, 2007.

[93] I-Y. Lee. The GAMMASPHERE. *Nucl.Phys. A*, **520**:c641, 1990.

[94] A. Staszczak, A. Baran, W. Nazarewicz. Spontaneous fission modes and lifetimes of super-heavy elements in the nuclear density functional theory. *Phys. Rev. C*, **87**:024320, 2013.

[95] A.Baran, et. al. Fission barriers and probabilities of spontaneous fission for elements with Z $\geq$ 100. *Nucl.Phys. A*, **944**:442, 2015.

[96] G. Korschinek, W. Kutschera. Mass spectrometric searches for superheavy elements in terrestrial matter. *Nucl.Phys. A*, **944**:190, 2015.

[97] W. Kutschera, G. Korschinek. Searching for Superheavy Elements in Terrestrial Matter with Accelerator Mass Spectrometry. *Fission and Properties of Neutron-Rich Nuclei, Proceedings of the Sixth International Conference on ICFN6, World Scientific*, page 222, 2017.

[98] H. Gäggeler, et. al. Search for Superheavy Elements in the ^{238}U + ^{238}U Reaction. *Phys. Rev. Lett.*, **45**:1824, 1980.

[99] K. Zelga, et. al. ΔE - E Detector System For Searching Long Lived Heaviest Nuclei In Activated Scintillators. *JPS Conf. Proc., Proc. 13th Int. Conf. on Nucleus-Nucleus Collisions*, **32**:010019, 2020.

[100] K. Zelga, et. al. Dedicated ΔE–E detector system for searching long-lived heaviest nuclei deposited in scintillators. *Acta Phys. Pol. B*, **50, No. 3**:579, 2019.

[101] S.W. Smith. The Scientist and Engineer's Guide to Digital Signal Processing Second Edition. 1999. California Technical Publishing San Diego, California.

[102] A. Farsoni. Digital Filters in Radiation Detection and Spectroscopy. *Digital Radiation Measurement and Spectroscopy NE/RHP 537*. Oregon State University.

[103] http://www.srim.org/SRIM/SRIMLEGL.htm.

[104] S. Barlini, et. al. New digital techniques applied to A and Z identification using pulse shape discrimination of silicon detector current signals. *Nucl. Instrum. Meth. Phys. Res. A*, **600**:644, 2009.